Role of WNT1-inducible signaling pathway protein-1 (WISP1) in liver injury

DISSERTATION

ZUR ERLANGUNG DES AKADEMISCHEN GRADES DES DOKTORS
DER NATURWISSENSCHAFTEN (DR. RER. NAT.)
FAKULTÄT FÜR CHEMIE UND CHEMISCHE BIOLOGIE DER
TECHNISCHEN UNIVERSITÄT DORTMUND

VORGELEGT VON

DANIELA FERNANDA GONZÁLEZ LEIVA, M. SC.

DORTMUND 2020

1. GUTACHTER: PROF. DR. JAN G. HENGSTLER
2. GUTACHTER: PROF. DR. CARSTEN WATZL

Eidesstattliche Versicherung (Affidavit)

Name, Vorname
(Surname, first name)

Matrikel-Nr.
(Enrolment number)

Belehrung:

Wer vorsätzlich gegen eine die Täuschung über Prüfungsleistungen betreffende Regelung einer Hochschulprüfungsordnung verstößt, handelt ordnungswidrig. Die Ordnungswidrigkeit kann mit einer Geldbuße von bis zu 50.000,00 € geahndet werden. Zuständige Verwaltungsbehörde für die Verfolgung und Ahndung von Ordnungswidrigkeiten ist der Kanzler/die Kanzlerin der Technischen Universität Dortmund. Im Falle eines mehrfachen oder sonstigen schwerwiegenden Täuschungsversuches kann der Prüfling zudem exmatrikuliert werden, § 63 Abs. 5 Hochschulgesetz NRW.

Die Abgabe einer falschen Versicherung an Eides statt ist strafbar.

Wer vorsätzlich eine falsche Versicherung an Eides statt abgibt, kann mit einer Freiheitsstrafe bis zu drei Jahren oder mit Geldstrafe bestraft werden, § 156 StGB. Die fahrlässige Abgabe einer falschen Versicherung an Eides statt kann mit einer Freiheitsstrafe bis zu einem Jahr oder Geldstrafe bestraft werden, § 161 StGB.

Die oben stehende Belehrung habe ich zur Kenntnis genommen:

Official notification:

Any person who intentionally breaches any regulation of university examination regulations relating to deception in examination performance is acting improperly. This offence can be punished with a fine of up to EUR 50,000.00. The competent administrative authority for the pursuit and prosecution of offences of this type is the chancellor of the TU Dortmund University. In the case of multiple or other serious attempts at deception, the candidate can also be unenrolled, Section 63, paragraph 5 of the Universities Act of North Rhine-Westphalia.

The submission of a false affidavit is punishable.

Any person who intentionally submits a false affidavit can be punished with a prison sentence of up to three years or a fine, Section 156 of the Criminal Code. The negligent submission of a false affidavit can be punished with a prison sentence of up to one year or a fine, Section 161 of the Criminal Code.

I have taken note of the above official notification.

Ort, Datum
(Place, date)

Unterschrift
(Signature)

Titel der Dissertation:
(Title of the thesis):

Ich versichere hiermit an Eides statt, dass ich die vorliegende Dissertation mit dem Titel selbstständig und ohne unzulässige fremde Hilfe angefertigt habe. Ich habe keine anderen als die angegebenen Quellen und Hilfsmittel benutzt sowie wörtliche und sinngemäße Zitate kenntlich gemacht.
Die Arbeit hat in gegenwärtiger oder in einer anderen Fassung weder der TU Dortmund noch einer anderen Hochschule im Zusammenhang mit einer staatlichen oder akademischen Prüfung vorgelegen.

I hereby swear that I have completed the present dissertation independently and without inadmissible external support. I have not used any sources or tools other than those indicated and have identified literal and analogous quotations.

The thesis in its current version or another version has not been presented to the TU Dortmund University or another university in connection with a state or academic examination.*

*Please be aware that solely the German version of the affidavit ("Eidesstattliche Versicherung") for the PhD thesis is the official and legally binding version.

Ort, Datum
(Place, date)

Unterschrift
(Signature)

TABLE OF CONTENTS

SUMMARY

Liver diseases are a global burden and a better understanding of factors controlling disease progression is required. In the last decade, much progress has been achieved in understanding the relevance of the extracellular matrix. Alterations in this dynamic structure can either facilitate or impair the repair of damaged liver tissue. Therefore, matricellular proteins of the CCN family, have emerged as new targets in liver pathophysiology. These highly conserved secreted proteins specifically interact with and signal through various extracellular partners, like integrins, which enable them to play crucial roles in various processes including development, wound healing and diseases such as cancer and fibrosis. We have discovered that WISP1 (Wnt1-inducible signaling pathway protein-1) also named CCN4, is induced upon CCl_4-induced liver damage and may play an important role in the remodeling process of the extracellular matrix. Therefore, I aimed to identify the cell type that produces WISP1, studied its influence in cell migration and used WISP1 KO mice to understand its role in the pathogenesis of liver fibrosis.

Isolation of individual liver cell types and quantification of WISP1 expression and secretion showed a higher mRNA expression and TGF-β-induced secretion of WISP1 in non-parenchymal cells, especially in stellate cells compared to hepatocytes. Furthermore, WISP1 facilitates the migration of isolated mouse hepatic stellate cells through collagen lattices, suggesting the interaction of WISP1 with one of the main components of the extracellular matrix and affecting its architecture. Additionally, gene expression analysis and Sirius Red staining showed differences in the development of CCl_4-induced fibrosis between WISP1 wild type and knockout mice. Upregulation of collagen type I and α-SMA is reduced in WISP1 KO mice and less collagen deposition is also observed.

In conclusion, WISP1 is mainly expressed and secreted by stellate cells which may influence their migration upon liver injury and consequently, ameliorating the degree of liver fibrosis.

ZUSAMMENFASSUNG

Weltweit sind Menschen von Lebererkrankungen betroffen und ein besseres Verständnis der Faktoren, die das Fortschreiten der Krankheit steuern, ist erforderlich. In den letzten Jahren wurden in der Erforschung der Relevanz der extrazellulären Matrix große Fortschritte erzielt. Veränderungen in dieser dynamischen Struktur können die Reparatur des geschädigten Lebergewebes entweder verbessern oder beeinträchtigen. Daher haben sich matrizelluläre Proteine der CCN-Familie als neue Ziele in der Leberpathophysiologie herauskristallisiert. Diese hochkonservierten sekretierten Proteine interagieren spezifisch mit verschiedenen extrazellulären Partnern, wie zum Beispiel Integrine, und können die Signalkaskade durch diese starten. Dadurch können sie eine entscheidende Rolle bei verschiedenen Prozessen spielen, einschließlich Entwicklung, Wundheilung und Krankheiten wie Krebs und Fibrose. Wir entdeckten, dass WISP1 (Wnt1-induzierbarer Signalweg Protein-1), auch CCN4 genannt, bei CCl_4-induzierten Leberschäden hochreguliert wird und eine wichtige Rolle bei dem Umbauprozess der extrazellulären Matrix spielen kann. Daher war das Ziel dieser Dissertation die Identifizierung des Zelltyps, welches WISP1 produziert, seinen Einfluss auf die Zellmigration zu untersuchen und WISP1-KO-Mäuse zu verwenden, um seine Rolle bei der Pathogenese der Leberfibrose zu verstehen.

Die Isolierung der einzelnen Leberzelltypen und Quantifizierung der WISP1 Expression und Sekretion zeigten eine höhere mRNA Expression und TGF- β-induzierte Sekretion von WISP1 in nicht parenchymalen Zellen, insbesondere in hepatischen Sternzellen im Vergleich zu Hepatozyten. Des Weiteren verbesserte WISP1 die Migration der isolierten hepatischen Sternzellen durch Kollagengitter, das auf die Wechselwirkung von WISP1 mit einer der Hauptkomponenten der extrazellulären Matrix hindeutet und deren Architektur beeinflusst. Zusätzlich zeigte die Genexpressionsanalyse und die Sirius Rot Färbung Unterschiede in der Entwicklung der CCl_4-induzierten Fibrose zwischen WISP1-Wildtyp- und KO-Mäusen. Die Hochregulation von Kollagen Typ I und α-SMA ist bei WISP1-KO-Mäusen verringert und es wird eine geringere Kollagenablagerung beobachtet.

Zusammenfassend können wir festhalten, dass WISP1 hauptsächlich von hepatischen Sternzellen exprimiert und sekretiert wird, die ihre Migration bei Leberschäden beeinflussen und folglich den Grad der Leberfibrose verbessern können.

ABBREVIATIONS

%	Percent
°C	Celsius degree
ACK	Ammonium-Chloride-Potassium
FADGRE1	Adhesion G protein-coupled receptor E1
AIF	Apoptosis-inducing factor
Akt	Protein Kinase B
ALT	Alanine transasminase
ALP	Alkaline phophatase
ANG2	Angiopoietin-2
APAP	Acetaminohen
Arg1	Arginase 1
AST	Aspartate transaminase
Bax	Bcl-2-assoctiated X protein
BC	Bile canaliculi
bp	Base pairs
BSA	Bovine Albumin Fraction V
Bsep	Bile Salt Export Pump
C/EBP	Ccaat-enhancer-binding proteins
ca.	circa
Ca	Calcium
CCl3*	Trichloromethyl free radical
CCl3OO*	Trichloromethylperoxy radical
CCl_4	Carbon tetrachloride
CMC	Collagen monolayer confluent
CO_2	Carbon dioxide
Col I	Collagen type I
Cps1	Carbamoyl-phosphate synthase
Ct	Ct value
CV	Central vein

CXCR4	C-X-C chemokine receptor type 4
CXCR7	C-X-C chemokine receptor type 7
CYP2e1	Cytochrome P450 enzyme 2e1
CYPs	Cytochrome P450 superfamily
d	Day(s)
DAB	3,3’-Diaminobenzidine
DAMPS	Damage-associated molecular patterns
DEPC	Diethylpyrocarbonate
DMEM	Dulbecco’s Modified Eagle’s Medium
DMSO	Dimethyl Sulfoxide
DNA	Deoxyribonucleic acid
DTT	DL-Dithiothreitol
ECM	Extracellular matrix
EDTA	Ethylenediaminetetraacetic acid
EGF	Epidermal growth factor
EGTA	Ethylene glycol tetraacetic acid
ELISA	Enzyme-linked immunoabsorbent assay
EMT	Epithelial to mesenchymal transition
ERK	Extracellular Signal-Regulated Kinase
EtOH	Ethanol
FBS	Fetal bovine serum
FCS	Fetal calf serum
FH	Fresh hepatocytes
Fn	Fibronectin
G	Standard gravity
g	Gram
GAPDH	Glyceraldehyde 3-phosphate dehydrogenase
Gls2	Glutaminase 2
Glt-1	Glutamate transporter 1
Gly	Glycine
Gs	Glutamine synthetase

GSH	glutathione
h	Hour(s)
H&E	Hematoxylin and eosin
H_2O	Water
HGF	Hepatocyte growth factor
HKG	Housekeeping Gene
HNF	Hepatocyte nuclear factor
HPC	Hepatic progenitor cell
HRP	Horseradish peroxidase
HSC	Hepatic stellate cell
Hyp	Hydroxyproline
i.p.	Intraperitoneal
ICAM	Intercellular Adhesion Molecule
IF	Immunofluorescence
IHC	Immunohistochemistry
IL	Interleukin
IPF	Idiopathic pulmonary fibrosis
ITS	Insulin-Transferrin-Selenium media supplement
JAK	Janus Kinase
JNK	c-Jun N-terminal Kinase
K^+	Potassium cation
KC	Kupffer cell
KCl	Potassium Chloride
kg	Kilogram
KH_2PO_4	Potassium dihydrogen phosphate
KO	Knockout
L	Liter
LAP	Latency associated protein
LLC	Large latent complex
LSEC	Liver sinusoidal endothelial cell
LSM	Laser Scanning Microscope

LTBP	Latent TGF-β binding protein
LTC	Latent TGF-β complex
mAB	Monoclonal antibody
MAPK mAB	Monoclonal antibody
MAPK	Mitogen-activated protein kinases
Mc	Monolayer confluent
MHC	Major histocompatibility complex class
mg	Miligram
min	Minute(s)
ML	Median lobe
mL	Mililiter
mm	Milli meter
MMP	Matrix metalloproteinases
MPT	Membrane permeability transition
mRNA	messenger RNA
Na^+	Sodium cation
NaOH	Sodium hydroxide
NEMO	NF-kB essential modulator
NF-kB	Nuclear Factor-Kappa B
ng	Nano gram
NK	Natural killer cells
NO	nitric oxide
NPC	Non parenchymal cell
NTCP	Na+ /taurocholate co-transporting polypeptide
O/N	Overnight
p-	Phosphorylated/phospho-
pAB	Polyclonal antibody
PAGE	Polyacrylamide gel electrophoresis
PAMPs	Pathogen-associated molecular patterns
PBS	Phosphate buffered saline solution
PCNA	Proliferating cell nuclear antigen

PCR	Polymerase chain reaction
PFA	Paraformaldehyde
PHx	Partial hepatectomy
PIP-3	Phosphatidylinositol-3,4,5-trisphosphate
PKC	Protein kinase C
PLC	Phospholipase C
PMSF	Phenylmethylsulfonyl fluoride
PPARα	Peroxisome proliferator-activated receptor alpha
Pro	Proline
PV	Portal vein
PXR	Pregnane X receptor
RhBg	Rh Family B Glycoprotein
qRT-PCR	Quantitative real time PCR
RNA	Ribonucleic acid
ROS	Reactive oxygen species
rpm	Revolutions per minute
RT	Room temperature
RT-PCR	Reverse transcriptase PCR
s	Second
SDS	Sodium dodecyl sulfate
STAT	Signal transducer and activator of transcription
STAT	Signal Transducers and Activators of Transcription
t	Time
TEY	Thr-Glu-Tyr
TF(s)	Transcription factor(s)
Thr	Threonine
Thy	Tyrosine
TIMPs	Tissue inhibitor metalloproteinases
TLR	Toll-like receptor
TNF-α	Tumor necrosis factor α
TPY	Thr-Pro-Tyr

Tris	Tris(hydroxymethyl)aminomethane
V	Volt
VEGFR	Vascular endothelial growth factor receptor 2
VEGF	Vascular endothelial growth factor
WB	Western blotting
Wnts	Wnt pathway ligands
WT	Wild type
x	Fold
α-SMA	Alpha-smooth muscle actin
µg	Micro gram
µl	Micro liter
µm	Micro meter

1 INTRODUCTION

1.1 Liver

The liver is the largest visceral organ of the body and its weight represents about 2% of the total body weight. It is located in the right upper quadrant of the abdominal cavity and it has a main role in metabolic homeostasis because it is responsible for the metabolism, synthesis, storage and redistribution of nutrients, carbohydrates, fats and vitamins. Furthermore, it is the main detoxifying organ of the body, removing wastes and xenobiotics by metabolic conversion and biliary excretion. Almost all of these functions are carried by the main cell type of the liver: the hepatocytes, or parenchymal cells, which comprehends around 80% of the hepatic cells. The other 20% includes the non-parenchymal cells, including Kupffer cells, liver sinusoidal endothelial cells, stellate cells, cholangiocytes and lymphocytes [1], [2].

1.1.2 Liver structure

The hepatocyte population accounts for approximately 78% of the liver tissue volume, while non-parenchymal cells constitute about 6.3% in which about 2.8% are endothelial cells, 2.1% Kupffer cells and 1.4% hepatic stellate cells. The remaining 15.7% of the liver tissue volume corresponds to the extracellular space [3].

The liver is highly vascularized, approximately 80 % of the blood supply comes from the portal vein, containing nutrient-rich blood from the intestine. The portal blood also contains substances secreted by the pancreas, spleen and intestine. The remaining 20 % of blood supply comes from the hepatic artery, which provides oxygenated blood from the aorta [3], [4].

The classical structural unit of the liver is the hepatic lobule. It consists of a roughly hexagonal arrangement of plates of hepatocytes, which extend forming liver cell plates of 15–25 hepatocytes in length (Figure 1). The corners of the hexagon are formed by the portal triads, which are constituted by the portal vein, bile duct and the hepatic artery. Plates of hepatocytes or “cords” radiate from the central vein to the perimeter of the lobule to define the basic functional unit of the liver, known as the acinus. In the cords, the hepatocyte membranes are interconnected and face the sinusoids at either side. The hepatic sinusoids are lined by liver sinusoidal endothelial cells and are also populated with resident

macrophages, the Kupffer cells. Importantly, there is a small space between the endothelial cell lining and the apical membrane of the hepatocytes called the Space of Disse, which is involved in lymph draining and provides a residence niche for hepatic stellate cells. The blood flows through the sinusoids from the portal triad via the central vein and channels into the hepatic vein, which then leaves the liver and reaches the systemic circulation [3], [5], [6], [7].

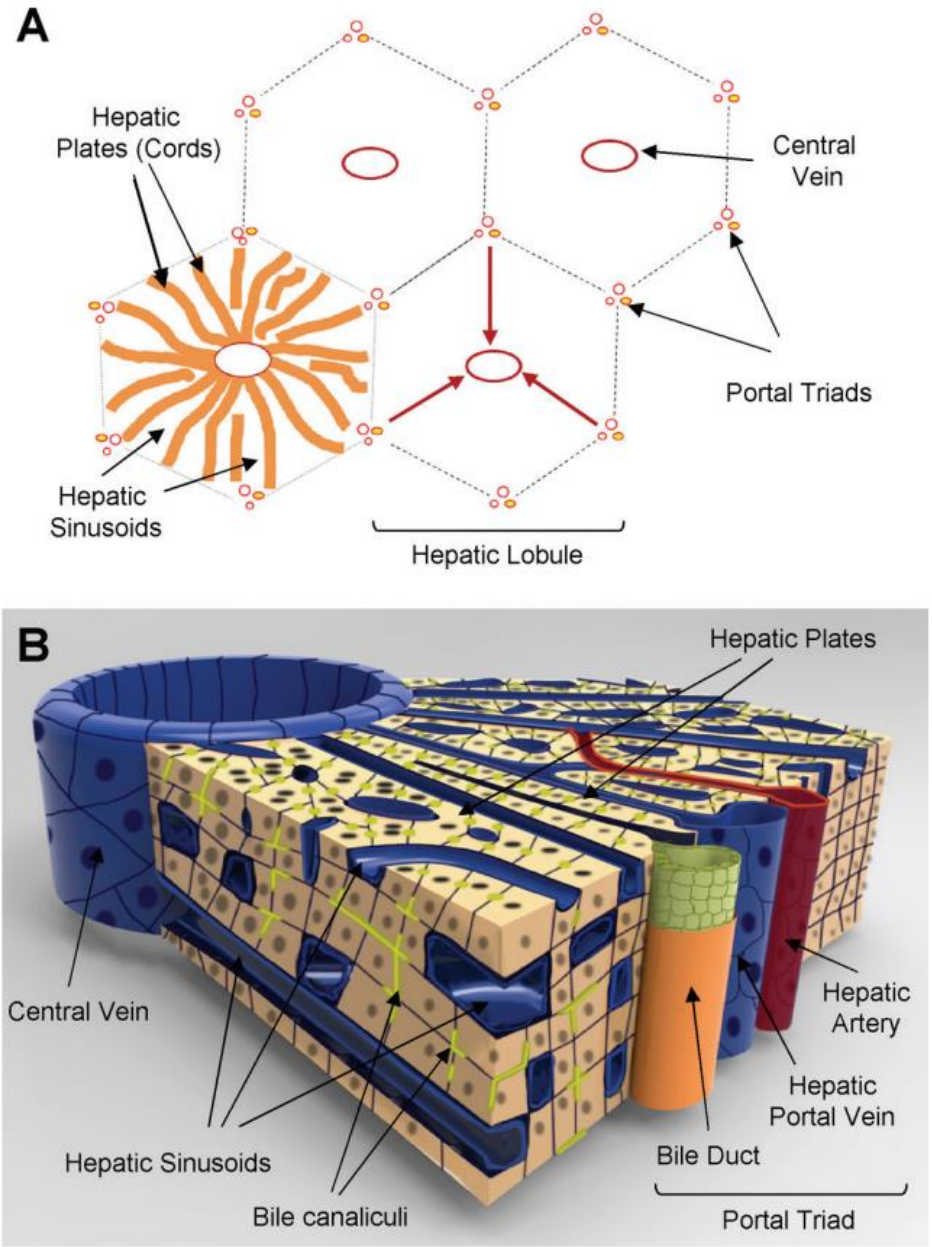

Figure 1. Structure of a hepatic lobule. A) Diagram of the basic hepatic lobule substructure showing the relative direction of the blood flow from portal triads towards the central veins (red arrows). B) Diagram illustrating the three-dimensional structure of the liver between a portal triad and the central vein. From the central vein, plates of hepatocytes (cords) radiate

to the perimeter of the lobule. The blood flows through hepatic sinusoids from the portal triad to the central vein [7].

1.1.3 Liver zonation

The maintenance of the liver homeostasis relies on its metabolic function. To achieve this, the liver parenchyma displays a functional organization known as metabolic zonation. The hepatocytes have a specialized function based on their position along the porto-central axis of the liver lobule that determines their fate as either "periportal" or "perivenous" hepatocytes [5].

Despite the almost homogeneous appearance on the histological level, the liver lobules or acini display a great heterogeneity regarding subcellular, biochemical and physiological functions. Initially two zones were distinguished, one around the portal triads (the periportal zone or zone 1) and a second one around the central vein (the perivenous, pericentral, centrilobular zone or zone 3) [4], [6]. Later, an additional intermediary zone (transitional zone or zone 2) was included (Figure 2).

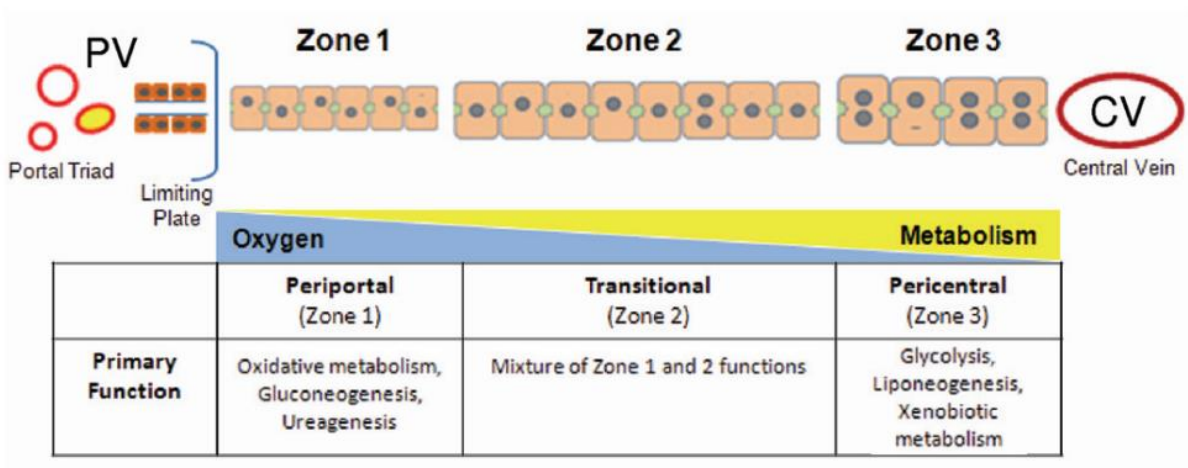

	Periportal (Zone 1)	Transitional (Zone 2)	Pericentral (Zone 3)
Primary Function	Oxidative metabolism, Gluconeogenesis, Ureagenesis	Mixture of Zone 1 and 2 functions	Glycolysis, Liponeogenesis, Xenobiotic metabolism

Figure 2. Structural and functional zonation of the liver. Zones of the liver between the portal vein (PV) and the central vein (CV) illustrating the differences in cell size, phenotype and gradients in oxygen tension and metabolism [7].

The glucose metabolism is one of the most studied zonated functions together with ammonia detoxification and metabolism of drugs and xenobiotics. Gluconeogenesis and metabolism of ammonia are performed by periportal hepatocytes. In contrast, glycolysis and metabolism of drugs and xenobiotics occur mostly in the perivenous area [5].

Importantly, functional zonation is mainly controlled by differential expression of genes encoding enzymes responsible for the functions of the liver. As shown by microarray studies, transcriptional mechanisms seem to be crucial. These studies confirmed that zonation of glucose, ammonia and drug metabolism was mainly under the control of mRNA levels [5], [8]. Moreover, the Wnt/β-catenin pathway, which has been strongly conserved through evolution, plays an important role in development and in liver zonation. The zonal metabolic pathways affected by changes in β-catenin signaling include those mediating ammonia metabolism. β-catenin exerts strict positive control over the perivenous genes encoding glutamine synthetase (Gs or glu1), a transporter of glutamate (Glt-1) and a transporter of ammonia (RhBg). It negatively regulates periportal genes such as the glutaminase 2 (Gls2), arginase 1 (Arg1) and carbamoyl-phosphate synthase (Cps1) which are key enzymes of the urea cycle. Additionally, Wnt signaling controls the expression of the two major Cyp450 enzymes, Cyp2e1 and Cyp1a2 [5][9].

1.2 Liver cell types

The liver is constituted by cells that are broadly divided into two categories: parenchymal cells and non-parenchymal cells. The parenchymal fraction consists of hepatocytes and the non-parenchymal one includes a heterogeneous fraction both in cell type and in function. It is composed by liver sinusoidal endothelial cells (LSEC), hepatic stellate cells (HSC), Kupffer cells (KC), bile duct epithelial cells (or cholangiocytes) and pit cells (intrahepatic lymphocytes) (Figure 3). These have also been shown to have functional heterogeneity in relation to their zonal placement. Kupffer cells are distributed in the ratio 4:3:2 across the acinus from zone 1 to zone 3, with the periportal cells having a tendency to be larger in size and more phagocytically active. Pit cells are a distinct population of lymphocytes, especially natural killer (NK) cells within the sinusoids, and they differ slightly, both structurally and functionally, from those in the general circulation. Similar to the Kupffer cells, these are located within the sinusoids, lodged on the walls. There are greater numbers of these cells in zone 1, and the cells themselves can be separated into two distinct populations based on their ditensity, although it is uncertain as to whether the zonal heterogeneity is associated with the heterogeneity in density. The stellate cells, which are situated in the space of Disse, are similarly more numerous in zone 1 [7], [10].

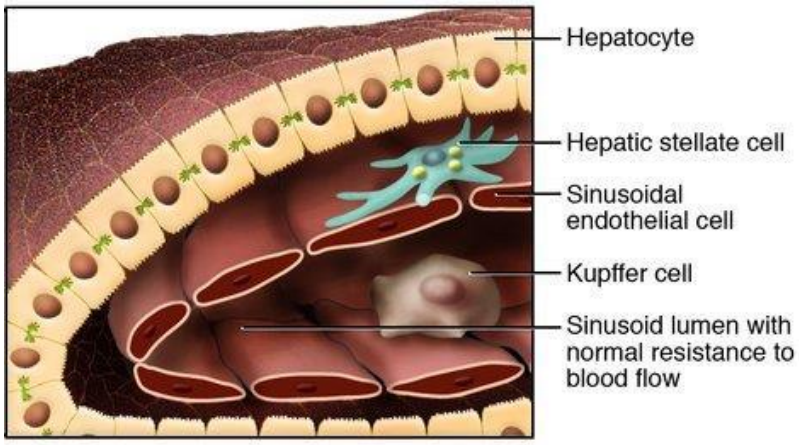

Figure 3. Cell types in the liver. Several diverse cell types are located in the liver: hepatocytes, liver sinusoidal endothelial cells, Kupffer cells, hepatic stellate cells, cholangiocytes and lymphocytes. Kupffer cells are localized in the hepatic sinusoids, which separate hepatic cords from one another. Hepatic stellate cells are localized in the space of Disse [11].

1.2.1 Hepatocytes

The hepatocyte is one of the largest cells of the body. It has a size of 20-30 µm with a volume of 11 000 μm^3 and comprehends a complex system which has to fulfil several complex functions at the same time. It is a polarized cell possessing three different specialized membrane domains: the basolateral or sinusoidal domain, the canalicular domain and the lateral domain. The basolateral domain faces the sinusoids and the perisinusoidal space of Disse. This domain constitutes 70% of the total cell surface and it presents itself with 25-50 microvilli/µm. The canalicular or apical domain constitutes 15% of the total hepatocyte surface and forms the bile canaliculus along with the canalicular domain of the opposite hepatocyte. The last 15% of the total surface corresponds to the lateral domain ranging from the edge of the canalicular domain to the edge of the sinusoidal domain. The border between the lateral and the canalicular domains is represented by junctional complexes that include tight junctions, gap junctions and desmosomes [2].

1.2.2 Liver sinusoidal endothelial cells

Liver sinusoidal cells (LSECs) are thin and elongated cells that from the lining of liver sinusoids. They possess multiple fenestrae throughout the cells and they lack of an underlying basement membrane. Those features distinguish them from other endothelial cells in other organs and in larger liver vessels. The fenestrations or small pores are 50-200 nm in diameter and allow free diffusion of many substances, but not particles of the size of chylomicrons and whole

cells, between the blood and the hepatocyte basolateral surface [2], [7]. LSECs play three important roles in maintaining overall hepatic homeostasis: they act as a “selective sieve” for substances passing from the blood to the hepatocytes and vice versa. Furthermore, they serve as a “scavenger system”, clearing the blood of macromolecular waste products that originate from turnover processes in various tissues. Lastly, the play a role in hepatic immunity to foreign pathogens and immune tolerance to neo-antigens formed during the metabolism of xenobiotics [7]. Moreover, LSECs also function as antigen-presenting cells in the context of both MHC-I and MHC-II restriction with the resulting development of antigen-specific T-cell tolerance [7], [12]. They are also active in the secretion of cytokines, endothelin-1, nitric oxide and some extracellular matrix components [7].

Interestingly, LSECs also play a significant role in the clearance and bioactivation of drugs and are a target of some types of chemical-induced hepatotoxicities. For example, toxicity of acetaminophen is observed in LSECs in the absence of hepatocytes, suggesting that they are capable of generating the reactive metabolite of acetaminophen and mimic its cytotoxic effects [7].

1.2.3 Kupffer cells

Kupffer cells (KCs) constitute 80-90% of the tissue macrophages present in the body. They reside within the lumen of the liver sinusoids, adherent to the endothelial cells that compose the blood vessel walls. KCs are found in great numbers in the periportal area and constitute the first macrophage population of the body to be in contact with bacteria, bacterial endotoxins and microbial debris derived from the gastrointestinal tract and transported to the liver via the portal vein. These KCs are larger and more active in phagocytosis in contrast with centrilobular KCs that are more active in the production of cytokines and inflammatory responses [2], [7], [13].

The activation of Kupffer cells is necessary for the optimal regeneration of the liver through the release of cytokines such as TNF-α and IL-6. These cytokines initiate hepatocyte proliferation mostly through NF-κβ and STAT-3 translocation [2].

1.2.4 Hepatic stellate cells

Hepatic stellate cells (HSCs) are located in the space of Disse in close contact with hepatocytes and sinusoidal endothelial cells. In the human liver, they are disposed along the sinusoids with a nucleus-to-nucleus distance of 40 µm and they constitute approximately 5-8% of the total number of liver cells. The clearest ultrastructural feature of HSCs in the normal adult liver is the presence of cytoplasmic lipid droplets ranging from 1 to 2 µm in diameter. These lipid droplets are involved in the hepatic storage of retinyl esters (vitamin A) [2]. In a normal liver, HSCs maintain a non-proliferative, quiescent phenotype. Following liver injury they become activated, transdifferentiating from vitamin-A-storing cells to myofibroblasts, which are proliferative, contractile, inflammatory chemotactic and are characterized by enhanced extracellular matrix production [14]. These features identified them as the major fibrogenic cell type and a key player in the process of hepatic fibrosis.

1.2.5 Cholangiocytes

Cholangiocytes, or intrahepatic bile duct cells, are biliary epithelial cells that line the bile ducts. Like hepatocytes, they are polarized with structural features that include well-defined apical and basolateral membrane domains. Functionally, they play an important role in the formation of bile by altering primary canalicular bile through a series of secretory and re-absorptive events. Furthermore, they can interact with immune cells directly or regulate localized immune responses through secretion of cytokines and other mediators that influence invading inflammatory cells [2], [7].

1.3 Liver extracellular matrix

The hepatic extracellular matrix (ECM) is a complex network of macromolecules that comprises less than 3% of the relative area on a tissue section and approximately 0.5% of the wet weight. It plays two important roles: provides cells an extracellular physical scaffold and modulates biological processes through signals that maintain the differentiated function of surrounding cells [2], [15].

The ECM undergoes continuous remodeling not only during development but also through differentiation and wound healing. The ECM remodeling is a complex but highly coordinated process that results from the balance between synthesis, secretion, degradation and

reorganization of its components. Synthesis and deposition of ECM elements occur in response to signals carried by cell surface receptors where integrins appear to have a major role [16]. After an insult, ECM is generated as a wound-healing response but also degradated upon elimination of the primary insult. If the injury persist, excessive deposition of ECM proteins occurs, which is the major characteristic of chronic liver disease and where also the transition of a normal liver to fibrotic involves both quantitative and compositional changes in the ECM. The changes in the ECM composition alter cell signaling and facilitate either normal regeneration or lead the way for liver diseases [2], [16], [17].

Components of the hepatic ECM include collagens, non-collagenous glycoproteins, glycosaminoglycans, proteoglycans, matrix-bound growth factors and matricellular proteins [2]. In normal liver, the dense, interstitial ECM is largely found in Glisson's capsule, around large vessels and in the portal triad. On the other hand, the perisinusoidal matrix in the space of Disse has special characteristics since it is composed of both interstitial and basement membranes (BM) like low-density ECM [2], [18].

1.3.1 Collagen

Collagen is the major fibrillar protein present in the ECM, representing up to 30% of the total protein content in the body; therefore, it constitutes the principal structural protein in mammalian tissues. So far, 28 collagens encoded by 49 genes have been identified in vertebrates [16], [19].

The defining feature of collagen is an elegant structural motif in which three parallel polypeptide strands in a left-handed, polyproline II-type (PPII) helical conformation coil around each other with a one-residue stagger to form a right-handed triple helix. The tight packing of PPII helices within the triple helix dictates that every third residue must be Gly, resulting in a repeating XaaYaaGly sequence, where Xaa and Yaa can be any amino acid. The amino acids in the Xaa and Yaa position of collagen are often (2S)-proline (Pro, 28%) and (2S,4R)-4-hydroxyproline (Hyp, 38%), respectively, resulting in ProHypGly, the most common triplet in collagen. Individual collagen triple helices, known as tropocollagen (TC), assemble in a complex, hierarchical manner that ultimately leads to the macroscopic fibers and networks observed in tissue, bone, and basement membranes (Figure 4) [20].

The distinct collagens have been grouped into two main molecular classes: the relatively homogeneous group of fibril-forming collagens and the rather heterogeneous group of non-fibrillar collagens. In the liver, types I, III and V (fibril-forming collagens) are the main components in the dense interstitial ECM in portal tracts and central vein walls. Among the non-fibrillar collagens, types IV, VI, VIII, XIV, XIX, XV and XVIII are found with different locations and functions in the liver. However, in the perisinusoidal matrix both fibril-forming and non-fibrillar collagens are found. These include fibrillar types I, II and V, microfibrillar collagen VI, BM collagens IV and XVIII, and FACIT (fibril-associated collagens with interrupted triple helices) collagen [2].

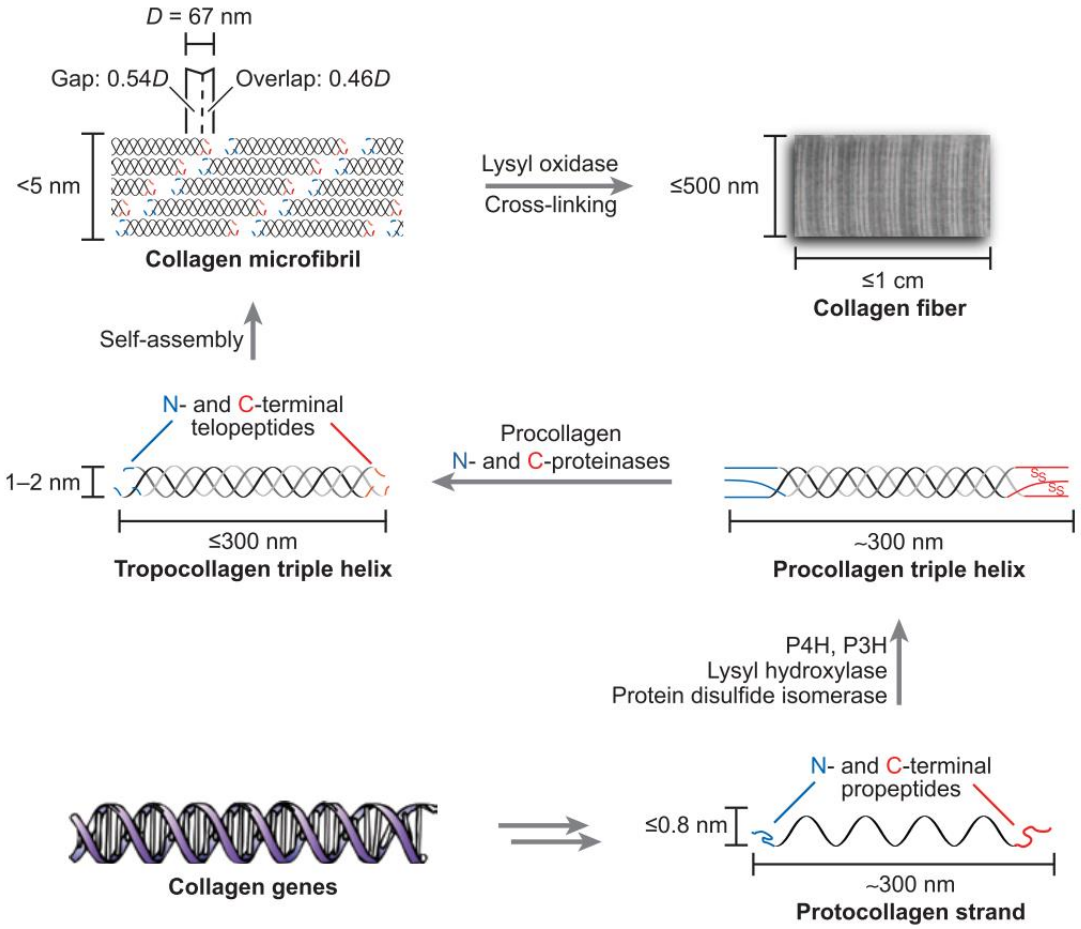

Figure 4. Biosynthetic route to collagen fibers. Size and complexity are increased by posttranslational modifications and self-assembly. Individual Tropocollagen (TC) monomers self-assemble into mature fibrils after procollagen N- and C-proteinases cleave the collagen propeptides at each triple-helix terminus that generate the TC monomers (beginning of fibrillogenesis). Oxidation of lysine side chains leads to the spontaneous formation of hydroxylysyl pyridinoline and lysyl pyridinoline cross-links [20]. P4H: prolyl 4-hydroxylase; P3H: prolyl 3-hydroxylase; nm: nanometer.

1.4 The CCN family

Among matricellular proteins, the CCN protein family is a group of highly conserved secreted proteins that have been identified by differential expression screening since the late 80´s [21]–[23]. The first three members described were CYR61 (cysteine-rich 61; CCN1), CTGF (connective tissue growth factor; CCN2) and NOV (nephroblastoma overexpressed; CCN3), and they provided the acronym for the CCN family. CCN4 (WISP1), CCN5 (WISP2) and CCN6 (WISP3) were later identified as Wnt-inducible secreted proteins [24], [25] and together they composed a family of six members that has been involved in a wide range of important functional pathways, including adhesion, mitogenesis, migration and chemotaxis, cell survival, apoptosis, differentiation, angiogenesis, chondrogenesis, tumorigenesis and wound healing [23], [25], [26].

The unifying feature of this family of proteins is their structure, consisting of modules that share identity with functional domains of other regulatory molecules. A prototypical CCN protein contains an N-terminal secretory signal peptide and four domains: an insulin-like growth factor binding protein-like module (IGFBP), a von Willebrand factor type C repeat module (VWC), a thrombospondin type-1 repeat module (TSP-1) and a cysteine-knot-containing module (CT) (Figure 5) [26]. All CCN proteins exhibit the same type of organization and share a close primary structure, except CCN5 which lacks the CT module and CCN6 which lacks four cysteine residues in the VWC domain [23], [26].

CCN proteins bind several groups of multi-ligand receptors similarly as other matricellular proteins (Figure 5). The most extensively documented among CCN-binding receptors are integrins, including αvβ3, αvβ5, α5β1, α6β1, αIIbβ3, αMβ2, and αDβ2, which mediate diverse functions of CCN proteins in various cell types. The ability of CCNs to bind multiple receptors in various cell types may account for the noteworthy versality of their functions and underline the diverse signaling pathways that mediate their activities [27]. Although CCN proteins do not contain the canonical RGD sequence (the tripeptide Arg-Gly-Asp) that binds to several integrins, they interact with integrins through their non-canonical binding sites [23]. Site-directed mutations in these binding sites abolish specific activities for which the related integrins are responsible, both *in vitro* and *in vivo*, providing strong evidence for the role of these integrins mediating the functions of CCN proteins [23], [28], [29].

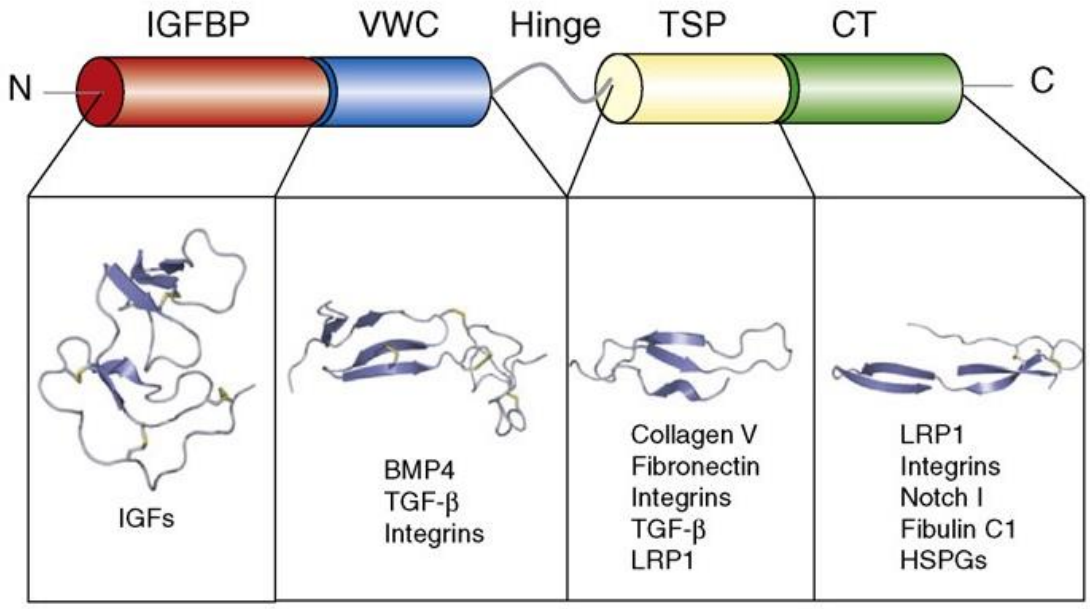

Figure 5. Domain arrangement of CCN proteins. Diagram showing the four domains: insulin-like growth factor (IGFBP) in red, von Willebrand factor C repeat (VWC) in blue, thrombospondin type-1 repeat (TSP) in yellow and cysteine knot (CT) in green. The protein is split in two halves, separated by a variable "hinge" region. Some of the known binding partners of each module are also listed. IGFs: insulin-like growth factors; BMP4: bone morphogenic protein 4; TGF-b: transforming growth factor beta; LRP-1: LDL receptor protein 1; HSPGs: heparin sulphated proteoglycans.[26]

1.4.1 Wnt1-inducible signaling pathway protein-1 (WISP1)

WISP1 or CCN4 was originally identified as one of the genes that was differentially expressed between parental mouse mammary epithelial C57MG cells and Wnt-1 expressing C57MG cells [24]. The higher expression level of WISP1 in the Wnt-1-transformed C57MG cells was reported to be due to the fact that the WISP1 promoter element responds transcriptionally to Wnt-1 and β-catenin signaling. Moreover, it was characterized as an oncogene regulated by Wnt-1-β-catenin pathway [30].

The WISP1 gene is located on chromosome 15 in murine and in human on chromosome 8q24.1-8q24.3. Both are composed of five exons and four introns, and the cDNA length is 1,766 bp and 2,830 bp, respectively. The human WISP1 encodes a protein of 367 amino acids with four potential N-linked glycosylation sites [24], [31].

Regarding WISP1 protein expression, it has been reported to be present in multiple organs along the body and it is expressed in different organs like heart, lung, kidney, intestine and brain among others, and it is linked to processes such as cell death, extracellular matrix

production, cellular migration and proliferation as for the other members of the CCN family [32]. However, a clear role in liver has not been yet reported.

1.5 Liver injury and regeneration

The most frequent cause of acute liver failure is acetaminophen hepatotoxicity. Even though it is a safe and effective analgesic and antipyretic drug, an overdose can cause hepatotoxicity in experimental animals and humans. That is why it has been extensively used as a model toxicant for *in vitro* and *in vivo* studies. Among the other most popular liver injury models is carbon tetrachloride (CCl_4) with acute administration of a large dose causing severe necrosis or chronic administration of lower doses to induce hepatic fibrosis [33].

1.5.1 Acetaminophen induced liver injury

The toxicity of acetaminophen (APAP, paracetamol, N-acetyl-*p*-aminophenol) is strongly dependent on the metabolism by cytochrome P450 enzymes, such as Cyp2E1 and Cyp1a2 [34]. Once APAP is metabolized by Cyp2E1, reactive intermediate N-acetyl-p-benzoquinone imine (NAPQI) is generated and then rapidly conjugated to glutathione (GSH) for detoxification (Figure 6). However, toxic doses cause cellular and mitochondrial GSH depletion, which leads to excessive reactive metabolite formation that produces later protein adduct formation. Modification of mitochondrial proteins causes mitochondrial damage, ATP depletion and oxidative stress, leading to the activation of JNK pathway. Activated JNK translocates to the mitochondria and further increases reactive oxygen species (ROS) formation, resulting in mitochondrial membrane permeability transition (MPT) and collapse of the membrane potential. The initial translocation of Bax [35] (a pro-apoptotic pore-former protein) to the outer membrane and the matrix swelling and rupture of the outer mitochondrial membrane after the MPT generate the release of endonucleases apoptosis-inducing factor (AIF) and endonuclease G (EndoG) from the mitochondria. These endonucleases translocate to the nucleus and cause nuclear DNA fragmentation, finally leading to oncotic necrosis [33], [36], [37].

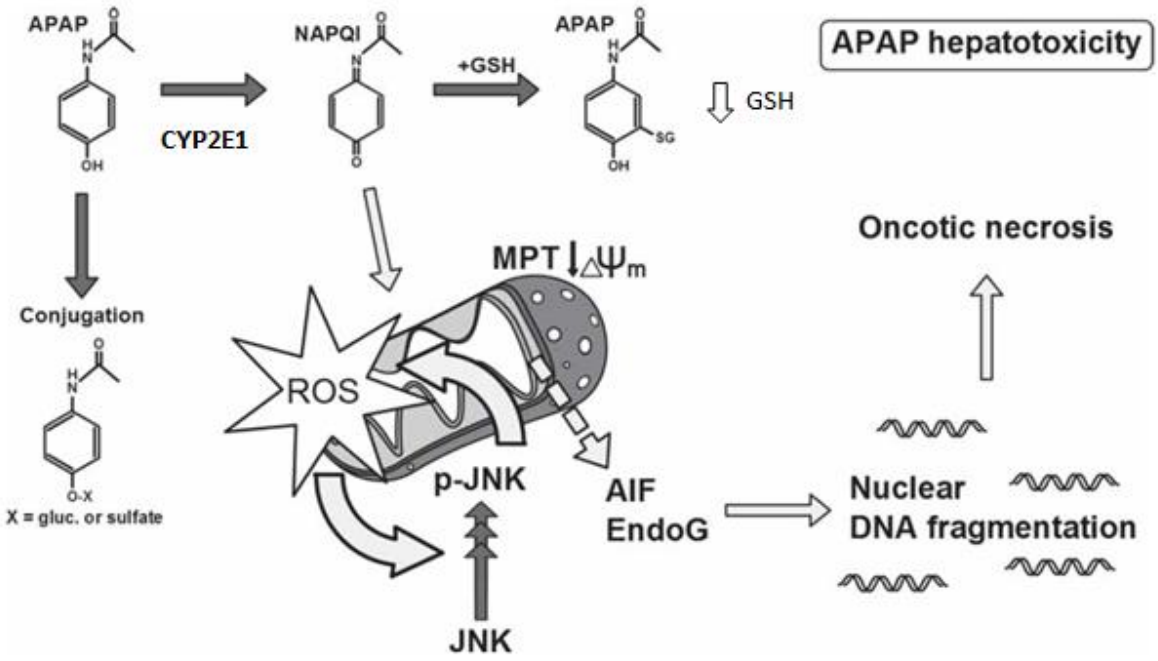

Figure 6. Mechanism of Acetaminophen hepatoxicity. APAP is metabolized to NAPQUI by CYP2E1. After an overdose, the excess of NAPQI depletes mitochondria GSH and the reactive metabolite NAPQUI binds covalently to proteins. Mitochondrial protein alkylation leads to oxidative stress which activates multiple signaling pathways converging on the JNK. Activated JNK (pJNK) then translocates into the mitochondria and increases the oxidative stress, leading to eventual mitochondrial membrane permeability transition (MPT). Matrix swelling and lysis of the outer mitochondrial membrane and translocation of Bax facilitate the release of the endonucleases AIF and EndoG from the membrane space. These endonucleases later translocate to the nucleus and fragment nuclear DNA, causing finally cell death by oncotic necrosis. (Modified image from [36]).

1.5.2 Liver regeneration

Normally in an adult liver, hepatocytes do not undergo cell division but they maintain the ability to proliferate in response to toxic injury and infection. Approximately 95% of hepatic cells re-enter the cell cycle from G0 to S phase after partial hepatectomy (PHx). In the rat liver, the rate of DNA synthesis in hepatocytes begins to increase after 12 hours and peaks around 24 hours starting in cells that surround the portal vein of the liver lobule and proceeds towards the central vein [1]. In contrast, in non-parenchymal cells the induction of DNA synthesis occurs later. For example, the biliary epithelial cells start to proliferate a little later than hepatocytes, and the endothelial cells start two or three days afterwards and finalize around four to five days after the partial hepatectomy [38].

The regeneration process requires a coordinated response of immune cells, mobilization of liver growth factors, matrix remodeling and a fast but tightly controlled epithelial proliferation to achieve the restitution of the liver mass [39]. The histological restitution of the liver mass after surgical resection of 2/3 parts can be achieved between seven and ten days in rodents [38] and may take up to eight weeks in humans [40]. Additionally, the complete restauration of the lobule architecture after CCl_4 intoxication has been reported to be achieved in about ten days [41].

Non-parenchymal cells also play a central role in the regenerative process (Figure 7B). LSECs of the vascular endothelium contribute to the liver regeneration in the early phases in a vascular endothelial growth factor receptor 2 (VEGFR-2)-dependent manner, which stimulates LSEC production of angiocrine factors Wnt2 and hepatocyte growth factor (HGF), triggering hepatocyte proliferation and liver regeneration [39].

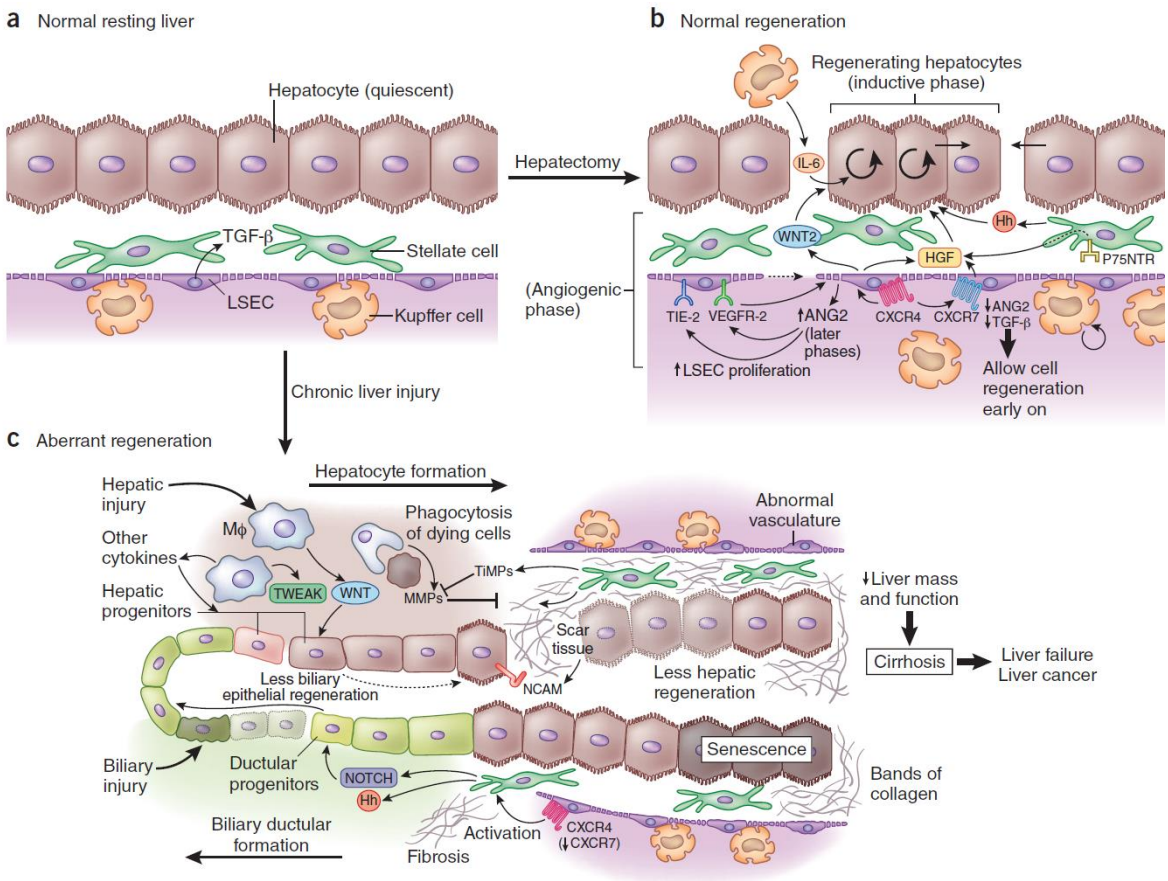

Figure 7. Regeneration in liver. A) Normal adult liver, where hepatocytes are in phase G0 of the cell cycle. LSECs secret TGF-β, which acts as a proliferative break on hepatocytes. B) Normal regeneration after hepatectomy or acute liver injury. LSECs downregulate ANG2 and TGF-β during the early phase after injury and in the later phase ANG2 is expressed to activate

VEGFR-2 and TIE-2 signaling. They also secrete HGF and WNT2 and the cytokines CXCR7 and CXCR4. Stellate cells secrete HGF and hedgehog (Hh); and Kupffer cells secrete IL-6. These factors act with circulating factors to stimulate hepatocyte and biliary epithelial proliferation, followed by proliferation of LSECs, KCs and HSCs. C) In the chronically damaged liver, there is an increased expression of TIMPs, which oppose the scar-resolving function of MMPs. CXCR7 is downregulated and CXCR4 is upregulated, and excessive scar is deposited inhibiting the proliferation of mature epithelial cells. Hepatocytes are often increasingly senescent. In this setting, ductular proliferation is activated by macrophage-derived TWEAK. When there is biliary damage, Notch signaling promotes biliary regeneration, and collagen is deposited. During hepatocyte damage, macrophages phagocytose hepatocyte debris and upregulate Wnt expression, stimulating hepatic regeneration [39].

When the liver injury is prolonged, as it is in chronic hepatitis due to viral infection or alcohol excess, there is an excessive deposition of ECM, and hepatocyte and biliary epithelial cell proliferation is impaired and thus, compromising regeneration (Figure 7C). Part of this complex process is due to the upregulated profibrotic CXCR4 activation and reduced CXCR7-Id1 signaling displayed by LESCs due to CXCR7 inhibition by constitutive activation of fibroblast growth factor receptor-1, resulting in proliferation and activation of hepatic stellate cells. HSC-derived factors such as HGF and hedgehog, fail to stimulate liver growth plus the deposition of scar tissue from stellate cells inhibit hepatocyte and hepatic progenitor cell-mediated regeneration, resulting in reduced liver mass and function [39].

Hepatic myofibroblasts respond to chronic injury by releasing tissue inhibitors of metalloproteinases (TIMPs), which counteract the scar-resolving matrix metalloproteinases (MMPs) that are typically expressed by macrophages. During the resolution of the scar, an antifibrotic milieu develops where TIMP expression is reduced while MMP activity is increased as the macrophages acquire a predominantly antifibrotic phenotype and myofibroblasts revert to quiescent phenotype or undergo apoptosis [39], [42].

1.5.2.1 TGF-β signaling pathway in fibrogenesis

During acute and chronic liver injury, transforming growth factor (TGF-β) is activated from deposits in the ECM and expressed and released from various cell types such as KCs. An important target of TGF-β in this scenery are HSCs that are induced to activate and transdifferentiate to myofibroblasts as mentioned previously. Together with other signaling pathways, TGF-β signaling is considered the key fibrogenic pathway that drives HSCs activation and induces ECM production. In normal liver, quiescent HSCs express a small amount of TGF-β, which is fast upregulated after liver injury. [43].

TGF-β is synthesized in the form of a latent precursor that needs to be cleaved by furin-like proteases to become activated. Then, the C-terminus of the TGF-β molecule binds to the N-terminus of the latency associated protein (LAP) to form the latent TGF-β complex (LTC). The LTC is then released and deposited in the surrounding ECM through binding to latent TGF-β binding protein (LTBP), forming the large latent complex (LLC). The integrin interactions are considered the principal activating mechanism for latent TGF-β. Through integrin binding to certain collagen molecules in the ECM, traction forces are applied, which induce a conformational change in the LLC, and hence facilitating the accessibility of proteases that mediate the liberation of the active form of TGF-β [44].

During liver fibrosis, the composition of the hepatic ECM changes, among others from collagen type IV and laminin towards collagen types I and III [43]. The most potent stimulus for production of collagen I and other matrix components by HSCs is TGF-β1. Signals downstream of TGF-β include the family of bifunctional molecules known as Smads, upon which many extracellular and intracellular signals converge to fine-tune and enhance TGF-β's effects during fibrogenesis [45][46]. In addition to the major role of Smad proteins, TGF-β stimulates collagen in HSCs through a hydrogen peroxide and C/EBPβ-dependent mechanism [47].

1.5.3 Liver fibrosis

Hepatic fibrosis is a common wound-healing response to chronic liver injury involving excessive deposition of extracellular matrix [15]. The accumulation of pro-fibrogenic myofibroblasts is a central feature of tissue fibrosis due to their role as master regulators of the fibrotic response as a result of their acquisition of scar-producing, proliferative, migratory, contractile, immunomodulatory and phagocytic properties [48]. The progressive accumulation of extracellular matrix ultimately leads to the development of cirrhosis, which is historically a morphological definition describing an abnormal liver architecture encompassing fibrous bands surrounding regenerative nodules. Importantly, fibrosis and cirrhosis, whilst sometimes used interchangeably, are clinically distinct entities [49] (Figure 8).

Liver fibrosis is a dynamic, bidirectional process that has an intrinsic ability for recovery and remodeling (Figure 8). Moreover, some clinical studies have shown that even cirrhosis can

regress, for example, patients with chronic hepatitis B virus infection that have been treated with the antiviral drug during five years have shown extensive histological regression and thus, no longer considered as cirrhotic patients [48]. Nevertheless, even if liver fibrosis almost always has some potential for regression, it can fail and that is why increasing understanding of the mechanisms that regulate liver fibrosis and repair can provide a logical framework to develop novel therapeutic approaches.

Models of liver fibrosis can be divided in three big groups: cell culture models, human tissues taken as biopsies or following hepatic resection and experimental animal models. Each group has specific advantages and disadvantages; however, animal models allow serial sampling of tissue for detailed studies of cellular and molecular pathogenesis. Additionally, the development of modern molecular tools and genetically modified mice allows the mechanistic studies of fibrosis in detail [50].

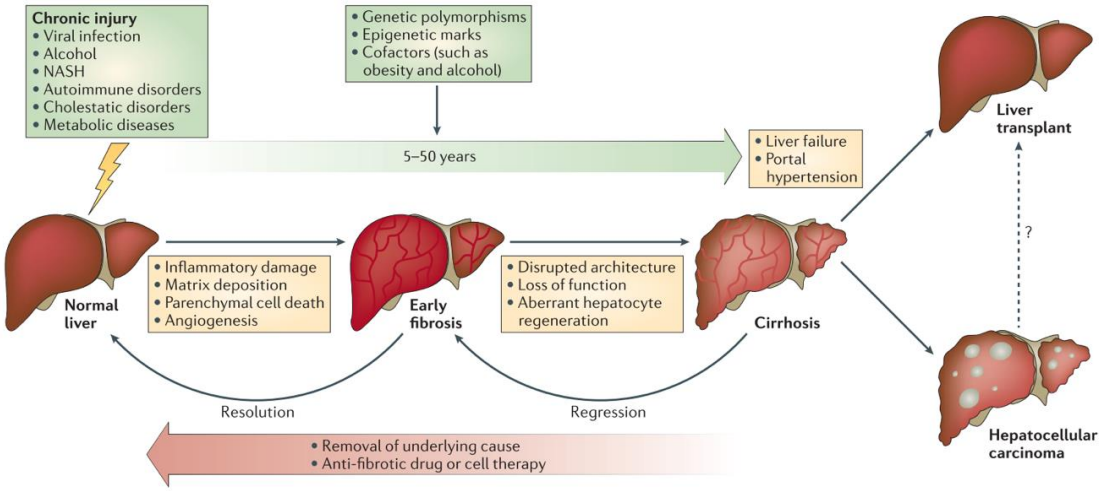

Figure 8. Liver fibrosis regression and resolution. Following chronic liver injury, liver fibrosis can develop and depending on the duration of the injury it can progress into cirrhosis and finally liver failure. Nevertheless, cessation of the liver insult may allow fibrosis regression in early stages [48].

1.5.3.1 CCl_4-induced liver fibrosis

Carbon tetrachloride was a popular industrial chemical that now, due to its toxicity, is strictly regulated in many countries. When it is metabolized, trichloromethyl radicals are produced and can bind to proteins and DNA causing direct damage to these macromolecules [33].

The liver is the principal site for CCl_4-induced effects to manifests themselves, but there is no specific “receptor” for its actions. However, it is well known that CCl_4 metabolism begins with the formation of trichloromethyl free radical CCl_3* through the action of the mixed function cytochrome P450 oxygenase system of the endoplasmic reticulum (Figure 9) [51]. In the presence of oxygen, the CCl_3* radical is converted to the trichloromethyl peroxy radical, CCl_3OO*. This radical is more reactive and thus more short- lived than the CCl3* radical. The lifetime of these radicals is in the range of a millisecond and they disappear from the tissue by reacting with suitable substrates in order to rehabilitate their electron pair. The radical CCl_3OO* is more likely to take a hydrogen from polyunsaturated fatty acids, initiating the process of lipid peroxidation [52]. On the other hand, CCl_3* is more likely to established primary or direct formation of a covalent bond. However, which of these radical-induced events plays the principal role in liver cell necrosis is so far controversial [51].

Many of the mostly inflammatory events identified to follow CCl_4 intoxication are not mediated by hepatocytes, but by mainly Kupffer cells and stellate cells. Kupffer cells release TNF-α, nitric oxide, TGF-β, IL-1, IL-6 and IL-10 [53], [54]. Stellate cells take on the fibroblast-like phenotype and release nitric oxide, and they also begin to over-produce type-I collagen and thus promote hepatic fibrosis.

The CCl_4 model can be applied to both rats and mice, where mice are more commonly used. In the most routinely followed strategy, CCl_4 is injected intraperitoneally two or three times per week during four to six weeks at a dose range of 300 to 1000 µl/kg [55]. This model is very popular among the researchers due to its reproducibility and ease of handling, and most importantly because it shows great similarities with the human liver fibrosis and its progress from a fibrotic into a cirrhotic stage, and reverse the fibrosis upon withdrawal of the insult [56][55].

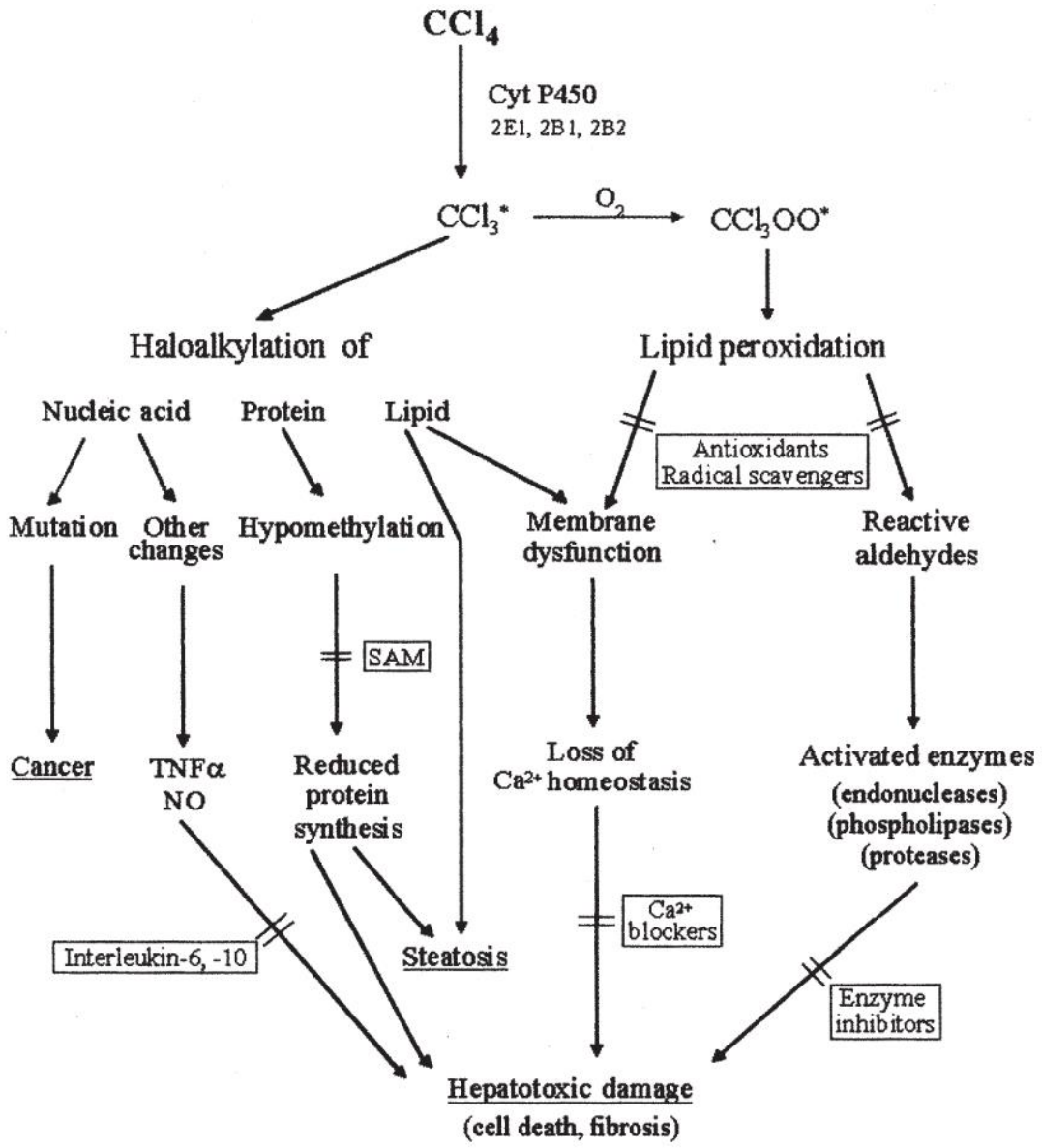

Figure 9. Mechanisms of CCl4-induced liver injury. Mechanisms of action of CCl_4, including points of beneficial intervention. SAM = S-adenosyl methionine; TNFα = tumor necrosis factor α; NO = nitrous oxide. Blocked arrows indicate interruption of toxication pathways with the help of different agents [51].

1.6 Aim of this work

The aim of this work was to investigate the role of WISP1 in the process of liver damage. For this purpose, a well-established WISP1 knockout mouse line was used in well-known toxicant-induced liver injury models. To accomplish that goal, the specific tasks were structured as following:

- Identify the cell source of WISP1 expression and secretion by isolating the different liver cell subpopulations.
- Study the influence of WISP1 on the migration of isolated hepatic stellate cell through collagen lattices *in vitro*.
- Study the influence of WISP1 knockout on hepatic stellate cell migration *in vivo* after APAP-induced liver injury.
- Investigate the effect of WISP1 knockout on liver fibrosis using a CCl_4-induced chronic liver damage.

2 MATERIALS AND METHODS

2.1 MATERIALS

2.1.1 Technical equipment

Table 1: Equipment

Equipment	Description, company
Autoclave	5075 ELV, Tuttenauer
autoMACS Pro Separator	Miltenyi Biotec
Balance	EW, Kern
Benches	HERA-Safe, Heraeus
Centrifuge	Centrifuge 5425 R, Eppendorf MiniSpin®/ MiniSpin® plus, Eppendorf Megafuge 1.0R, Heraeus
Centrifuge with cooling function	5424R, Eppendorf Biofuge Fresco, Heraeus
Chemistry analyzer	1100-1001 Piccolo xpress
Electrophoresis Chamber	Mini-PROTEAN® Tetra Cell Systems, BioRad
Electrophoresis Chamber	Sigma-Aldrich® MSMINIDUO horizontal, Sigma-Aldrich
Freezer	Liebherr (-20 °C) Thermo Scientific (-80 °C)
Fridge	Siemens Bosch
Heating blocks	HTM 130, Haep Labor Consult PHMT-PSC20, Grant Instruments HX-2, VWR Peqlab
Ice machine	AF 100, Scotsman
Image acquisition system	E-BOX CX5, Vilber Lourmat
Incubators	CO2 Incubator C150 R Hinge 230, Binder
Infinite M200 Pro Plate reader	Tecan
Laminar Flow Hood	Electronics FAZ 2, Waldner
Magnetic stirrer	IKAMAG RCT, IKA
Microscope	Eclipse TS100, Nikon
Microscope CCD-Camera	AxioCam ICm 1
Minishaker	MS 2, IKA
pH meter	CG 842, Schott
Piccolo Xpress Analyzer	Abaxis
Pipettes	Research plus, Eppendorf Reference, Eppendorf
Pipette Aid	PIPETBOY, INTEGRA
Power Supplies	Power Pack P25 T, Biometra Power Pack™ HC, BIO RAD
Precision balance	EW 150-3M, Kern

Real-Time PCR	7500 Fast & 7500 Real-Time PCR System, Applied Biosystems
Safety Cabinet	Herasafe™, Heraeus Tecnoflow, INTEGRA Biosciences Clean Air, Clean Air Systems
Shaker	KS 260 basic, IKA Rocking Platform Shaker, VWR Dual-Action Shaker KL 2, Edmund Bühler
Slide Scanner	Axio Scan.Z1, Zeiss
Software Sonicator	Zen, Zeiss SONOPULS mini20, Bandelin
Spectrometer	NanoDrop 2000, PeQLab Biotechnologie GmbH
Thermocycler	TGRADIENT, Biometra
Vacuum pump	Diaphragm Vacuum Pump, Vacuumbrand
Vortex	Testtube shaker, VWR Vortex-Genie 2, Bender&Hobein
Water purification system	Maxima Ultra-Pure Water, ELGA
Waterbath	GFL 1083, Gesellschaft für Labortechnik

2.1.2 Consumables

Table 2: Consumables

Consumable	Description, Company	Catalog No
Adhesive Film	MicroAmp® Optical Adhesive Film, Applied Biosystems	
autoMACS Columns	Miltenyi Biotec	130-021-101
Biosphere Filtered Tip, 1000uL	Sarstedt, Numbrecht, Germany	70.762.211
Biosphere Filtered Tip, 200uL	Sarstedt, Numbrecht, Germany	70.760.211
Biosphere Filtered Tip, 100uL	Sarstedt, Numbrecht, Germany	70.760.212
Biosphere Filtered Tip, 20uL	Sarstedt, Numbrecht, Germany	70.1116.210
Biosphere Filtered Tip, 2.5uL	Sarstedt, Numbrecht, Germany	
Cell culture microtiter plate, 96 well	Greiner bio-one	655986
Culture plates (150 mm)	Sarstedt, Numbrecht, Germany	
Cell scraper	Sarstedt, Numbrecht, Germany	83.183
Corning™ 96-Well Clear Bottom White	Costar 3610, Thermo Scientific, Braunschweig, Germany	07-200-566
Cover glass, 24 x 32 mm	VWR International (Argos Technologies)	631-0711
Falcon ® 24-well TC-treated Plate	Corning	353504
Falcon ®Permeable Support 24-well With 8.0 µm PET membrane	Corning	353097
Falcon tube, 15mL	Sarstedt, Numbrecht, Germany	62.554.512
Falcon tube, 50mL	Sarstedt, Numbrecht, Germany	62.547.254

Gloves	TouchNTuff®, Ansell	
Hypodermic Needle, 26G x 5/8	BD Bioscience, San Jose, USA	304300
Hypodermic Needle, 30G x 5/8	BD Bioscience, San Jose, USA	
Hypodermic Needle, 20G x 5/8	BD Bioscience, San Jose, USA	
Kimtech Science Delicate Task Wipes	Kimberly-Clark Professionals, Roswell, USA	7216
MicroAmp Optical 96-well Reaction Plate	Applied Biosystems, California, USA	N801-0560
MicroAmp Optical Adhesion Film	Applied Biosystems, California, USA	4311971
PCR SingleCap 8er-SoftStrips 0.2ml	Biozym Scientific GmbH, Germany	710988
Pestle & microtube 1,5 ml	VWR International (Argos Technologies)	431-0098
Pipette Tips, 1000uL	Sarstedt, Numbrecht, Germany	70.762
Pipette Tips, 200uL	Sarstedt, Numbrecht, Germany	70.760.002
Pipette Tips, 20uL	Sarstedt, Numbrecht, Germany	70.1116
RNase-free Microfuge Tubes 1.5 mL	Ambion, Thermo Fischer Scientific, Waltham, USA	AM12400
RNaseZap® RNase Decontamination Solution	Ambion, Thermo Fischer Scientific, Waltham, USA	AM9780/AM9782
SafeSeal 0.5mL microtube	Sarstedt, Numbrecht, Germany	72.699
SafeSeal 1.5mL micotube	Sarstedt, Numbrecht, Germany	72.706
SafeSeal 2.0mL microtube	Sarstedt, Numbrecht, Germany	72.695.500
Serological Pipette, 5mL	Sarstedt, Numbrecht, Germany	86.1253.001
Serological Pipette, 10mL	Sarstedt, Numbrecht, Germany	86.1254.001
Serological Pipette, 25mL	Sarstedt, Numbrecht, Germany	86.1685.001
Sterile filter, Filtrapur S0.2	Sarstedt, Numbrecht, Germany	83.1826.001
Tissue Culture Plate Flat-Bottom 6-Well Plate	Sarstedt, Numbrecht, Germany	83.1839
Tissue Culture Plate Flat-Bottom 12-Well Plate	Sarstedt, Numbrecht, Germany	
Tissue Culture Plate Flat-Bottom 24-Well Plate	Sarstedt, Numbrecht, Germany	
Vacuum Filtration Unit, 0.22um, 250mL	Sarstedt, Numbrecht, Germany	83.1822.001
WypAll L30 wipes	Kimberly-Clark Professionals, Roswell, USA	7301

2.1.3 Chemical reagents and kits

Table 3: Chemicals and kits

Chemical	**Company**	**Catalog No**
Acetic acid	Carl Roth, Karlsruhe, Germany	3738.5
Agarose	Biozym Scientific GmbH, Hessisch Oldendorf, Germany	840004

Alanine Aminotransferase Activity Assay Kit	Sigma-Aldrich Corp., St. Louis, MO, USA	MAK052
Amino acid solution (Costumer formulation)	PAN Biotech GmbH, Aidenbach, Germany	SO-33100
APS	Sigma-Aldrich Corp., St. Louis, MO, USA	3678-25g
Aquatex	Sigma-Aldrich	1085620050
Aspartate Aminotransferase (AST) Activity	Sigma-Aldrich Corp., St. Louis, MO, USA	MAK055
autoMACS Running buffer	Miltenyi Biotec	130-091-221
autoMACS Washing solution	Miltenyi Biotec	130-092-987
Avidin/Biotin Blocking Kit	Vector Laboratories, Lörrach, Germany	SP-2001
Benzonase	Sigma-Aldrich Corp., St. Louis, MO, USA	
BioChemistry Panel Plus	Abaxis	REF 400-0035
Bovine Albumin Fraction V (BSA)	Carl Roth, Karlsruhe, Germany	8076.4
Bromophenol Blue	Merck, Darmstadt, Germany	108122
Buffer concentrate A	Carl Roth, Karlsruhe, Germany	L510.1
Buffer concentrate K	Carl Roth, Karlsruhe, Germany	L511.1
Calcium chloride ($CaCl_2$)	Sigma-Aldrich Corp., St. Louis, MO, USA	5239.1
CCl_4	Sigma-Aldrich Corp., St. Louis, MO, USA	7345.1
Cell Lysis Buffer 2	R&D Systems, Minneapolis, USA	895347
Cell Titer Blue Assay	Promega, Wisconsin, USA	G8081
Chloroform	Carl Roth, Karlsruhe, Germany	7331.2
Citric acid monohydrate	Carl Roth, Karlsruhe, Germany	3958.2
Collagen I	Advanced BioMatrix	5005-100ML
Collagenase from Clostridium hystolyticum	Sigma-Aldrich Corp., St. Louis, MO, USA	C2674
Complete feed for Rats&Mice - Maintenance	Ssniff Spezialdiaeten, Soest, Germany	V1534-000
D-(+)- Glucose monohydrate	Sigma-Aldrich Corp., St. Louis, MO, USA	49159
DAB Peroxidase substrate kit	Vector Laboratories, Lörrach, Germany	SK 4100
Dako Pen	Dako, Hamburg, Germany	REF S2002
DEPC Treated Water	Invitrogen GmbH, Darmstadt, Germany	750024
di-Sodium Hydrogen Phosphate anhydrous (Na2HPO4)	Carl Roth, Karlsruhe, Germany	P030.2
DMSO	Sigma-Aldrich Corp., St. Louis, MO, USA	34869
DNA ladder, 2-log	New England Biolabs	N0550S
DNAse I	Roche	10104159001

DNAZap™ PCR DNA Degradation Solutions	Invitrogen	AM9890
DTT (DL-Dithiothreitol)	Sigma-Aldrich Corp., St. Louis, MO, USA	D9779
DPBS	Sigma-Aldrich Corp., St. Louis, MO, USA	
EDTA	Carl Roth, Karlsruhe, Germany	8040.3
EGTA	Carl Roth, Karlsruhe, Germany	3054.2
Eosin Y disodium salt	Sigma-Aldrich Corp., St. Louis, MO, USA	E4382
Ethanol	Merk, Darmstadt, Germany	100983
Ethanol, 70%	Walter CMP, Kiel, Germany	WAL10506
Ethidium Bromide	Invitrogen GmbH, Darmstadt, Germany	15585-011
Glycerin	Carl Roth, Karlsruhe, Germany	3783.2
Glycine	Carl Roth, Karlsruhe, Germany	HN07.3
HEPES	Carl Roth, Karlsruhe, Germany	9105.4
HBSS	PAN Biotech	P04-34500
High Capacity cDNA Reverse Transcription Kit	Applied Biosystems, Karlsruhe, Germany	4368813
Hydrochloric Acid, 32%	Carl Roth, Karlsruhe, Germany	P074.4
Hydrogen peroxide 30% (H2O2)	Sigma-Aldrich Corp., St. Louis, MO, USA	H1009
Ketamin-ratiopharm® 50 mg O.K. Injection Solution	Ratio pharm, Ulm, Germany	N64477.04
Iodixanol	Sigma-Aldrich Corp., St. Louis, MO, USA	
L- Glutamine	Sigma-Aldrich Corp., St. Louis, MO, USA	G3126
Magic Mark XP Western Protein Standard	Invitrogen GmbH, Darmstadt, Germany	LC5602
Magnesium sulfate (MgSO4)	Carl Roth, Karlsruhe, Germany	P027.2
Mayer´s Hemalum solution	Merck, Darmstadt, Germany	1.09249.0500
Methanol	Sigma-Aldrich Corp., St. Louis, MO, USA	322415
Microscopy Entellan	Merck, Darmstadt, Germany	1.07960.0500
Mouse/Rat WISP-1/CCN4 Quantikine ELISA Kit	R&D Systems, Minneapolis, USA	MWSP10
Nycodenz	Progen	1002424
Olive oil	Sigma-Aldrich Corp., St. Louis, MO, USA	75343-1L
Paracetamol (4-Acetamidophenol 98 %)	Sigma-Aldrich Corp., St. Louis, MO, USA	A 7302
Paraffin Histowax Surgipath paraplast	Leica Microsystems, Wetzlar, Germany	3901006
p-Coumaric acid	Sigma-Aldrich Corp., St. Louis, MO, USA	C9008
Percoll™	GE Healthcare	17-0891-01

Phire Animal Tissue Direct PCR Kit	Thermo Scientific, Braunschweig, Germany	F-140WH
Phosphatase Inhibitor Cocktail II	Sigma-Aldrich Corp., St. Louis, MO, USA	P5726
Phosphatase Inhibitor Cocktail III	Sigma-Aldrich Corp., St. Louis, MO, USA	P0044
Pierce BCA Protein Assay Kit	Thermo Scientific, Braunschweig, Germany	23225
Potassium Chloride (KCl)	Carl Roth, Karlsruhe, Germany	6781 .1
Potassium dihydrogen phosphate (KH2PO4)	Carl Roth, Karlsruhe, Germany	3904.1
Precision Plus Protein standard	Bio-Rad Laboratories, Munich, Germany	161-0374
Pronase E		
Protease Inhibitor Cocktail	Sigma-Aldrich Corp., St. Louis, MO, USA	P8340
Qiazol Lysis Reagent	Qiagen, Hilden, Germany	79306
Recombinant Mouse TGF-beta 1 Protein (TGF-β)	R&D Systems	
Recombinant WISP1 (AA23-367) protein	Antibodies-Online GmbH	ABIN2018457
Rompun 2%	Bayer Health Care, Leverkusen, Germany	
Roti Histofix 4%	Carl Roth, Karlsruhe, Germany	P087.5
Roti-Histol	Carl Roth, Karlsruhe, Germany	6640.1
Rotiphorese® Gel 30 (37,5:1)	Carl Roth, Karlsruhe, Germany	3029.1
SDS pellets	Carl Roth, Karlsruhe, Germany	CN30.1
Sera Plus (Special Processed FBS)	PAN Biotech GmbH, Aidenbach, Germany	3702-P103009
Silver nitrate	Merck, Darmstadt, Germany	
Sircol Collagen assay	Biocolor	S4000
Sodium carbonate	Carl Roth, Karlsruhe, Germany	
Sodium chloride (NaCl)	Carl Roth, Karlsruhe, Germany	3957.2
Sodium deoxycholate	Sigma-Aldrich Corp., St. Louis, MO, USA	D6750
Sodium hydroxide pellets	Merck, Darmstadt, Germany	1.06482
Taq DNA Polymerase kit	5-Prime, Hamburg, Germany	2900169
TaqMan® Universal Master Mix II, with UNG	Applied Biosystems, Karlsruhe, Germany	4440038
Trichloroacetic Acid	Carl Roth, Karlsruhe, Germany	8789.2
Trichloromethane/Chloroform	Carl Roth, Karlsruhe, Germany	7331.2
TRIS	Carl Roth, Karlsruhe, Germany	4855.2
Tris-HCl	Sigma-Aldrich Corp., St. Louis, MO, USA	T3253
Triton X-100	Carl Roth, Karlsruhe, Germany	3051
Trizma base	Sigma-Aldrich Corp., St. Louis, MO, USA	33742

Trypan Blue	Sigma-Aldrich Corp., St. Louis, MO, USA	T6146
Tween 20	Sigma-Aldrich Corp., St. Louis, MO, USA	P7949
Tween 80	Sigma-Aldrich Corp., St. Louis, MO, USA	P8074
VECTASTAIN Elite ABC Kit (Rat IgG)	Vector Laboratories, Lörrach, Germany	PK-4004
Xylol AnalaR Norampur	VWR, Langenfeld, Germany	UN1307

2.1.4 Buffers for liver perfusion and in vivo collection

Table 4: Buffers for liver perfusion and in vivo collection

Buffer	Chemical	Amount
Collagenase buffer	Amino acid solution	30 ml
	$CaCl_2$ solution (19 g/l $CaCl_2$* 2 H_2O)	10 ml
	Collagenase Type 1	100 mg
	Glucose solution (9 g/l)	155 ml
	Glutamine (7 g/ml)	2.5 ml
	HEPES (60 g/l) (pH 8.5)	25 ml
	KH buffer	25 ml
EGTA buffer	Amino acid solution	60 ml
	EGTA solution (47.5 g/l)	1.6 ml
	Glucose solution (9 g/l)	248 ml
	Glutamine (7 g/l)	4 ml
	KH buffer	30 ml
	HEPES (60 g/l) (pH 8.5)	30 ml
KH buffer	Potassium chloride	1.75 g
	Potassium dihydrogene phosphate	1.6 g
	Sodium chloride	60 g
	filled to 1 L with H_2O	
	set pH to 7.4	
PBS (10x)	Potassium chloride	10 g
	Potassium dihydrogene phosphate	10 g
	Sodium chloride	400 g
	di-Sodium Hydrogen Phosphate anhydrous	46 g
	filled up to 5 L with distilled H_2O	
	Set pH to 7.4	
Suspension buffer	Albumin Fraction V	400 mg
	Amino acid solution	30 ml
	CaCl2 solution (19 g/l $CaCl_2$ * 2 H_2O)	1.6 ml
	Glucose solution (9 g/l)	124 ml
	Glutamine (7 g/ml)	2 ml
	HEPES (60 g/l) (pH 7.6)	20 ml
	KH buffer	20 ml

	$MgSO_4$ solution (24.6 g/l $MgSO_4$ * 7 H2O)	0.8 ml
Pronase E solution	Amino acid solution	30 ml
	Glucose solution (9 g/l)	155 ml
	KH Buffer	25 ml
	HEPES (60 g/l) (pH 8.5)	25 ml
	$CaCl_2$ (19 g/L)	10 ml
	Glutamine (7 g/l)	2.5 ml
	Pronase E	150 mg
Collagenase solution	Amino acid solution	30 ml
	Glucose solution (9 g/l)	155 ml
	KH Buffer	25 ml
	HEPES (60 g/l) (pH 8.5)	25 ml
	$CaCl_2$ (19 g/L)	10 ml
	Glutamine (7 g/l)	2.5 ml
	Collagenase Type 1	190 mg
Solution D	Amino acid solution	30 ml
	Glucose solution (9 g/l)	155 ml
	KH Buffer	25 ml
	HEPES (60 g/l) (pH 8.5)	25 ml
	$CaCl_2$ (19 g/L)	10 ml
	Glutamine (7 g/l)	2.5 ml
	Collagenase Type 1	190 mg
	Pronase E	150 mg
	DNAse I	2.5 ml
Nycodenz solution	Nycodenz in 27.5 ml GBSS/A solution	8 g
GBSS/A solution	KCl	370 mg/l
	$MgCl_2$ x 6H2O	210 mg/l
	$MgSO_4$ x 7H2O	70 mg/l
	Na_2HPO_4	59.6 mg/l
	KH_2PO_4	30 mg/l
	$NaHCO_3$	2270 mg/l
	$CaCl_2$ x 2H2O	225 mg/l
	Glucose (9 g/l)	100ml/l
	Set pH to 7.36	

2.1.5 Chemicals cell culture

Table 5: Chemicals reagents for hepatocyte cell culture

	Final concentration	**For 500mL Medium**	**Company**	**Catalog No**
William's Medium E	-	-	PAN Biotech	P04-29510
Dexamethasone	100 nM	20 µl from 2.5 mM stock in EtOH	Sigma-Aldrich	D4902-25MG

Gentamycin	10 µg/ml	500 µl	PAN Biotech	P06-13001
Insulin (ITS) 100x	2 ng/ml	5 µl	Sigma-Aldrich	I3146
Penicillin/Streptomycin	100 U/ml	5 ml	PAN Biotech	P06-07100
Stable L-Glutamine	2 mM	5 ml	PAN Biotech	P04-82100
Sera Plus	10 %		PAN Biotech	3702-P103009

Table 6. Chemicals reagents for non-parenchymal cell culture

	Final concentration	**For 500mL Medium**	**Company**	**Catalog No**
DMEM	-	-	Sigma-Aldrich	D1145-500ML
Penicillin/Streptomycin	100 U/ml	5 ml	PAN Biotech	P06-07100
Stable L-Glutamine	2 mM	5 ml	PAN Biotech	P04-82100
Sera Plus	10 %		PAN Biotech	3702-P103009

2.1.6 Buffers for immunohistochemistry

Table 7. Buffers for immunohistochemistry

Buffer	**Chemical**	**Amount**
TBS (10x)	NaCl	80 g
	KCl	2 g
	Tris	30 g
	filled to 5 L with distilled H_2O	
	Set pH to 7.4	
1 x TBS-T	1xTBS	1 l
	Tween 20	5 ml
Citrate buffer	Citric acid monohydrate	2.1 g
	Filled to 1 l with distilled H_2O	
	Set pH to 6.0	
Unmasking buffer	Tris (10mmol/l)	1.2114 g
	EDTA (1mmol/l)	0.3722
	Filled to 1 l with distilled H_2O	
	Set pH to 9.0	

2.1.7 Buffers for PCR

Table 8. TAE-buffer

Buffer	**Chemical**	**Amount**
TAE (10x)	Tris	48.4 g
	Glacial acetic acid	11.4 ml
	EDTA disodium salt	3.7 g

	Filled to 1 l with distilled H_2O	

2.1.7.1 Primers for PCR

Table 9. Primers for genotyping

Primer	Type	Sequence 5´ -> 3´
Alt Puro 3a	Forward	AATTGCATCGCATTGTCTGAGTAGG
Wisp-alt6	Forward	TACGCAATAGGAGTGTGTGCACG
Wisp-alt9	Reverse	GGCAGTGTCTCCATATCATTTGATAGG

2.2 METHODS

2.2.1 Animal models

All animals were kept and treated according to the animal welfare and European laboratory animal regulations. Mice had free access to water and food (Ssniff R/M-H, 10 mm standard diet, Ssniff, Soest, Germany), the room temperature was kept between 18 °C to 26 °C, humidity between 30% and 70% and a 12-hour light/dark cycle.

All experiments were either performed with BALB/c or WISP1 knockout and wild type mice.

2.2.2 WISP1 knockout mice

Heterozygous WISP1 mice (B6;129S5-Wisp1tm1Lex/Orl) were purchased from Lexikon Pharmaceuticals (Lexko-1174) and bred in our animal facility to obtain homozygous WISP1 KO and WT mice. The strategy for the knock down of the gene was to replace Exon 2 of WISP1 by a construct containing puromycin resistance cassette for clone selection, and a stop codon at its 3' end to inhibit transcription of WISP1 (Figure 10)

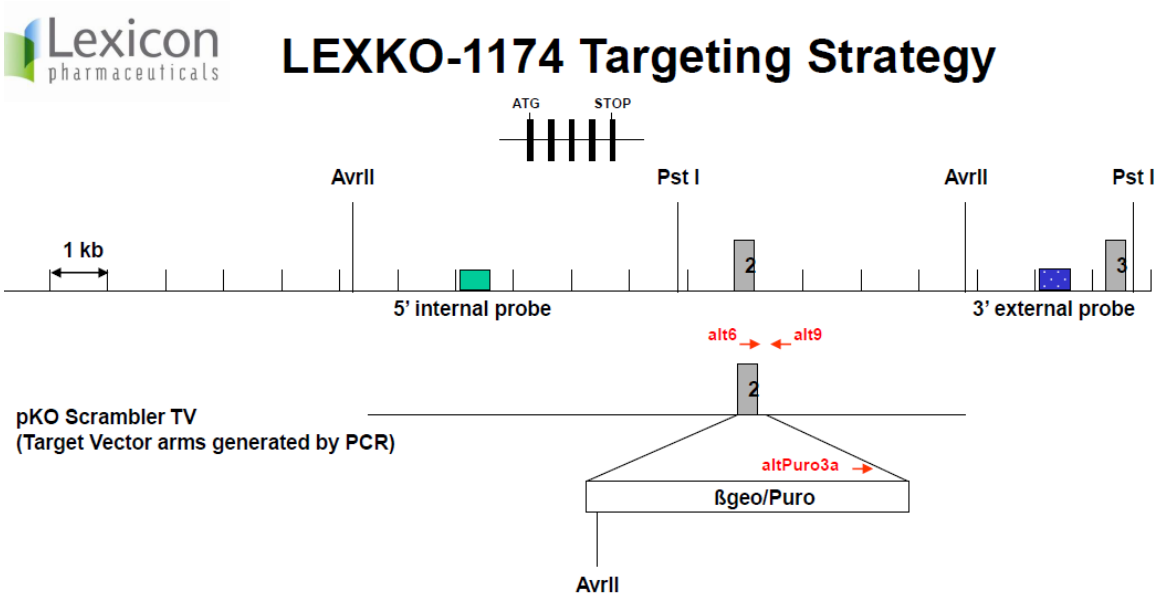

Figure 10. Generation of WISP1 knockout mice. Exon 2 of the WISP1 gene was exchanged by a construct that contains puromycin resistance and a stop codon at its 3' end inhibiting WISP1 transcription.

2.2.3 Genotyping of WISP1 mice

For the WISP1 mice genotyping, Phire Animal Tissue Direct PCR Kit (Thermo Scientific) was used. Ear punch tissue from mice was collected in a microtube containing 25 µl of the Dilution buffer and 1.5 µl of DNARelease Additive were added to release the DNA from the tissue. Afterwards, the samples were heated in a thermo shaker at 98°C for 25 min with gentle agitation followed by a short centrifugation step. The reaction mixture for one PCR reaction is listed in table 10, and the PCR primers are specified in table 11. For the wild type mice, the PCR primers Alt6 and Alt9 were used; whereas, for the mutant samples Alt9 and Puro3A primer pairs were used at a concentration of 10 pmol/µl. Finally, 1 µl of DNA was added to each wild type and mutant PCR. The reaction steps for PCR reaction are listed in table 12.

Afterwards, the PCR products were analyzed on a 1.5% agarose gel containing ethidium bromide. Gel electrophoresis was performed at 100 V in 1x TAE buffer. PCR products in the agarose gel were visualized with E-BOX C5 (Vilber Lourmat, Germany).

Table 10. Master Mix conditions for PCR reaction.

Phire Animal Tissue Direct PCR Kit	Volume per reaction (µl)
Phire Animal Tissue PCR Buffer	10
Primer Forward	5
Primer Reverse	5
Phire Hot Start II DNA Polymerase	0.4
DNA	1

Table 11. PCR primers set up

	Wild type	Mutant
Primers	Alt6 + Alt9	Alt Puro 3A + Alt9
PCR product	363 bp	459 bp

Table 12. PCR reaction program

Step	Temperature (°C)	Time (min)	Note
1	94	3	
2	94	0.5	
3	58	1	
4	72	1	Go to step 2, repeat 39 cycles
5	72	10	
6	Pause at 4		

2.2.4 CCl_4-induced chronic liver damage

To study the role of WISP1 in the pathology of liver fibrosis, a dose of 1g/kg CCl_4 dissolved in olive oil was administrated intraperitoneally (i.p.) twice a week for two months and nine months. Control group received only olive oil as vehicle control. All mice were fed ad libitum along the entire experimental period and six days after the last injection, the mice were sacrificed and samples were collected.

2.2.5 Paracetamol

As a model of acute liver injury, the hepatotoxic compound Acetaminophen was used. Mice were starved overnight and a single dose of 300 mg/kg paracetamol, dissolved in sterile 1x PBS, was administered intraperitoneally. For this purpose, a solution of 14.9 g/l paracetamol was first prepared by dissolving in a water bath at 55°C to ensure solubilization [37]. Afterwards, the solution was cooled at room temperature and sterile filtered. The final volume injected to the mice was 20 µl/g. Control mice were injected with sterile 1x PBS as the vehicle control. All solutions were freshly prepared before the injection.

2.2.6 Blood sampling and organ collection

At the indicated time point, mice were anesthetized using a mixture of sedative Rompun 2 % (20 mg/kg) and anesthetic Ketamine (120 mg/kg) that was administered via i.p. After the loss of all mouse reflexes, the abdominal wall was opened carefully while the mouse was fixed in a dorsal position on a grid.

2.2.6.1 Blood sampling and plasma separation

To analyze the activity of liver enzymes and WISP1 secretion, blood samples were collected from three positions in mice as described previously [57] from the portal vein (representing the liver inflow), from the liver vein (representing the liver outflow), and from the right heart chamber (representing the mixed venous blood). Briefly, to collect blood from the hepatic vein the median liver lobe was carefully lifted up to expose the left liver lobe which was gently pulled caudally. With a 30-gauge needle the liver vein was reached and the blood was collected slowly. In order to expose the portal vein, the abdominal viscera was gently pulled outside of the abdominal cavity and blood was collected by inserting a 30-gauge needle into

the portal vein. To collect blood from the heart a 25-gauge needle was passed through the diaphragm and inserted directly into the right heart chamber. Approximately 100µl of blood were collected from each site using EDTA (32mg/ml) coated syringes. After collection, the blood was directly centrifuged at 13,000 rpm for 10 min at 4°C, the plasma separated in 0,5ml tubes and stored at - 80°C until analysis.

2.2.6.1.1 Biochemical analysis

To analyze the liver function the Biochemistry Panel Plus and the Piccolo Xpress chemistry analyzer (Abaxis) were used. The panel included disks containing different dry reagents for the determination of 14 substances like albumin, transaminases and alkaline phosphatase (ALP). For the analysis, plasma samples were diluted with 1 x PBS in a 1:1 ratio. 100 µl of the dilution were pipetted into the chamber of the disk and the system spun it automatically. The samples reached the reagents chambers, the reactions ran, and the signals were detected by the system.

For most samples and liver damage markers, the Piccolo Xpress chemistry analyzer system was used, however, alanine transferase and aspartate transaminase were in some cases measured with the following assays (2.2.6.1.1.1).

2.2.6.1.1.1 Transaminases assay

Alanine transferase (ALT), also known as serum glutamic-pyruvic transaminase (SGPT) and Aspartate transaminase (AST), also known as serum glutamic-oxaloacetic transaminase (SGOT) were measured colorimetrically using the Alanine Aminotransferase Activity Assay Kit (Sigma) and the Aspartate Aminotransferase Activity Assay Kit (Sigma), respectively.

The transfer of an amino group from alanine to α-ketoglutarate results in the generation of pyruvate, leading to a colorimetric product that can be detected at 570nm wavelength, which is proportional to the ALT enzymatic activity. One unit of ALT is defined as the amount of enzyme that generates 1.0 µmole of pyruvate per min at 37°C.

In the case of AST, the transfer of an amino group from aspartate to α-ketoglutarate results in the generation of glutamate, resulting in the production of a colorimetric product that can be measured at 450 nm wavelength. One unit of AST is the amount of enzyme that will generate 1.0 µmole of glutamate per minute at pH 8.0 at 37°C.

Both assays were performed as described by manufacturer's instructions. All samples were diluted with assay buffer (1:20) and measurement was taken with the microplate reader Infinite M200 Pro.

2.2.6.1.2 ELISA

In order to determine the concentration of WISP1 in blood plasma, liver tissue and supernatant from plated liver isolated cells, Quantikine® ELISA Mouse/Rat WISP-1/CCN4 immunoassay was used. The principle of this assay is the sandwich ELISA which is 2-5 times more sensitive compared to the other ELISA assay types.

All plasma samples were diluted 1:10 with the Calibrator Diluent RD6-31 (1:2). Liver tissue samples were prepared from snap frozen tissue. First, the weight of every frozen tissue was measured and later homogenized with a pestle in 150 µl PBS plus150 µl Cell lysis Buffer 2. Next, the samples were mix with gentle agitation in a thermo shaker at room temperature for 30 minutes. Finally, samples were centrifuged at 13.000 rpm at 4°C for 10 minutes and supernatants were transferred into a new microtube. The assay was performed as described by the manufactures' protocol. The concentration of WISP1 was calculated according to the standard curve and dilution sample for blood plasma and normalization to pg/mg for liver tissue and cell number for cell supernatant.

2.2.6.2 Collection of tissue samples

After blood collection, the whole liver was carefully excised and briefly rinsed with 1X PBS. The left liver lobe was divided into two halves. One half was collected in Tissue-Loc™ HistoScreen™ Cassettes for paraffin embedding and the other half was cut into small pieces (0.5 cm2) and snap-frozen in liquid nitrogen. Snap frozen samples were stored at -80°C for further analyses. The right segment of median liver lobe was also collected for paraffin embedding. All other lobules were cut into smaller pieces and transferred into a 1.5 ml tube and snap-frozen.

2.2.6.2.1 Paraffin embedding of mouse tissues

Half of the left liver lobe and the median liver lobe were fixed in 4% PFA for 48h at 4°C. Afterwards, the samples were washed with PBS for 48h at 4°C and later embedded in paraffin using a spin tissue processor STP120 embedding automate (Microm, Walldorf, Germany). The

embedding program is shown in table 13. Finally, the tissue samples were submerged in paraffin using EC 350 – Modular tissue embedding center.

Table 13. Embedding program for mouse liver tissue

Step	Treatment	Time (min)
1	70% ethanol	30
2	70% ethanol	60
3	90% ethanol	30
4	90% ethanol	30
5	99% ethanol	30
6	99% ethanol	35
7	99% ethanol	60
8	Xylol	30
9	Xylol	35
10	Xylol	30
11	Paraffin Histowax	80
12	Paraffin Histowax	105

2.2.7 Histology

For histological analyses, the liver tissue was sliced in 4 µm sections using the HM 450 Sliding Microtome (Microm, Walldorf, Germany) followed by a fixation on glass microscopy slides at 60°C for 20 min. All tissue slides were stored at 4°C until further usage.

2.2.7.1 Hematoxylin and eosin staining

For the Hematoxylin and Eosin staining (H&E), slides were deparaffinized in Roti-Histol for three times ten minutes and rehydrated in a declining alcohol range (100 %, 90 %, 80 %, 70 % and dH_2O) for five minutes each. After rehydration, the tissue slides were incubated in Mayer´s hematoxylin solution (1:5 diluted with distilled water) for 5 min. Subsequently, the slides were washed for 15 min under running tap water followed by an incubation in 1 % Eosin solution for 3 min. Thereafter, the slides were washed in distilled water for 10 s and dehydrated in ethanol gradient for 5 s each (70 %, 80 % and 90 %). Finally, the sections were incubated two times for 5 min in 100 % ethanol followed by 3 min incubation in Roti-Histol. Subsequently, the stained tissue was preserved with Entellan, allowed to dry overnight, and images were acquired with whole slide scanner (Axio Scan.Z1, Zeiss) for later image analysis.

2.2.7.2 Sirius red staining

In order to visualize collagen deposition in fibrosis, picrosirius red staining was performed [58], [59]. The sections were incubated in Roti-Histol four-times 5 min each. After deparaffinization, the sections were rehydrated in in a declining alcohol range (100 %, 90 %, 80 %, 70 %, 50% and dH_2O) for five minutes each. Afterward, the tissue sections were incubated in hematoxylin solution for 8 minutes and subsequently rinsed for 10 minutes under tap water. Afterwards, the sections were immersed in Sirius Red solution (Sirius red F3B in saturated aqueous solution of picric acid) for 60 minutes followed by washing in acidified water (200µl 32% HCl in 100ml dH_2O) two times. Next, sections were dehydrated in a graded ethanol series (dH2O, 50%, 70%, 80%, 90% and 100%), 1 min each and then incubated in Roti-histol for 3 min. Finally, the sections were preserved by mounting with Entellan. Images were acquired with whole slide scanner (Axio Scan.Z1, Zeiss) for later image analysis.

2.2.7.3 Immunohistochemistry (α-SMA, Desmin)

For immunohistochemical staining, paraffin slides of 4 µm thickness were used. For deparaffinization, the slides were incubated four times in Xylol for 5 min each. Afterwards, rehydration was performed using a descending ethanol gradient (100 %, 90 %, 70 %) for 5 min each followed by an incubation in distilled water for 5 min and another incubation for 5 min in 1 x TBS. For antigen retrieval, the slides were boiled with citrate buffer (2.1 g/L in distilled water, pH 6.0) for 15 to 20 min followed by a cool down with fresh citrate buffer for 30 min. Afterwards, the slides were washed in distilled water for 5 min and blocked for endogenous peroxidase activity for 10 min at room temperature followed by another washing step in distilled water one time and two times in 1 x TBS. Thereafter, unspecific binding sites were blocked by incubation in blocking solution for minimum 1 hour at room temperature in a humidified chamber. After overnight incubation with the primary antibody, the slides were washed three times in TBS-T for 3 min followed another blocking step for 30 minutes. Afterwards, the slides were incubated with the secondary antibody, 30 minutes for α-SMA and 1 hour for desmin with the respective antibodies. Next, the slides were washed again two times in TBS-T for 5 min, followed by one washing time in TBS for 5 min and one time in 0.1M Tris/HCl for 5 minutes. Thereafter, for the color development, the slides were incubated in the dark with the AEC substrate for α-SMA or DAB substrate for Desmin. DAB/AEC substrate

incubation times are listed in table 14. Next, the slides were washed in TBS for 5 minutes followed by incubation with Mayer´s Hemalum solution (1:5 diluted with distilled water, filtered before use) for 2 min. Subsequently, because of the AEC substrate, the α-SMA stained slides were washed with running tap water for 10 min and immediately preserved by mounting with Aquatex and covered with a glass slide. On the other hand, the desmin stained slides were dehydrated in an ethanol gradient, after the washing step under running tap water, for 1 min each (30 %, 50 %, 70 %, 90 %, 95 %, 100 %), followed by an incubation in Roti-Histol for 3 min. Finally, the slides were fixed with Entellan and covered with a glass slide.

All stained slices were scanned with the Axio Scan.Z1 (Zeiss, Jena, Germany) and analyzed with the software ZEN 3.1 (blue edition) (Zeiss, Jena, Germany).

Table 14. Conditions for primary antibodies

Antigen	Origin	Dilution	DAB/AEC substrate	Company	Catalog No.
A-SMA	rabbit	1:100	4-7 min	Abcam	Ab150301
Desmin	rabbit	1:400	6 min	Thermo Fisher Scientific	RB-9014p0

Table 15. Secondary antibodies

Antibody	Origin	Enzyme	Company	Catalog No.
Anti-rabbit	goat	HRP	Dako	K4003
Anti-rabbit	Pig	HRP	Dako	P0217

2.2.8 RNA collection and isolation

RNA was isolated from mouse liver tissue, isolated primary mouse liver cells using QIAzol Lysis Reagent and phenol/chloroform method according to the manufacturer´s description.

Snap frozen liver tissue: Sections of about 0.5 cm2 were homogenized with a plastic pestle in a 1.5 ml tube using 1 ml of QIAzol while kept on ice.

Freshly isolated hepatocytes, NPCs, LSECs, KCs and HSCs: Volume needed for at least 1 million cells was calculated, transferred into a new 1.5 ml tube and centrifuged at 13,000 rpm for 10 min at 4°C. Subsequently, the supernatant was removed and cells were lysed using 0.5-1ml QIAzol.

After the homogenization step, the samples were sonicated on ice for 30 sec (5 sec pulse, 2 sec break) and stored at -80°C until RNA isolation. For 1 ml Qiazol, 200 µl of chloroform was added and samples were strongly shaken for 15 sec. After 2-3 min incubation at room temperature, samples were centrifuged at 4°C for 20 min at 12,000 rpm, the upper aqueous phase was carefully transferred into a new RNase free 1.5 ml tube and RNA was precipitated using 500 µl of isopropanol. Samples were incubated at room temperature for 10 min, followed by a centrifugation step at 4°C for 20 min at 12,000 rpm. Afterwards, the supernatant was removed and RNA pellet was re-suspended in 800 µl of 100 % ethanol and centrifuged at 12,000 rpm at 4°C for 5 min. The supernatant was discarded and RNA pellet was re-suspended with 800 µl of 75 % ethanol and centrifuged for 5min at 4°C at 12,000 rpm. Thereafter, the supernatant was removed and RNA pellet was air-dried under fume hood. Finally, the RNA pellet was dissolved in RNase-free water depending on the pellet size. RNA concentration and integrity were determined spectrophotometrically using the NanoDrop 2000. Extracted RNA was stored at -80°C until further usage.

2.2.9 cDNA synthesis

In the next step, a double stranded cDNA is synthesized by using the biomolecular technique reverse transcriptase polymerase chain reaction (RT-PCR). This technique is using the isolated RNA samples as a template to generate a complementary DNA (cDNA) with the enzyme reverse transcriptase (RT). The cDNA synthesis was performed with the High Capacity cDNA Reverse Transcription Kit (Applied Biosystems). The reaction mixture is shown in table 16.

Table 16. Master Mix for cDNA synthesis

Reagent	Volume per reaction (µl)
10x RT-Buffer	2
25x dNTP	0.8
Random primer	2
Reverse transcriptase	1
DEPC-water	4.2
Total volume 1	10
RNA	Calculated for 2µg
DEPC-water	Up to 10
Total volume 2	10
Final total volume	20

The samples were mixed, centrifuged and the PCR was started (Table 17) using the thermocycler TGRADIENT from Biometra. After the PCR was finished, the resulting cDNA was diluted with DEPC-water to a final concentration of 10 ng/µL and stored at -20°C or directly used for qRT-PCR analysis.

Table 17. Program for RT-PCR

Step	Temperature (°C)	Time
Incubation	25	10 min
Reverse Transcription	37	120 min
Inactivation	85	5 sec
	4	Hold

2.2.10 Quantitative Real Time PCR (qRT-PCR)

The quantitative real time PCR was performed by using Taq-Man-PCR technology with a 7500 Real-Time PCR System using TaqMan® Universal Master Mix II. Reagents were purchased from Applied Biosystems and Taqman probes are listed in table 18. The composition of master mix reaction for qRT-PCR is shown in table 19.

Samples were measured in technical duplicates. For negative control, DEPC-water was used instead of cDNA. The qRT-PCR program is shown in table 20.

Table 18. Taqman probes

Target gene	Gene name	Assay Catalog No.
Adgre1	Adhesion G protein-coupled receptor E1	Mm00802529_m1
Acta2	Alpha smooth muscle actin	Mm00725412_s1
Col1a1	Collagen 1 alpha 1	Mm00801666_g1
Des	Desmin	Mm00802455_m1
Fn1	Fibronectin 1	Mm01256744_m1
GAPDH	Glyceraldehyde-3-phosphate dehydrogenase	4352932E
Mcam	Melanoma Cell Adhesion Molecule	Mm00522397_m1
Mmp9	Matrix Metallopeptidase 9	Mm00442991_m1
Mmp13	Matrix Metallopeptidase 13	Mm00439491_m1
Tgfb1	Tumor grow factor beta 1	Mm01178820_m1
WISP1	WNT1 inducible signaling pathway protein 1	Mm00457574_m1

Table 19. Master Mix composition for qRT-PCR

Reagent	Volume per sample (µl)
Universal PCR Master Mix	10
DEPC-water	6.5
Taqman probe	1
25ng cDNA	2.5
Final volume	20

Table 20. Conditions for qRT-PCR

Stage	Temperature (°C)	Time	Repetitions
1	50	2 min	1
2	95	10 min	1
	94	15 sec	
3	60	30 sec	40
	72	35 sec	
	95	15 sec	
4	60	20 sec	1
	95	15 sec	
	60	15 sec	

PCR products were analyzed using the 7500 Real-Time PCR System software. Glyceraldehyde-3-phosphate dehydrogenase (GAPDH) expression was used as the endogenous control for each sample. The expression levels in treated mouse liver and freshly isolated cell populations were normalized to mouse control liver tissue. For calculation the comparative threshold method (ΔΔCt method) was used [60].

2.2.11 Isolation and culture of primary mouse hepatocytes and non-parenchymal cells.

Primary mouse cells were obtained from male BALB/c mice [61] using a two-step perfusion or a three-step perfusion technique [62], [63]. Animals were between 12 weeks and 9 months old depending on the cell type isolation. Prior isolation, animals were weighed and anesthetized using an intraperitoneal injection containing a mixture of sedative 2% Rompun (20 mg/kg) and anesthetic Ketamin (120 mg/kg) with a 26G cannula in a 1ml syringe. After ensuring that the animals were fully narcotized, that is all reflexes were suppressed, they were placed on an operatic stand under a heating lamp and the abdominal cavity was opened for cannulation.

2.2.11.1 Perfusion of mouse livers to isolate primary hepatocytes

To obtained primary mouse hepatocytes a two-step perfusion was performed. After opening the abdominal cavity, the exposed inferior vena cava was cannulated with a 24G cannula connected to a peristaltic pump with a rate flow of 15ml/min. Successful cannulation of the liver could be observed by an instant and even color change of the liver tissue from red-brown to beige. Afterwards, the vena cava was incised to ensure proper outflow of the buffers. All buffers used during perfusion are described in Table 4. First, the livers were perfused with the EGTA buffer warmed up to 37 °C for approximately 15 min at a rate flow of 15 mL/min to remove the blood volume and Ca^{2+} dependent adhesion factors. The perfusion was then continued with the collagenase buffer warmed up to 37 °C for approximately 15 min at a rate flow of 15 mL/min to digest collagen in the extracellular matrix. Depending on the collagenase enzymatic activity, this step lasted between 5-15 min. Following collagen digestion, the liver was excised from the animal and transferred onto a Petri dish filled with suspension buffer. The liver capsule was carefully opened under a sterile hood using a forceps to release the liver cells in the suspension buffer. The cell suspension was filtered through a 100 µm cell strainer and centrifuged for 5 min at 4°C and 50 rpm. The supernatant contained the non-parenchymal cells and the pellet contained the larger and heavier hepatocytes. The phase containing the non-parenchymal cells was transfer to a new 50ml tube for further isolation of the different cell populations. Subsequently, the remaining hepatocyte pellet was further purified by washing twice with the suspension buffer and re-centrifuged. Finally, the hepatocyte-enriched pellet was re-suspended in 10 ml suspension buffer and placed on ice until counting, plating, and/or Percoll purification. For counting, an aliquot of the cell suspension was diluted 1:5 with suspension buffer and further mixed with 0.4 % trypan blue solution at a ratio of 1:1 for cell counting in a Neubauer chamber hemocytometer. Dead cells, which stained blue were counted together with unstained living cells in all four corner squares. The average of viable cells was multiplied by $1x10^5$ to achieve the cell number per milliliter of cell suspension. The viability varied from 90-95 % with total cell yield of 5-7 x 10^6 cells per ml.

For some experiments, freshly isolated hepatocytes were further purified from the remaining non-parenchymal cells, and cell debris removed by one Percoll centrifugation step. For this purpose, Percoll™ (GH Healthcare, 1.131 g/mL) was diluted with sterile PBS to a final density of 1.063 g/mL. Next, 5 mL from the hepatocyte-enriched cell suspension was gently added on top of the diluted Percoll™ solution and centrifuged twice for 5 min at 50G at 4°C. The

resulting cell pellet was washed with 25 mL of sterile suspension buffer and centrifuged for 5 min at 50G at 4°C. The cell pellet was then resuspended in 5 mL of suspension buffer and cells were counted as previously described.

2.2.11.1.1 In vitro culture of hepatocytes

Primary hepatocytes were cultured in a collagen monolayer confluent format. To obtain a rat collagen-I stock of 250 µg/mL, 10mg of rat-tail collagen-I was dissolved in 40 mL of 0.2 % acetic acid resulting in a solution of 250 µg/mL. This stock solution was used to pre-coat tissue culture plates used for collagen monolayer cultures and allowed to dry overnight under the tissue culture bench. Shortly before plating, all pre-coated plates were washed twice with PBS. During all experiments, cells were maintained at 37 °C and 5% CO2.

The appropriate cell number was seeded in William's E medium (Table 21) with 10% Sera Plus during the first 3h of attachment. Afterwards, unattached cells were removed by washing three times with medium, and the final volume of fresh DMEM plus additives was added.

Table 21: Collagen monolayer culture specifications

Plate format	Confluent condition Amount of cells (x 10^6)	Medium (mL/well)
6-well plate	1	2
12-well plate	0.5	1
24-well plate	0.2	0.5

2.2.11.2 Isolation of endothelial and Kupffer cells from non-parenchymal cell fraction

To isolate these cell populations, the magnetic-activated cell sorting (MACS) method was used from cell suspensions from 4 mice each time to obtain an appropriated cell number. The supernatant obtained after the first centrifugation step of the liver cell suspension (5 min, 50 G at 4°C) of each mouse, was collected into a 50 ml tube and 1mL of DNAse (2 mg/ml) was added and incubated for 15 min at 37°C with gentle shaking in between. After the incubation, cell suspensions were centrifuged for 10 min at 4°C at 300 G. The supernatants were discarded and the pellets were re-suspended in 3 ml ACK buffer each and incubated for 4 minutes at room temperature. To stop the reaction, 9 ml of 1x PBS was added and a centrifugation step at 300G for 10 min at 4°C was done. The pellets obtained were combined in a 15 ml tube and re-suspended in 10 ml of MACS buffer. An aliquot of the NPC cell

suspension was mixed with 0.4 % trypan blue solution at a ratio of 1:10 for cell counting in a Neubauer chamber hemocytometer. Cells were centrifuged at 300G for 10 min at 4°C and the pellet was re-suspended in a volume of MACS buffer depending on the cell number previously obtained. For 10^7 total cells, the pellet was re-suspended in 90 µl of MACS buffer plus 10 µl CD146 (LSEC) MicroBeads (Miltenyi) and incubated for 15 min in the refrigerator (2-8°C) to first label and isolate endothelial cells. Afterwards, the cells were washed by adding 1 ml of MACS buffer and centrifuged at 300G for 10 min at 4°C. The supernatant was completely aspirated and the pellet re-suspended in 500 µl of buffer. The cells were loaded into the autoMACS Pro Separator and the program Possel was used. The purified LSECs were placed in ice until counting and the flow through was taken to label and isolate Kupffer cells. First, cell suspension was centrifuged at 300 G for 10 min at 4°C and supernatant was discarded. Next, the pellet was re-suspended in 90 µl MACS buffer plus 10 µl Anti-F4/80 MicroBeads UltraPure (Miltenyi) and incubated for 15 min in refrigerator. Same procedure was done as for LSECs with the difference that the program Posseld2 was used. Finally, an aliquot of each cell suspension was mixed with 0.4 % trypan blue solution at a ratio of 1:1 for cell counting in a Neubauer chamber hemocytometer.

2.2.11.2.1 In vitro culture of liver sinusoidal endothelial and Kupffer cells

After cell counting, cell suspensions were centrifuged at 300 G for 10 min at 4°C in order to replace the MACS buffer for the appropriated cell culture medium. Cells were maintained in DMEM medium plus additives and 10% sera plus at 37 °C and 5% CO2.

Primary sinusoidal endothelial cells were cultured in a collagen monolayer confluent format. The collagen monolayer was done the same way as for primary hepatocytes (2.2.11.1.1). For a 24-well plate format, 800.000 cells were plated. Primary Kupffer cells were cultured in a confluent format without collagen coating. For a 24-well plate, 500.000 cells were plated.

2.2.11.2 Perfusion of mouse livers to isolate stellate cells

To obtained primary hepatic stellate cells, a three-step perfusion was performed in 6-9 months old mice. After opening the abdominal cavity, the exposed inferior vena cava was cannulated with a 24G cannula connected to a peristaltic pump with a rate flow of 15ml/min through the portal vein. Afterwards, the vena cava was incised to ensure proper outflow of the buffers. All buffers used during perfusion are described in Table 4. First, the liver was

perfused with the EGTA buffer warmed up to 37 °C for approximately ca. 2 min at a rate flow of 15 mL/min to remove the blood volume and Ca^{2+} dependent adhesion factors. The perfusion was then continued with the Pronase E solution warmed up to 37 °C for approximately 4 min at a rate flow of 15 mL/min for the hydrolysis of glycoprotein peptide linkages. Next, the liver was perfused with the collagenase solution for 5 minutes to digest collagen in the extracellular matrix. Later, the liver was excised from the animal and transferred onto a Petri dish filled with cold HBSS. The liver capsule was carefully opened under a sterile hood using forceps to release the liver cells in the HBSS buffer. Thereafter, the clumps were transferred to a small bottle with 100 ml of solution D and incubated 10 min at 37°C in water bath with gentle shaking. After the last digestion step, the solution was filtered through a 100 µm mesh and everything was washed with DMEM medium into 50 ml tubes. Next, a centrifugation step at 500 G for 10 min at 4°C was done and supernatants were discarded. Each pellet was gently re-suspended in 10 ml DMEM containing 150 µl DNAse I, then DMEM was added until 50 ml and centrifuged at 500 G for 10 min at 4°C. After discarding the supernatants, the pellets were re-suspended in 10 ml DMEM containing 150 µl DNAse I in one 50 ml tube and DMEM was added up to 34 ml, 13.5 ml of the Nycodenz solution were added and all was mixed carefully. Aliquots of 11.6 ml were placed into 15 ml tubes and 1 ml of DMEM was layered on top. In this way, the Nycodenz gradient was performed by centrifugation at 1.400 G for 20 min at 4°C without a break. The resulting white layers, under the clear DMEM solution layers, corresponding to the hepatic stellate cells were collected into a 50 ml tube with a few ml of cold DMEM. To wash the Nycodenz solution away, DMEM was added and cells were centrifuged at 500 G for 10 min at 4°C. Finally, the pellet was re-suspended in 2 ml of DMEM plus additives and an aliquot was mixed with Trypan blue 0.4% in a 1:10 ratio for cell counting in the Neubauer chamber.

2.2.11.2.1 In vitro culture of hepatic stellate cells

Primary hepatic stellate cells were cultured in a confluent layout and depending on the experiment, they were cultured in different plate formats. The appropriated cell number and medium volumes are shown in table 22.

Table 22. Hepatic stellate cells plate format

Plate format	Confluent condition Amount of cells (x 10^6)	Medium (mL/well)
6-well plate	1	2
12-well plate	0.5	1
24-well plate	0.25	0.5

2.2.12 Stimulation of primary hepatocytes and non-parenchymal cell populations with TGF-β

Stimulation of primary mouse hepatocytes, LSECs, KCs and HSCs was performed for 48 h. Recombinant human TGFβ protein was reconstituted in sterile 4 mM HCl containing 0.1 % bovine serum albumin to a final concentration of 10 ng/µl. Reconstituted protein was stored in 20-50 µl aliquots at -20°C. On the day of stimulation, a stock solution (10 ng/ml) in medium plus additives was prepared. Before stimulation, cells were washed with medium or 1 x PBS three times to remove dead cells followed by per well of prepared cytokine solutions. TGF-β stimulated cells were incubated for 48 h at 37°C. Subsequently, representative images were taken from each condition and supernatants were collected.

2.2.13 Simulation of hepatic stellate cells with recombinant WISP1

Plated hepatic stellate cells were stimulated with recombinant WISP1 for 24 h. Recombinant WISP1 was reconstituted in sterile 1 x PBS to a final concentration of 100 µg/ml. Before simulation, cells were washed very carefully 3h after seeding and the medium was changed to 1% sera plus to starve the cells. After ca. 16 h of starvation, a stock solution (25 µg/ml) was prepared in medium 1% sera and was added to the cells and incubated for 24 h at 37°C. At the end of the stimulation period, representative images were taken from each condition and RNA was collected for later qRT-PCR analysis.

2.2.13 Invasion and migration assay

To study cell migration and invasion, a Trans-well assay or also called Boyden chamber assay was used. This assay was originally introduced by Boyden for the analysis of leukocyte chemotaxis [64] and it is based on a chamber of two medium-filled compartments separated by a microporous membrane [65].

2.2.14.1 Trans-well assay

Collagen solutions were prepared as described previously [66]. Briefly, Col I (BioMatrix) was neutralized to pH 7.0 on ice by adding 0.1 M NaOH and mixed with 10 x PBS to yield a stock solution containing 2mg/ml collagen in 1 x PBS. Recombinant WISP1 (Antibodies-online) was reconstituted in 1 x PBS to a final concentration of 200 µg/ml. Bovine serum albumin was also prepared to a final concentration 200 µg/ml in 1 x PBS and later sterile filtered. Next, the stock solutions were used to prepare the different conditions as shown in table 23.

Table 23. Collagen solutions specifications

Condition	Collagen (µl)	1X PBS (µl)	WISP1 (µl)	BSA (µl)
Control	-	-	-	-
Col I 1.5 mg/ml	75	25	-	-
Col I 1 mg/ml	50	50	-	-
Col I 0.5 mg/ml	25	75		-
WISP1 50 µg/ml	75	-	25	-
WISP1 25 µg/ml	75	12.5	12.5	-
WISP1 5 µg/ml	75	22.5	2.5	-
BSA 50 µg/ml	75	-	-	25

A volume of 50 µl of all collagen solutions were then layered on membranes of 24-well trans-well inserts with 8 µm pore size (Corning) and incubated at 37°C for 3 h. Collagen lattices were then washed thrice with 1 x PBS and 100.000 isolated hepatic stellate cells in serum free media were seeded per the insert. Seeded cells were incubated for 20 min at 37°C and afterwards, serum containing media was added into the well. After 72 h of incubation at 37°C, medium was removed and with a moisten cotton swab with PBS, cells from the inner side of the insert were gently removed. Next, the clean inserts were added to a new well containing a 0.5 w/v Crystal Violet in methanol/water solution for 20 minutes at RT for cell fixation and staining. Inserts were then washed thrice with tap water and dried overnight. Finally, cells that invaded to the bottom chamber were imaged and later quantified with Image J. Six images from different fields were taken for the quantification and each condition was performed in duplicates.

2.2.14.2 Collagen quantification

To quantify the amount of collagen attached to the wells in the transwell assay, the Sircol collagen assay kit (Biocolor) was used and performed as described by manufacturer's instructions.

First, collagen was prepared as described above (2.2.14.1) and added to the inserts. After 3 h incubation, inserts were washed two times with 1X PBS at RT. Afterwards, 500 µl of 0.5M cold acetic acid was added and incubated overnight at 4°C. To concentrate and to extract the collagen, samples were placed in a 1.5 ml microcentrifuge tube and 50 µl of Acid neutralizing reagent was added followed by 100 µl of cold isolation and concentration reagent. After mixing by inversion, tubes were incubated at 4°C overnight. The next day, samples were centrifuged at 12.000 rpm for 10 min at RT and the pellets of hydrated transparent collagen were visible. The supernatant was removed and any rest of fluid was carefully removed with a cotton bud. Afterwards, the pellets were re-suspended in 100 µl of 0.5 M acetic acid and 1 ml of the Syrcol Dye was added on top. Collagen standards (1, 5, 10, 15 and 30 µg) were prepared with the Reference Standard stock solution in 0.5 M acetic acid in a final volume of 100 µl. 1 ml of the Syrcol Dye was also added on top and all samples, standards and blanks (100 µl 0.5 M acetic acid) were placed in a mechanical shaker and were mixed for 30 min at RT to form the collagen-dye complex and precipitate out from the soluble unbound dye. Next, samples were centrifuged at 12.000 rpm for 10 min and supernatants were removed carefully. On top of the pellets, 750 µl of ice-cold acid salt wash were layered to remove unbound dye. Then, a centrifugation step was done as previously and supernatants were drained and any fluid was carefully removed. 250 µl of Alkali reagent were added and a vortex step of 5 min was done or until the complete solutions were without clumps. Finally, 200 µl of each sample, standards and blanks were transferred to a clear 96 well plate and absorbance was measured at 555 nm in the microplate reader Infinite M200 Pro. Concentrations of collagen in the samples were calculated according to the standard curve and manufacturer's instructions.

2.2.15 Statistics

All experiments were performed with three or more biological replicates if stated differently. In order to determine significant differences between groups an unpaired t test two sided was used. P values of <0.05 were considered statistically significant. All data are shown as mean ± standard error of the mean (SEM). The calculations were performed using GraphPad PRISM 8.

3 RESULTS

3.1 WISP1 expression in mouse isolated liver cells

The purpose of the following experiments was to find the liver cell subpopulation that is the principal responsible for WISP1 expression and secretion. For this, the different cell types from the liver were isolated.

For the present experiment, BALB/c mice were used due to their significantly higher number of HSCs when compared to C57Bl/6 mice [61]. First, the livers were perfused and RNA was isolated from freshly isolated cells, or alternatively the cells were seeded for later stimulation with TGF-β for 48 h (Figure 10 A). Purity of the freshly isolated cells was analyzed by qRT-PCR for different cell markers. CD146, a cell adhesion molecule used as a marker for endothelial cell lineage, was highly expressed in enriched endothelial and stellate cells subpopulations. ADGRE1 also known as F4/80, a marker for macrophages, was high in Kupffer cells. Furthermore, desmin, an intermediate filament protein used as a marker for quiescent and active hepatic stellate cells, was strongly expressed in isolated stellate cells (Figure 10 B). Contamination from different cell types was observed in all cell subpopulations, nonetheless, morphology of the seeded cells showed high purity (Figure 10 C).

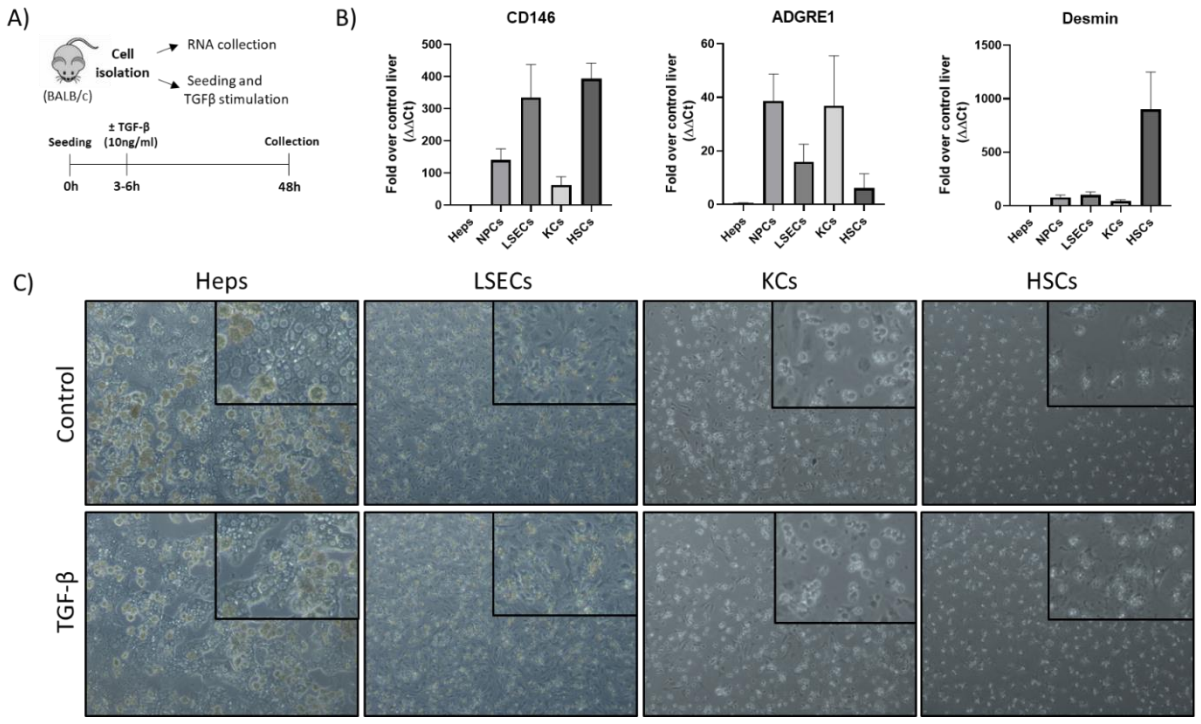

Figure 11. Liver cell populations are isolated with high purity. A) Experimental setup. B) qRT-PCR quantification of CD146, ADGRE1 and desmin. Results are plotted as log-fold increase

(ΔΔCt), compared to control liver and are presented as means ± standard errors of 3 biological replicates. C) Representative images from the isolated cell subpopulations (scale bar: 50µm). CD146: cluster of differentiation 146; ADGRE1: Adhesion G Protein-Coupled Receptor E1; Heps: hepatocytes; NPCs: Non-parenchymal cells; LSECs: liver sinusoidal endothelial cells; KCs: Kupffer cells; HSCs: hepatic stellate cells; TGF-β: Transforming growth factor beta.

In a next step, mRNA levels were quantified by qRT-PCR for WISP1 expression. WISP1 expression was higher in all non-parenchymal cells compared to hepatocytes, when compared to a control liver. Furthermore, hepatic stellate cells express significantly higher mRNA levels of WISP1 (Figure 11 A). In the same way, protein levels measured in supernatant by ELISA showed an approximately 7-fold stronger induction of WISP1 in stellate cells after stimulation for 48h with TGF-β compared to control conditions (Figure 11 B).

In conclusion, stellate cells strongly express WISP1 compared to other liver cell types. Additionally, the secretion of the protein can be further induced by the cytokine TGF-β.

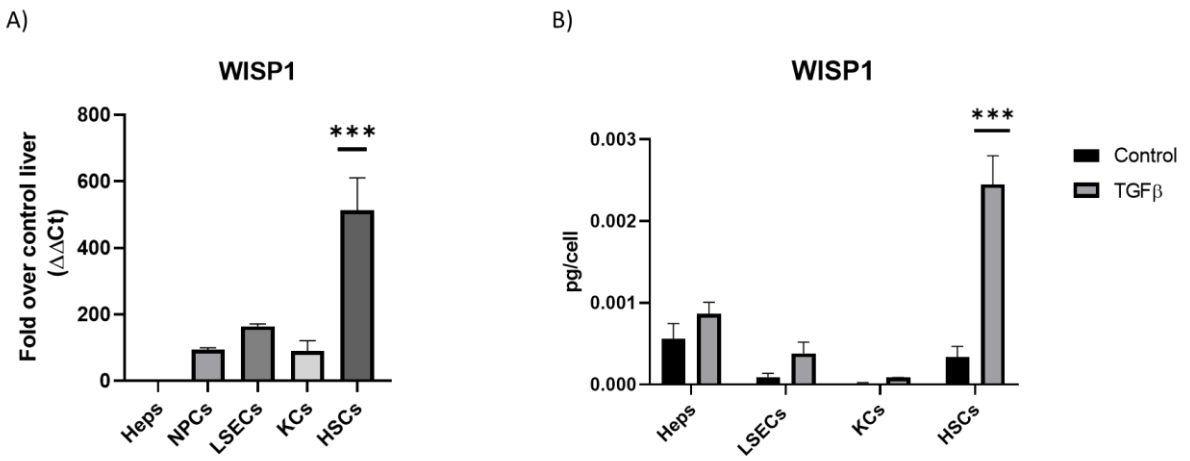

Figure 11. Hepatic stellate cells are the main cell type expressing and secreting WISP1 in liver. A) qRT-PCR quantification of WISP1 in different cell types compared to control liver. B) ELISA WISP1 protein quantification in cell supernatants normalized to cell number. Results are presented as means ± standard errors of 3 biological replicates. One and two-way ANOVA were used to calculate difference between groups. *** p <0.001. Heps: hepatocytes; NPCs: Non-parenchymal cells; LSECs: liver sinusoidal endothelial cells; KCs: Kupffer cells; HSCs: hepatic stellate cells.

3.2 Effect of WISP1 in cell migration

3.2.1. Migration of hepatic stellate cells through collagen lattices *in vitro*

The goal of the next presented experiments was to study the influence of WISP1 in the migration of hepatic stellate cells through collagen. Since stellate cells showed the greater expression and secretion of WISP1 after TGF-β stimulation, they were used to perform a transwell migration/invasion assay (Boyden chamber assay).

Cells were seeded on a filter membrane transwell insert coated with collagen I lattices formed in the absence or presence of WISP1 (50µg/ml). As a control protein, bovine serum albumin (BSA) (50µg/ml) was used. After 72 h, cells that migrated to the bottom chamber were stained with 0.5 w/v Crystal Violet, imaged and analyzed. HSCs migrated more efficiently through collagen I + WISP1 than through collagen alone or than through collagen + BSA (Figure 12). Migrating cells through collagen I + WISP1 reached similar cell number as control condition (no coating).

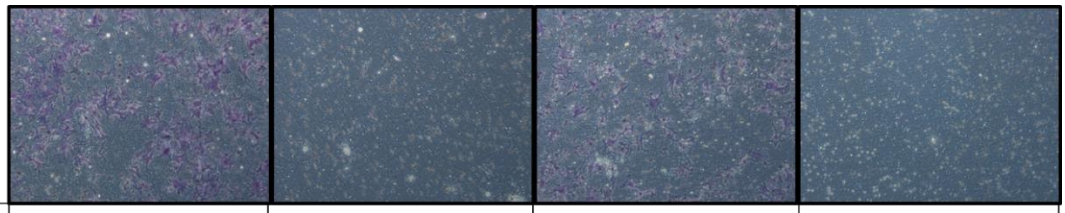

Collagen (1.5mg/ml)	-	+	+	+
WISP1 (50µg/ml)	-	-	+	-
BSA (50µg/ml)	-	-	-	+

Figure 12. WISP1 enhances HSCs migration through collagen. Hepatic stellate cells were cultured in transwell chamber plates for 72h and serum was used as a chemoattractant. Representative images of migrated cells (purple) (scale bar: 50µm). WISP1: Wnt1 inducible signaling pathway protein 1; BSA: Bovine serum albumin.

In the next step, it was determined if the addition of WISP1 affects the amount of collagen on the filter and thus, the level of cell migration. For this purpose, different collagen and WISP1 concentrations were tested and migrating cells as well as the collagen amount were quantified for each condition (Figure 13). HSCs migration increased as the collagen concentration decreased and it decreased as WISP1 concentration decreased. However, the highest concentration of WISP1 (50 µg/ml) significantly reduced the amount of collagen that attaches to the transwell insert membrane (Figure 13 D). Moreover, 25ug/ml WISP1 was

sufficient to enhance the migration of cells without significantly altering the amount of collagen. BSA control did not affect the collagen concentration nor the migration of stellate cells.

Finally, to assess if WISP1 influences hepatic stellate cell activation in vitro, the cells were stimulated with WISP1 25µg/mL for 24h and RNA was isolated to quantify mRNA levels of HSCs activation markers such as Col1a1 and α-SMA by qRT-PCR (Figure 14). No significant differences were found in the activation related markers after treatment with WISP1. TGF-β was used as a positive control of HSCs activation as reported previously [43]. Additionally, WISP1 was also quantified to address the question if WISP1 stimulation influences its own expression (Figure 14). Results showed no significant difference.

In conclusion, the experiments above gave a strong suggestion that WISP1 influences collagen structure, enhancing hepatic stellate cells migration without activating them.

3.2.2 Influence of WISP1 knockout in hepatic stellate cell migration after acute liver injury

Cultured HSCs on collagen lattices in the presence of WISP1 showed a strong evidence that WISP1 impacts cell migration perhaps by altering extracellular matrix component properties as it has been reported before [66]. To verify if WISP1 influences hepatic stellate cells migration in vivo, WISP1 knockout and wild type mice were treated with a single injection of high dose Acetaminophen (300mg/kg) and the livers were collected after different time points to analyze HSCs presence in the damaged area (Figure 15 A). Macroscopically, alteration patterns (small white spots) were observed in all time points after the APAP treatment. Paraffin embedded liver tissue sections were stained to assess pericentral necrotic lesions by H&E staining. Dead cell areas were observed in WISP1 WT and KO mice after 300mg/kg APAP administration, however, WISP1 KO mice showed less clear damage areas around the central veins after 18h. (Figure 15 B).

In the next step, paraffin embedded liver tissue sections were stained against desmin and α-SMA to detect all (quiescent and activated) and only activated hepatic stellate cells, respectively. Visual inspection of the whole slide images of every mouse from each group was done thoroughly. As expected, healthy control livers stained positive for desmin and negative for α-SMA, indicating that HSCs are quiescent (Figure 16 A). After 18 h and 24 h of APAP treatment, quiescent HSCs infiltrated into the dead cell area in both WISP1 WT and KO mice

with no clear difference between the groups. Activation of HSCs was only observed after 48 h the administration of Acetaminophen and WISP1 KO mice showed a slightly less positive staining for α-SMA, suggesting less activation.

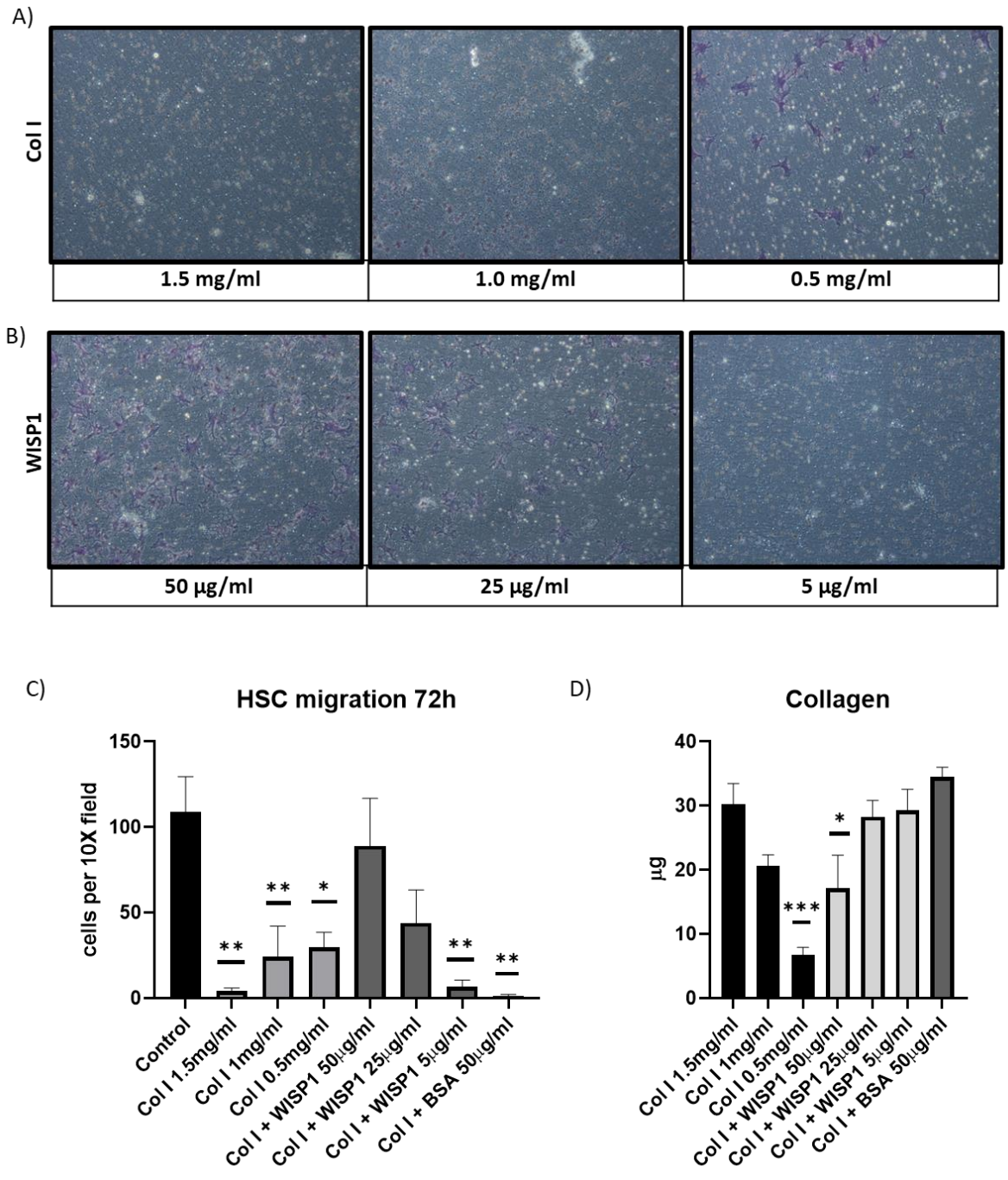

Figure 13. WISP1 influences cell migration through collagen lattices, regardless of the collagen amount. A) Representative pictures of migrated cells (purple) through collagen or B) collagen + WISP1 in different concentrations (scale bar: 50µm). C) Quantification of migrated cells after 72 h. D) Collagen quantification after formation of collagen lattices. The data are presented as means ± standard errors of 3 biological replicates. One-way ANOVA was used to calculate differences compared to control. * $p < 0.05$; ** $p < 0.01$; *** $p < 0.001$.

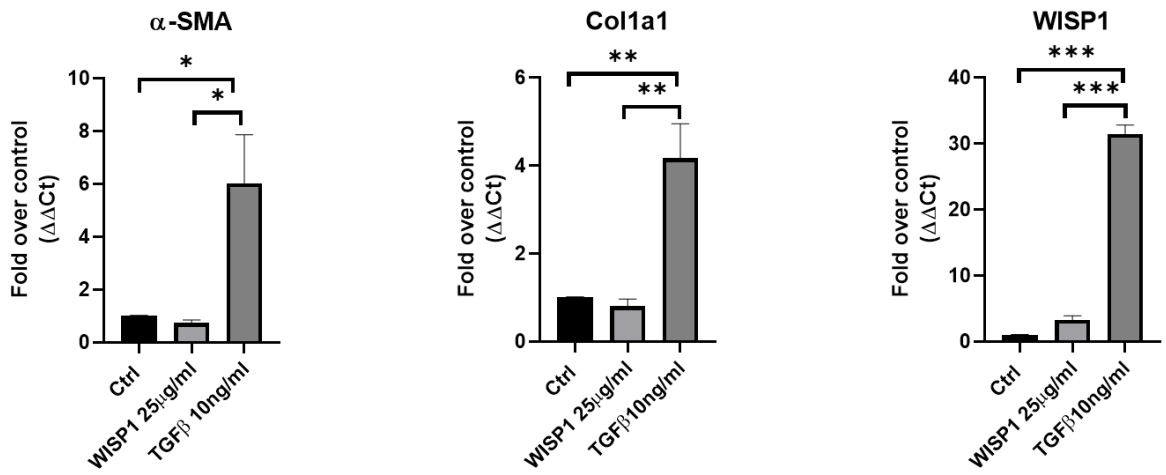

Figure 14. WISP1 does not activate hepatic stellate cells in vitro. qRT-PCR quantification of collagen type I alpha 1 (Col1a1), alpha smooth muscle actin (α-SMA) and Wnt1 inducible signaling pathway protein 1 (WISP1). Results are plotted as log-fold increase (ΔΔCt), compared to control and are presented as means ± standard errors of 3 biological replicates. One-way ANOVA was used to calculate differences between groups. * $p < 0.05$; ** $p < 0.01$; *** $p < 0.001$.

Additionally, it was analyzed if WISP1 knockout influences hepatic stellate cells proliferation and activation on the mRNA level. For that purpose, RNA isolated from homogenized liver tissue was quantified by qRT-PCR. Higher levels of desmin and α-SMA were detected at 48 h time point with no statistically significant difference observed between WISP1 WT and KO mice. However, the WISP1 KO group showed a tendency towards lower levels of hepatic stellate cell activation marker α-SMA, correlating with the result of the visual analysis of the α-SMA staining (Figure 16 B). Furthermore, WISP1 expression was analyzed and as expected, it was induced after liver injury (Figure 17).

In conclusion, there is no clear effect of the WISP1 knockout on hepatic stellate cell migration in vivo after APAP-induced acute liver injury. Nevertheless, the presented experiments gave us a hint that WISP1 may affect how hepatic stellate cells behave after liver damage.

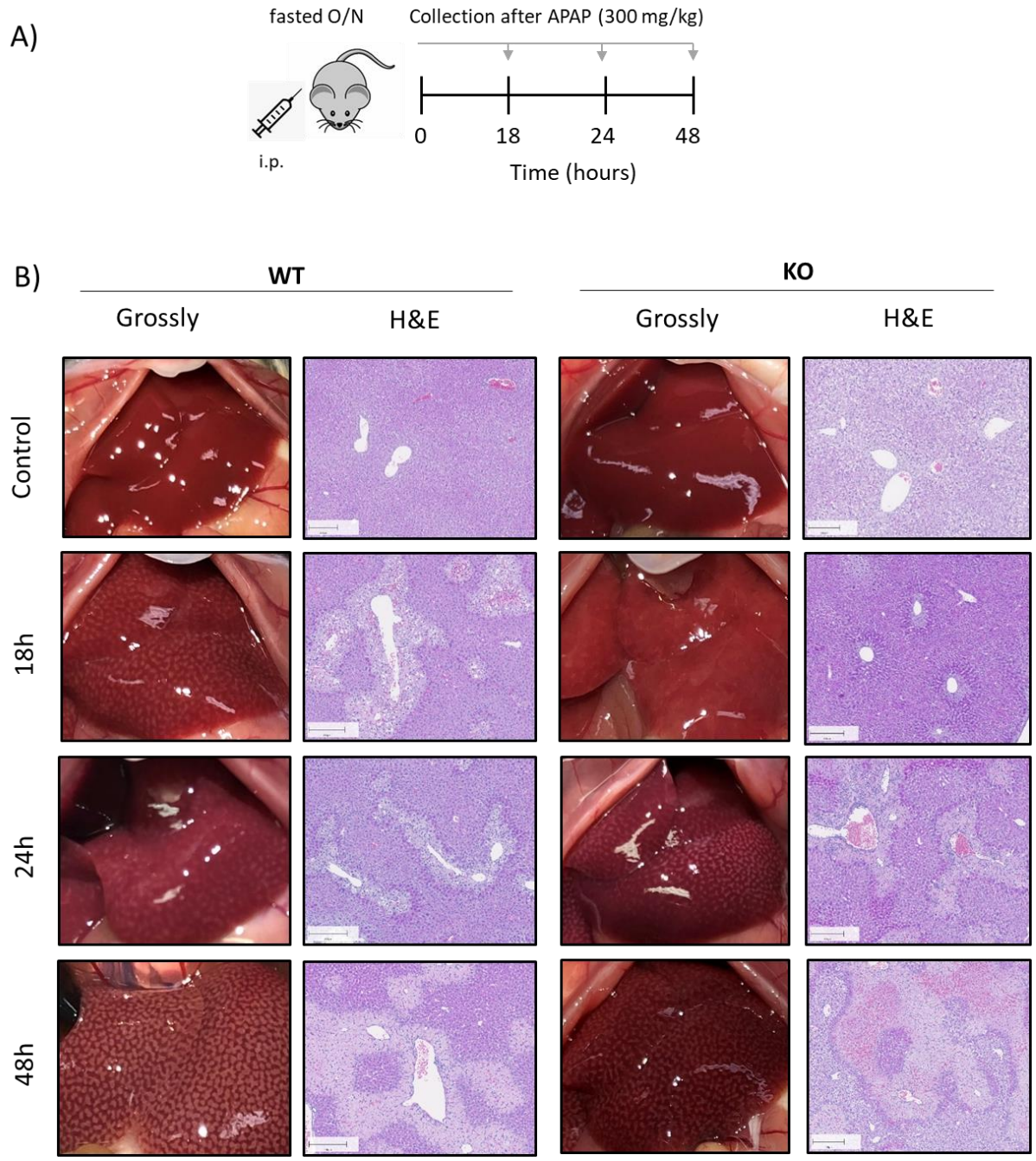

Figure 15. APAP-induced liver damage in WISP1 WT & KO mice. A) Experimental schedule. B) Representative images of gross pathology of the liver and H&E stained liver paraffin embedded tissue sections (Scale bars: 200µm). i.p.; intraperitoneal; WT: wild type; KO: knockout; APAP: Acetaminophen; O/N: overnight; H&E: hematoxylin and eosin staining.

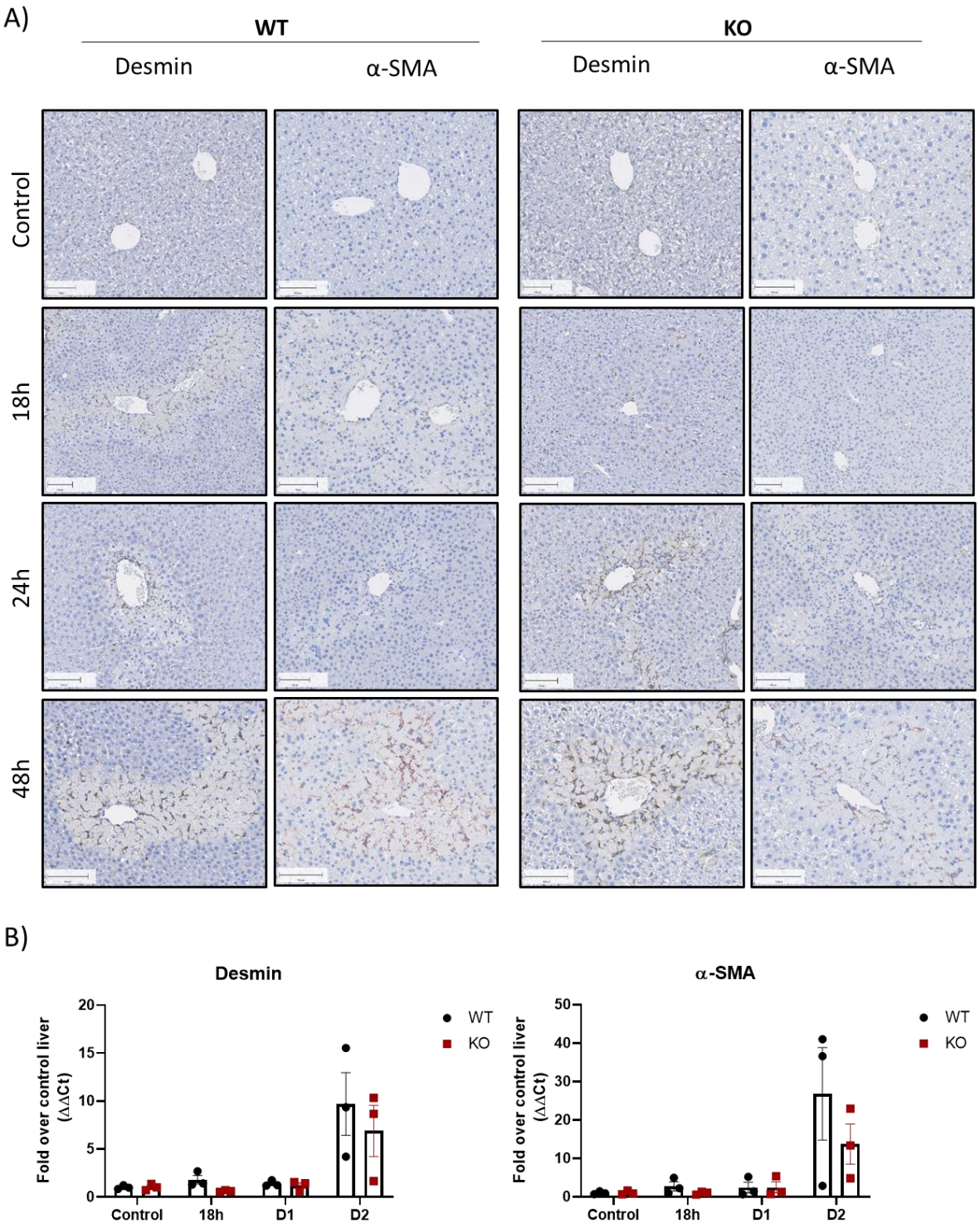

Figure 16. WISP1KO does not influence hepatic stellate cell migration *in vivo* after APAP-induced liver injury. A) Representative images of desmin and α-SMA stained liver paraffin embedded tissue sections (Scale bars: 100 µm). B) qRT-PCR quantification of desmin and alpha smooth muscle actin (α-SMA). Results are plotted as log-fold increase (ΔΔCt), compared to control liver and are presented as means ± standard errors of 3 mice per group. The multiple t-test was used to calculate differences between groups. WT: wild type; KO: knockout; D1: day one; D2: day two.

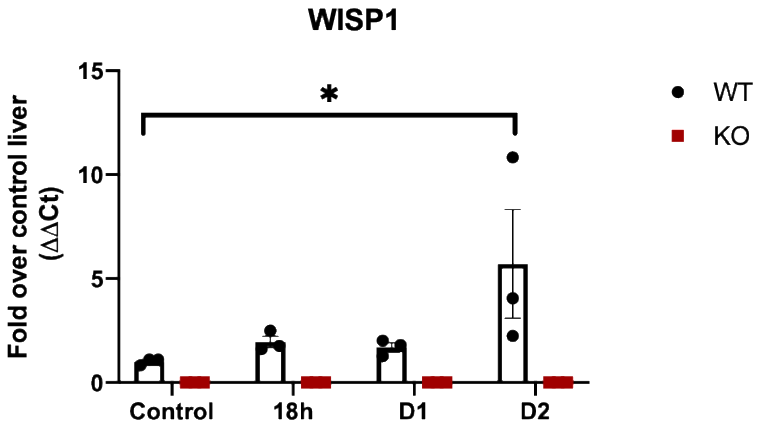

Figure 17. WISP1 is induced after acute liver injury. qRT-PCR quantification of WISP1. Results are plotted as log-fold increase (ΔΔCt), compared to control liver and are presented as means ± standard errors of 3 mice per group. Two-way ANOVA was used to calculate differences between groups. * p <0.05; WT: wild type; KO: knockout; D1: day one; D2: day two.

3.3 Influence of WISP1 knockout on liver fibrosis in chronic CCl_4 mouse models

The aim of the following experiments was to analyze if the constitutive knockout of WISP1 alters the extent of fibrosis in a mouse model where hepatotoxic doses of CCl_4 were administrated twice a week for different time periods.

In a first set of experiments, CCl_4 was administrated over two months (Figure 18 A). Macroscopically fibrotic alterations were seen after the end of the exposure period in both WT and KO mice (Figure 18 B). Sirius red staining was performed to visualize collagen deposition (Figure 19). As expected, the formation of fibrotic streets was observed in the CCl_4 treated livers, while the control livers showed collagen deposition only in large blood vessels. Furthermore, thorough visual inspection of the whole slide images of every mouse from each group, suggests a lower degree of collagen depositions and a reduced branching of fibrotic streets in the WISP1 KO mice. Moreover, the typical pericentral fibrosis induced by CCl_4 [67] was clearly observed in both groups. However, the clear central-to-central bridging of the fibrotic streets observed in the wild type mice was reduced in the WISP1 knockout mice, as shown in Figure 19.

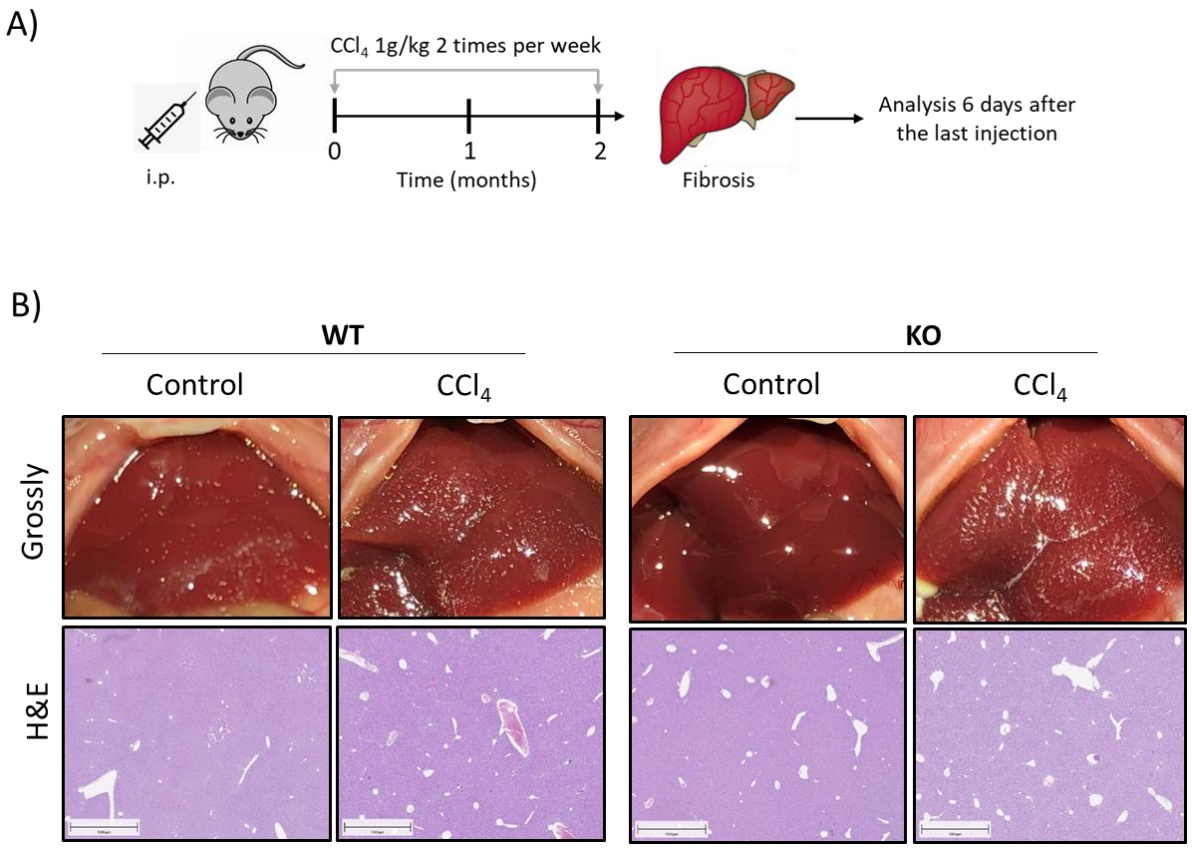

Figure 18. Histological analysis of WISP1 knockout and wild type mice after two month-CCl_4 induced liver fibrosis. A) Experimental schedule. B) Representative images of gross pathology of the liver, as well as H&E stained liver paraffin embedded tissue sections (Scale bars: 1000 µm). i.p.; intraperitoneal; WT: wild type; KO: knockout; CCl_4: Carbon tetrachloride; H&E: hematoxylin and eosin staining.

As a measure of hepatocyte death, the liver enzymes alanine aminotransaminase (ALT), aspartate transaminase (AST) and alkaline phosphatase (ALP) were quantified in plasma obtained from the right heart chamber at day 6 after the last injection (Figure 20). At this time a CCl_4 induced increase in liver enzymes was no longer detected.

In a next step it was analyzed if fibrosis associated mRNA species were altered by the WISP1 knockout at the end of the CCl_4 exposure period. For this purpose, RNA isolated from homogenized liver tissue was quantified by qRT-PCR. Knockout of WISP1 led to significantly lower levels of Col1a1, α-SMA, Fn1 and Tgfb1. In contrast, the matrix metalloproteinase Mmp13, which is known to remove collagen deposits, was significantly increased in the WISP1 knockout mice. A further matrix metalloproteinase Mmp9, showed no significant difference (Figure 21). The expression of these fibrosis markers, especially Col1a1, correlate well with the results observed by the Sirius red staining for collagen depositions (Figure 19).

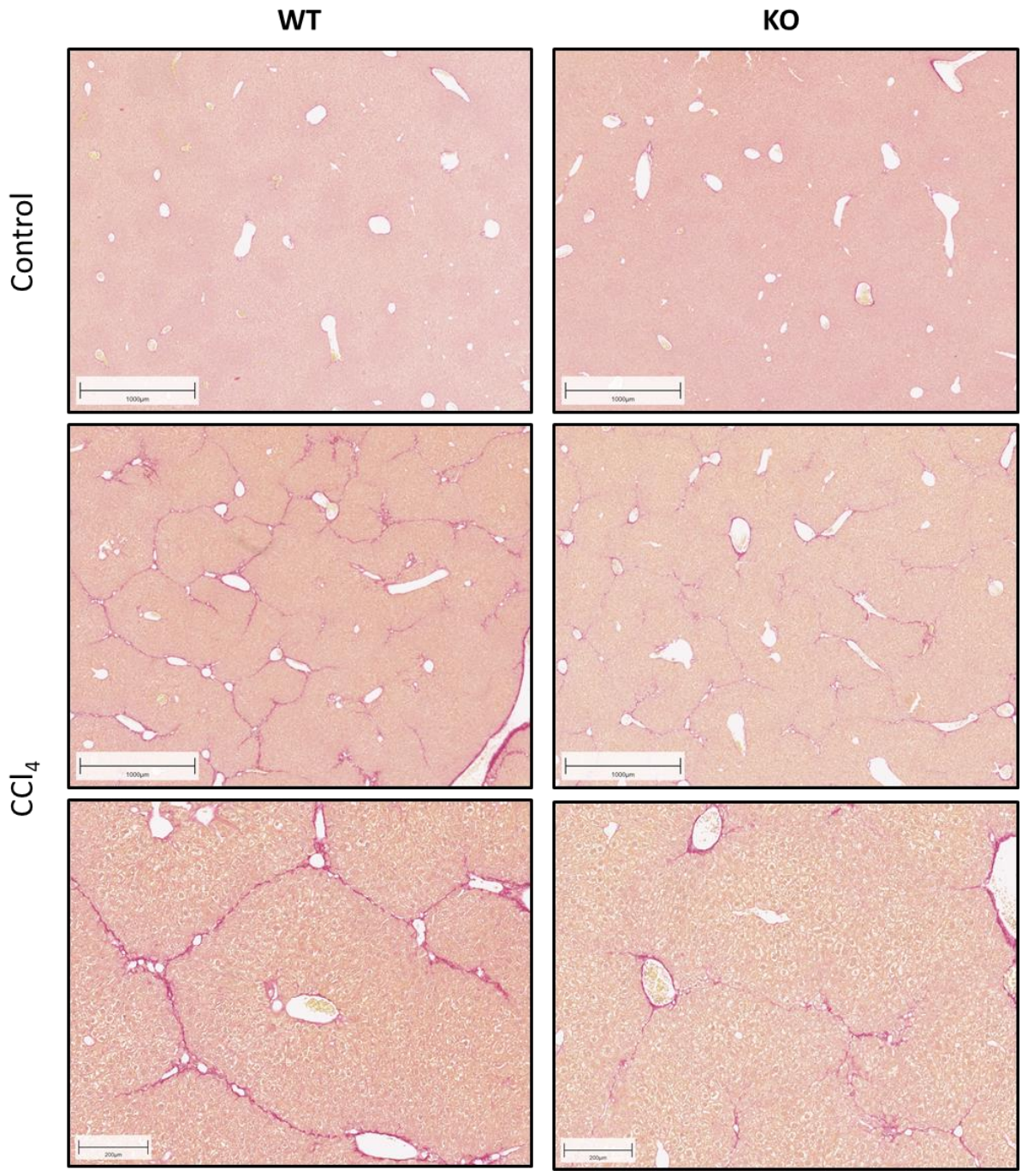

Figure 19. WISP1 KO ameliorates the degree of two month-CCl_4 induced liver fibrosis. Visualization of fibrosis by Sirius red staining. Representative images of whole slides from stained liver paraffin embedded tissue sections from at least 3 mice per group. Scale bars: 1000 µm and 200 µm. WT: wild type; KO: knockout; CCl_4: Carbon tetrachloride.

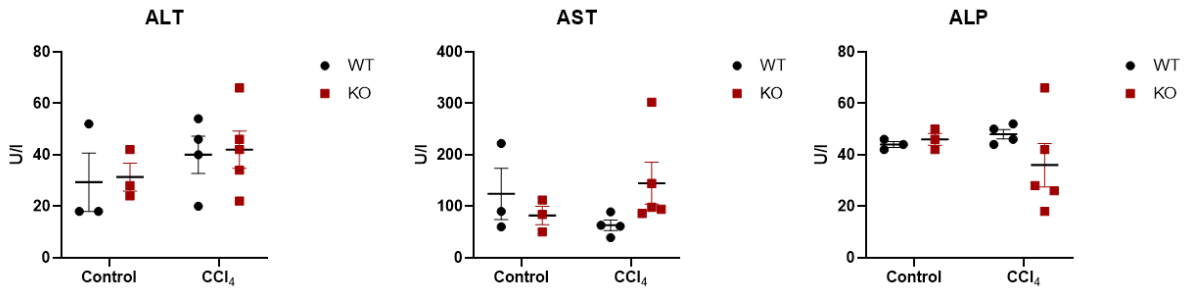

Figure 20. WISP1 KO does not decrees liver damage in liver fibrosis. Concentrations of liver enzymes in the blood plasma as units per liter. The data are presented as means ± standard errors of at least 3 mice per group. Multiple t-test was used to calculate difference between groups. ALT: alanine transaminase; AST: aspartate transaminase; ALP: alkaline phosphatase.

To analyze if chronic CCl_4 exposure influences WISP1 expression in liver tissue, RNA levels were quantified by qRT-PCR. No significant influence of CCl_4 exposure was obtained (Figure 22 A). Similarly, the protein levels measured by ELISA in liver homogenates remained unaltered (Figure. 22 B).

Finally, the question was addressed if chronic CCl_4 administration alters the levels of WISP1 secreted by the liver. For this purpose, WISP1 concentrations were quantified in plasma taken from the portal vein (the "inflow" of the liver), the hepatic vein (the "outflow" of the liver) and heart blood (Figure 22 C). No significance differences were observed.

In conclusion, the present experiments gave strong evidence that the knockout of WISP1 ameliorates the degree of fibrosis induced by repeated doses of CCl_4 over two months.

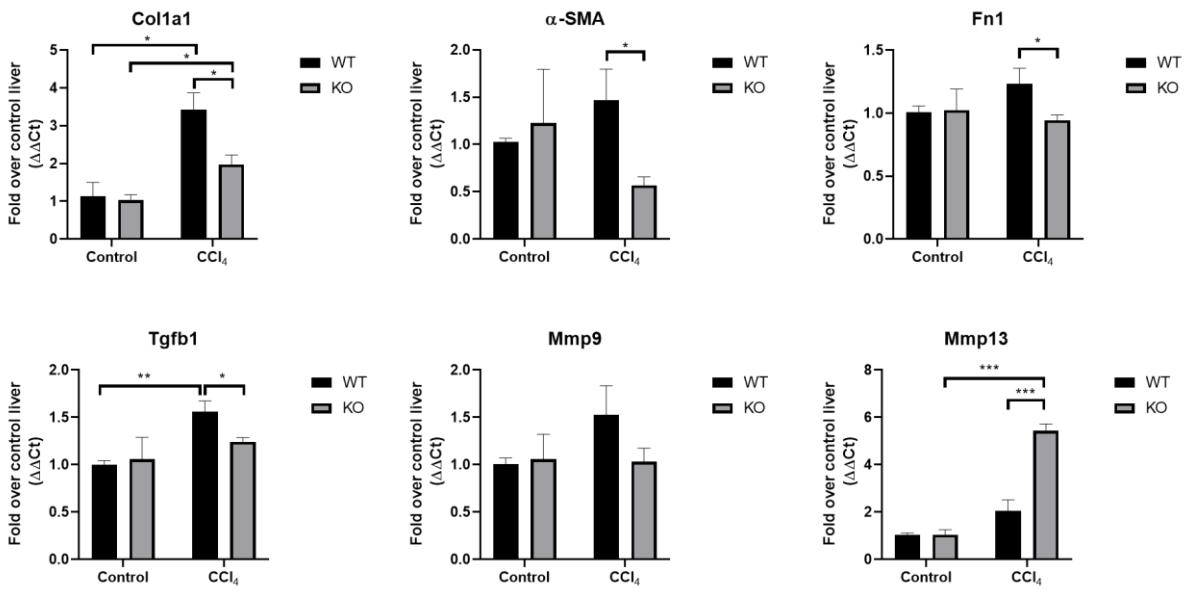

Figure 21. WISP1 KO attenuates the upregulation of fibrosis related genes. qRT-PCR quantification of collagen type I alpha 1 (Col1a1), alpha smooth muscle actin (α-SMA), fibronectin 1 (Fn1), transforming growth factor beta 1 (Tgfb1), matrix metalloproteinase 9 (Mmp9) and matrix metalloproteinase 13 (Mmp13). Results are plotted as log-fold increase (ΔΔCt), compared to control liver and are presented as means ± standard errors of at least 3 mice per group. Multiple t-test was used to calculate differences between groups. * p <0.05; ** p <0.01; *** p <0.001.

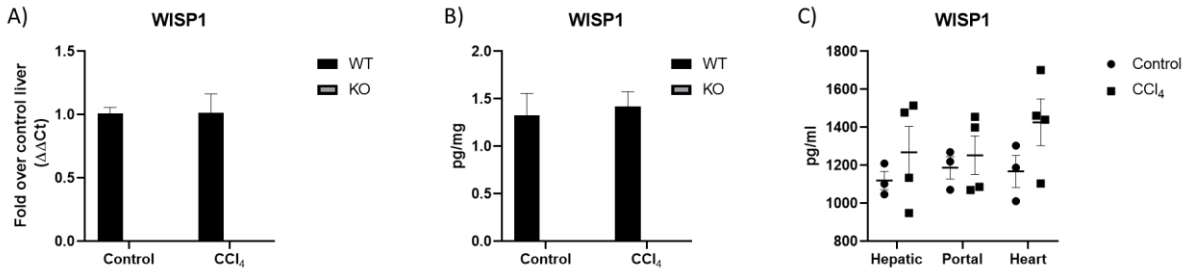

Figure 22. Repeated doses of CCl_4 do not alter WISP1 expression. A) qRT-PCR quantification of WISP1 mRNA from control and treated liver tissues. B) Protein quantification of WISP1 by ELISA in homogenized liver tissue and in plasma C) from hepatic vein, portal vein and heart blood. The data are presented as means ± standard errors of at least 3 mice per group. Multiple t-test was used to calculate differences between groups.

In a second set of experiments, CCl_4 was administrated over nine months (Figure 23 A). As for the two months experiment, macroscopically fibrotic alterations were seen after the end of the exposure period in both WT and KO mice (Figure 23 B). The same analyses were conducted to determine if the phenotype observed in the WISP1 KO mice remains after a longer exposure to the hepatotoxicant. Sirius red staining showed the formation of fibrotic streets in the CCl_4 treated livers, while control livers showed collagen deposition only in large blood vessels. Similarly to the two-month exposure period to CCl_4, the visual analysis of the positive Sirius red area suggests lower degree of the branching of fibrotic streets in the WISP1 KO mice (Figure 24). However, nine-month treated wild type mice showed a loss of central-to central-bridging of the fibrotic streets observed in the two-month treated wild type mice. Instead, WT mice showed a widespread Sirius red positive fibrotic street signal. Remarkably, WISP1 KO mice showed the pericentral CCl_4-induced liver fibrosis and reduced bridging of the fibrotic streets, as for the two-month period.

Liver enzymes, AST and ALT, showed no significant increase after 6 days of the last CCl_4 injection. However, alkaline phosphatase, an enzyme also involved in bone processes,

showed higher values for WISP1 KO mice after CCl_4 exposure compared to WT mice (Figure 25).

Next, it was analyzed if fibrosis associated mRNA species were altered by the WISP1 knockout at the end of the longer CCl_4 exposure period (Figure 26). qRT-PCR analysis revealed significantly lower levels of Tgfb1 in WISP1 KO treated mice compared to WT. Additionally, Col1a1 only shows a significant increase in the WT mice after CCl_4 treatment, which correlates with the increased collagen deposition observed in wild type mice by Sirius red staining (Figure 24). In contrast, the matrix metalloproteinase Mmp9 and Mmp13 were significantly increased in the WISP1 knockout mice. Finally, α-SMA showed no significant difference.

In conclusion, the present experiments gave strong evidence that the knockout of WISP1 ameliorates the degree of fibrosis induced by repeated doses of CCl_4, also over the longer exposure time period. Some differences at the mRNA level were observed, however, the main phenotype of WISP1 knockout on fibrotic branches remains.

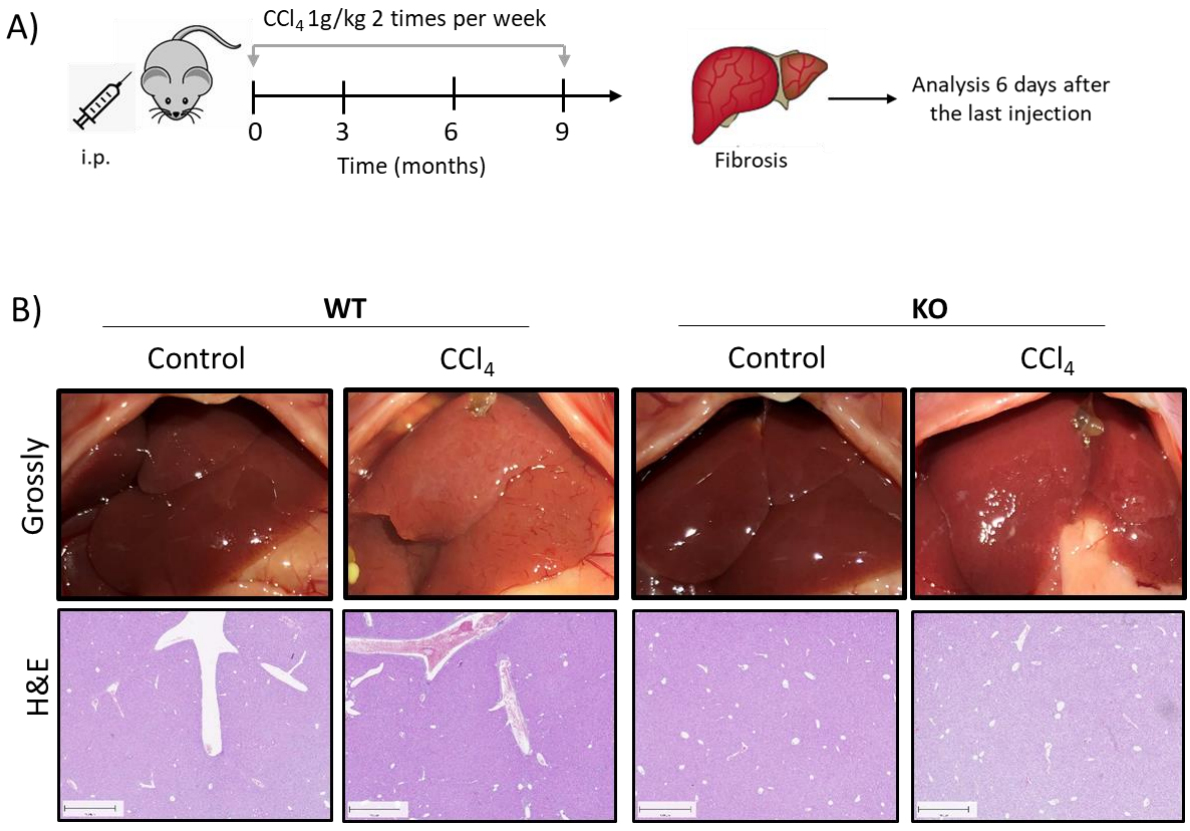

Figure 23. Histological analysis of WISP1 knockout and wild type mice after two month-CCl_4 induced liver fibrosis. A) Experimental schedule. B) Representative images of gross pathology of the liver, as well as H&E stained liver paraffin embedded tissue sections (Scale bars: 1000µm). i.p.; intraperitoneal; WT: wild type; KO: knockout; CCl_4: Carbon tetrachloride; H&E: hematoxylin and eosin staining.

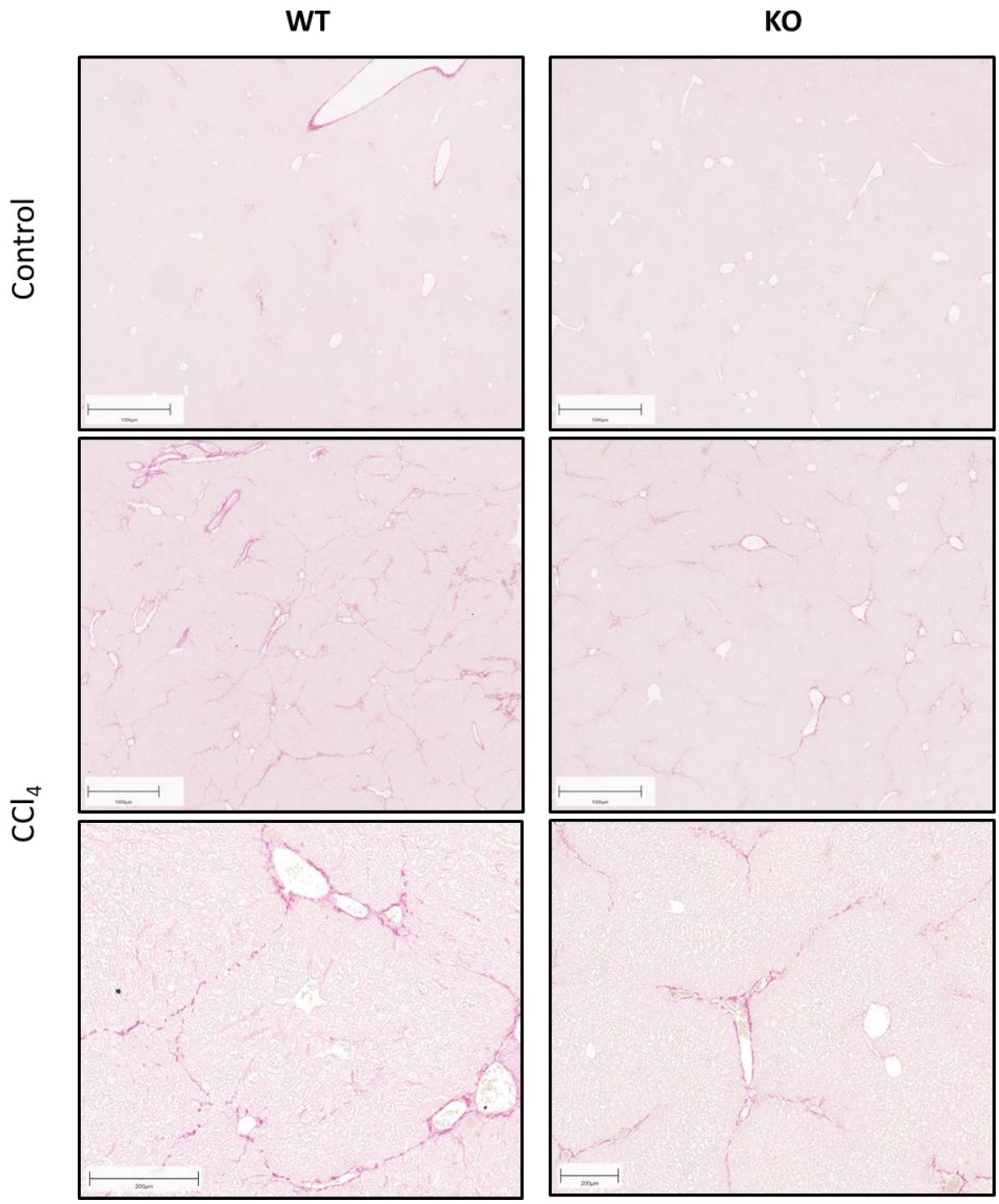

Figure 24. WISP1 knockout ameliorates the degree of nine month-CCl_4 induced liver fibrosis. Visualization of fibrosis by Sirius Red staining. Representative images of whole slides from stained liver paraffin embedded tissue sections from at least 3 mice per group. Scale bars: 1000 µm and 200 µm. WT: wild type; KO: knockout; CCl_4: Carbon tetrachloride.

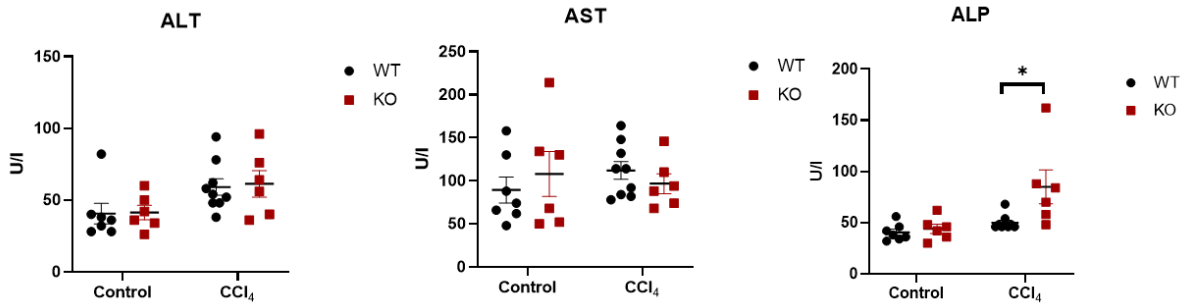

Figure 25. WISP1 KO does not decrease liver damage in liver fibrosis. Concentrations of liver enzymes in the blood plasma as units per liter. The data are presented as means ± standard errors of at least 3 mice per group. Multiple t-test was used to calculate difference between groups. ALT: alanine transaminase; AST: aspartate transaminase; ALP: alkaline phosphatase.

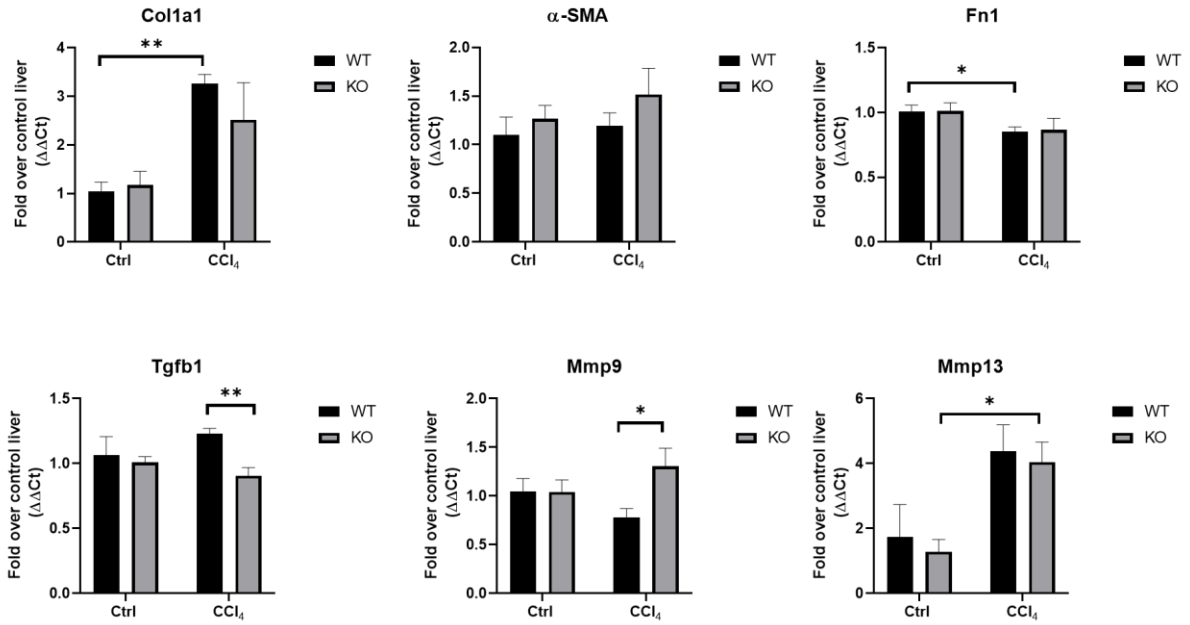

Figure 26. WISP1 KO attenuates the upregulation of fibrosis related genes. qRT-PCR quantification of collagen type I alpha 1 (Col1a1), alpha smooth muscle actin (α-SMA), fibronectin 1 (Fn1), transforming growth factor beta 1 (Tgfb1), matrix metalloproteinase 9 (Mmp9) and matrix metalloproteinase 13 (Mmp13). Results are plotted as log-fold increase (ΔΔCt), compared to control liver and are presented as means ± standard errors of at least 3 mice per group. Multiple t-test was used to calculate differences between groups. * p <0.05; ** p <0.01; *** p <0.001.

4 DISCUSSION

The principal findings of this thesis relate to the significance of WISP1 in liver, regarding expression and influence in cellular processes and disease models. The results demonstrate that **(1)** WISP1 is manly expressed and secreted by hepatic stellate cells and **(2)** helps them migrate through collagen lattices via changes in collagen properties and **(3)** can influence the development of chronic liver diseases such as fibrosis.

4.1 Expression of WISP1 in liver: parenchymal cells are not the main source of WISP1

Previously in our group, differentially expressed genes in mouse liver tissue after acute CCl_4 intoxication were determined after gene array analysis [68], [69]. One of the most upregulated genes among the CCN family members was Wnt-induced secreted protein-1 (WISP1). Furthermore, in Larissa Pütter's dissertation WISP1 expression upon CCl_4 administration was validated by qRT-PCR in a time- dependent manner confirming a strong induction of WISP1 within the early injury phase (2h up to D1) in C57Bl/6N mice. While performing qRT-PCR analysis of two different isolated cell populations from liver tissue, it was observed that the NPC fraction showed the highest WISP1 expression in control condition, whereas upon CCl_4 administration, the induction of WISP1 was stronger in hepatocytes [70]. Nevertheless, it was important to determine which cell type expresses and secrets WISP1 in the liver to understand its function and its relevance upon injury. The isolation of hepatic cells was the technique to use due to the unsuccessful liver tissue staining against WISP1 and an ineffective WISP1 reporter mouse.

Because WISP1 induction was stronger in hepatocytes after liver injury and because they are the structural and functional unit of the liver comprising the 80% of the liver cell mass, it was expected that WISP1 would be also efficiently secreted by the parenchymal cells. However, it has been well reported that CCN proteins are expressed in fibroblast [25], [71], therefore it was not surprising that hepatic stellate cells are 2.5 times more effective to secret WISP1 protein upon TGF-β stimulation, compared to hepatocytes.

WISP1 protein has been reported to be present in multiple sites throughout the body and it is expressed in different organs like the heart, lung, kidney, intestine and brain among others, and linked to processes such as cell death, extracellular matrix production, cellular migration and proliferation as the other members of the CCN family [32]. However, there are only few publications connecting WISP1 to liver injury until now [72], and they are mainly related to

chronic liver diseases and hepatocellular carcinoma [73]–[76]. Furthermore, the function of WISP1 in the liver has not yet been established, but it seems to be promoting and mediating hepatic diseases via TLR4 signaling [72], [74]. Nonetheless, it has not been related to any specific cell type until now.

4.2 Migration of hepatic stellate cells and collagen upon liver injury.

It has been previously reported that WISP1 is associated with cell adhesion and migration, mostly in fibroblasts [77]. Moreover, I found that hepatic stellate cells migrate more efficiently in the presence of WISP1 when seeded on collagen type I. Collagen coated inserts inhibit the migration of hepatic stellate cells and the presence of bovine serum albumin does not influence the result. In contrast, the presence of WISP1 can enhance the migration of the cells, not only at the highest concentration when the collagen concentration decreases, but also at 25 µg/ml when the collagen concentration is not significantly different from the control collagen condition. Moreover, when hepatic stellate cells were stimulated with WISP1 at the concentration of 25 µg/ml, no activation was detected when analyzing stellate cell activation markers via qRT-PCR, at least not after 24h of stimulation. Here, we can point out three important discoveries: (1) WISP1 can induce HSCs migration by (2) influencing collagen type I architecture and the process of fibrillogenesis as reported previously [66] and corroborated during this study (data not shown); (3) without activating them to myofibroblasts.

In the next step, it was important to support the *in vitro* data presented above by studying the migration of hepatic stellate cells *in vivo*. In that regard, the expected result was to observe a delayed or impaired migration of stellate cells to the damaged area in the WISP1 KO mice. For that purpose, I used APAP-induced liver injury mouse model in WISP1 KO and WT mice. After the single injection of high dose of APAP, I analyzed the migration of HSCs to the damaged area after different time points. It was described before [78] that HSCs migrate to the damaged area 24 h after acetaminophen exposure. Here, I included 18 h time point to observe the earlier stage of migration of the cells to the wound. However, WISP1 KO mice did not present a clear damage compared to the WT counterparts after 18 h of APAP injection (H&E staining, Figure 15 B). The cause may be due to a problem with the injection or the metabolization of the drug from the mice themselves. Nevertheless, after 24 h of the APAP challenge, all mice showed pericentral damage and the cells migrated into the dead cell area

and no clear differences were observed between WT and KO mice. The activation of HSCs was observed after 48 h in both groups (α-SMA staining, Figure 16) with no clear differences between them. However, the mRNA analysis showed a slight tendency of lower levels of desmin and α-SMA in the WISP1 KO mice, suggesting a possible influence of WISP1 in the activation of HSCs in vivo after acute induced-liver injury. The unclear *in vivo* results could be clarified with a larger cohort of mice, since only 3 mice per group were analyzed, and with an automated image analysis for quantification of infiltrating HSCs to the damage area. *In vivo* supporting data would give a stronger understanding of the *in vitro* evidence of WISP1 influencing collagen architecture and consequently cell migration.

Cell migration is essential in a variety of biological events such as regeneration and wound healing. Migration of hepatic stellate cells serves an important role in hepatic fibrosis, including ECM and growth factor production [79], [80]. In general, it has been well reported that activated HSCs migrate to fibrotic regions by transforming into myofibroblasts-like cells. In contrast, migration in early activation *in vivo* has not yet been well described. Here I showed that after 18 h of APAP administration HSC migrate to the dead cell area and only after 48 h they stained positive for alpha-SMA, displaying the activated phenotype. It seems that genes and signaling pathways involving migration are activated at early time points [81]. Activation of HSCs has been extensively studied and their significance in liver fibrosis reported [14], [82]. The activation refers to the transformation of quiescent, vitamin A-storing cells into proliferative, fibrogenic, and contractile myofibroblasts. Early events have been termed as “initiation” (or “preinflammatory”) which comprehends rapid changes in gene expression and phenotype that render the cells responsive to cytokines and other local stimuli. This process is associated with rapid gene induction resulting from paracrine stimulation by inflammatory cells and injured hepatocytes or bile duct cells, and from early changes in ECM composition. The cellular responses following the initiation have been named “perpetuation”, which involve those cellular events that amplify the activated phenotype through enhanced growth factor expression and responsiveness (Figure 27) [15].

In these processes, transforming growth factor-β plays an important role. TGF-β is generally considered as the most potent fibrogenic cytokine and is released by several cell populations in the liver. The binding of TGF-β and the phosphorylation of the type I receptor induces phosphorylation of downstream SMAD proteins, principally SMAD3. Activation of SMAD3 during HSC activation promotes transcription of type I and III collagen [14], [46]. Additionally,

as I showed previously, TGF-β induces WISP1 expression and secretion in HSCs (Figure 11). WISP1 could potentially be one of the genes in the initiation phase and in the later part of the perpetuation phase, remodeling the ECM in the fibrogenesis process where these fibril-forming type I and III collagens are abundant in fibrotic liver. Furthermore, HSCs express two types of collagen receptors, integrins and discoidin domain-containing receptors (DDRs). Each type receives signals from ECM components to regulate cell adhesion, differentiation, proliferation and migration [83], [84].

Integrins containing αv (αvβ1, αvβ3, αvβ5 and αvβ8) are expressed in HSCs and their depletion protects mice from CCl_4-induced liver fibrosis [14][83]. It has been reported as well that WISP1 interacts with integrins [85] [86] and therefore activates adhesion and migration pathways.

In conclusion, the data suggests WISP1 as an important matricellular TGF-β-induced protein that is able to bind collagen directly or via integrins and influence the ECM remodeling and cell migration upon liver injury.

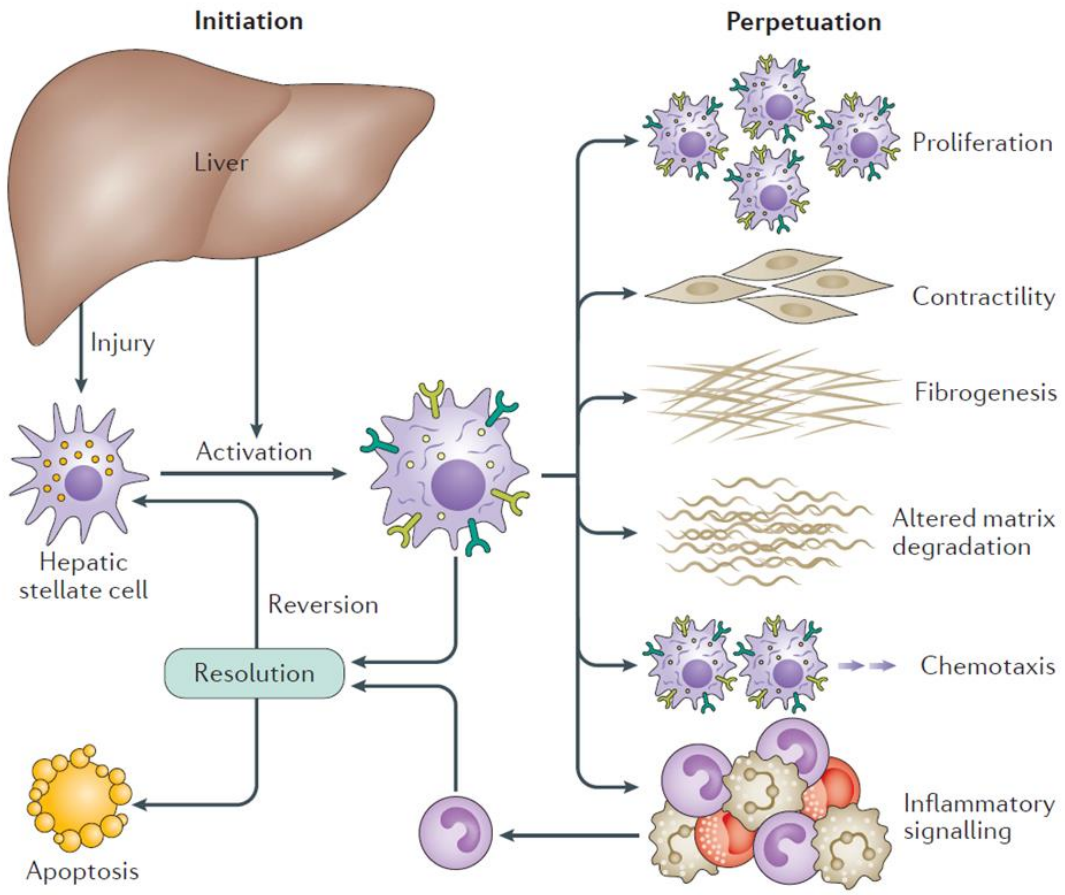

Figure 27. Roles, features and phenotypes of HSCs in normal and diseased livers. Stellate cells activate in response to liver injury in a two-stage process: Initiation and perpetuation. During resolution of hepatic fibrosis, activated HSCs can be cleared by apoptosis or reversion to an inactivated phenotype. [14]

4.3 WISP1: Regulator of signaling pathways or downstream effector to remodel extracellular matrix in liver diseases.

WISP1 was one of the differentially expressed genes in the Wnt-1-expressing mouse mammary epithelial cell line C57MG and it demonstrated oncogenic activities, inducing morphological transformation and accelerated cell growth when it was overexpressed in rat kidney fibroblast cells [30]. Since then, its expression has been linked to clinical significance in human cancers. In colorectal cancer, WISP1 appeared to act as a factor stimulating aggressiveness, however, it seemed to act as a tumor suppressor in breast cancer [31]. The contrasting roles of WISP1 in these two types of cancer hinted that its role may be tissue specific. In liver, the expression of WISP1 was higher in hepatocellular carcinoma (HCC) than in matched normal tissues. Additionally, HCC patients with WISP1 SNPs are associated with HCC development [75] and the inhibition of WISP1 expression can reduce the proliferation, migration and adhesion of mouse hepatocellular carcinoma cells [87].

Although WISP1 itself is a downstream target gene of Wnt/β-catenin signaling pathway, it also plays an essential role in regulating the complicated network composed of various signaling transduction pathways and it is associated with the progression of different biological processes in diverse tumor types such us angiogenesis, migration and motility [31].

WISP1 is highly expressed in many fibrosis diseases, such as liver fibrosis and idiopathic pulmonary fibrosis (IPF) [31]. However, here I showed that WISP1 expression in the liver is not altered by repeated doses of CCl_4 over two months, neither in mRNA nor in protein levels. Similarly, the secreted protein was not induced when quantified in blood plasma. This can be explained with the time point of collection after the last CCl_4 injection, which was six days, where the acute effect of the hepatotoxicant is resolved. These findings support that the induction of WISP1 expression happens at early time points after injury, as shown previously [70] and it is not maintained over time. Nevertheless, the knockout of WISP1 in a liver fibrosis model over two or nine months ameliorated the degree of the disease. The standard and robust technic for the analysis of fibrosis, Sirius Red staining [59], [88], showed reduced collagen depositions and bridging of the fibrotic streets in WISP1 KO mice, suggesting a lower degree of fibrosis. However, to confirm the observation made by visual inspection, automated image analysis and quantification should be performed in order to confirm these results. Furthermore, the upregulation of Col1a1, α-SMA, Fn1 and TGF-β was reduced in WISP1 KO

mice after the two-month period and interestingly, Mmp13, the interstitial collagenase of rodents, was strongly upregulated in these mice. Mmp13 has been reported to exhibit a beneficial function for the resolution of stable liver fibrosis but also complete the opposite at the onset of cholestasis-induced fibrosis [89].

Moreover, at the end of the nine-month period of repeated CCl_4 doses, only Col1a1 and Tgfb1 showed similar expression pattern compared to the two-month period. In contrast, Fn1 was downregulated in WT mice and the metalloproteinases Mmp9 and Mmp13 were upregulated in the KO mice. Relation between metralloproteinases expression and CCN proteins has been described, however in human chondrosarcoma CCN proteins induce MMP expression and they seem to enhance migration through integrin receptor, ERK and NF-κβ signaling pathways [90], [91].

Remarkably, the longer exposure to the insult did not increase the differences observed between WT and KO. The different progression may be due to stronger changes that occur after a longer exposure to the hepatotoxicant such as the disruption of liver zonation [67], which additionally explains the differences observed in the collagen depositions in WT mice after the nine-month exposure compared to the two-month CCl_4 exposure period.

Strangely, the location of WISP1 protein in the liver has not been determined and hence a possible zonation pattern is unknown. So far, the attempts done during my thesis to fulfil that purpose have failed, such as the use of a WISP1 reporter mice and liver tissue staining against WISP1. However, zonation of hepatic stellate cells, its major cell source, has been reported and recently different subsets of HSCs and myofibroblasts in liver fibrosis by single cell RNA sequencing have been identified [92].

Interestingly, a model of skin damage showed that WISP1 KO delays the wound closure accompanied by reduced expression of Col1a1 and Fn mRNA. Additionally, WISP1 induces migration of dermal fibroblasts and inhibits TNF-α-induced upregulation of two metalloproteinases (Mmp1 and Mmp3) in human dermal fibroblasts [85].

Taken together, the data suggests that WISP1 is expressed and secreted after acute injury to help the process of healing through cell migration of hepatic stellate cells. Genetic deletion of WISP1 may lead to a higher sensitivity to damage [70]. However, when the damage turns into chronic in a wild type situation, the migration of stellate cells and collagen deposition becomes excessive and therefore, blocking of WISP1 could help to reduce and ameliorates the degree of the fibrotic state, decreasing the migration of the cells that can produce extracellular matrix (Figure 28).

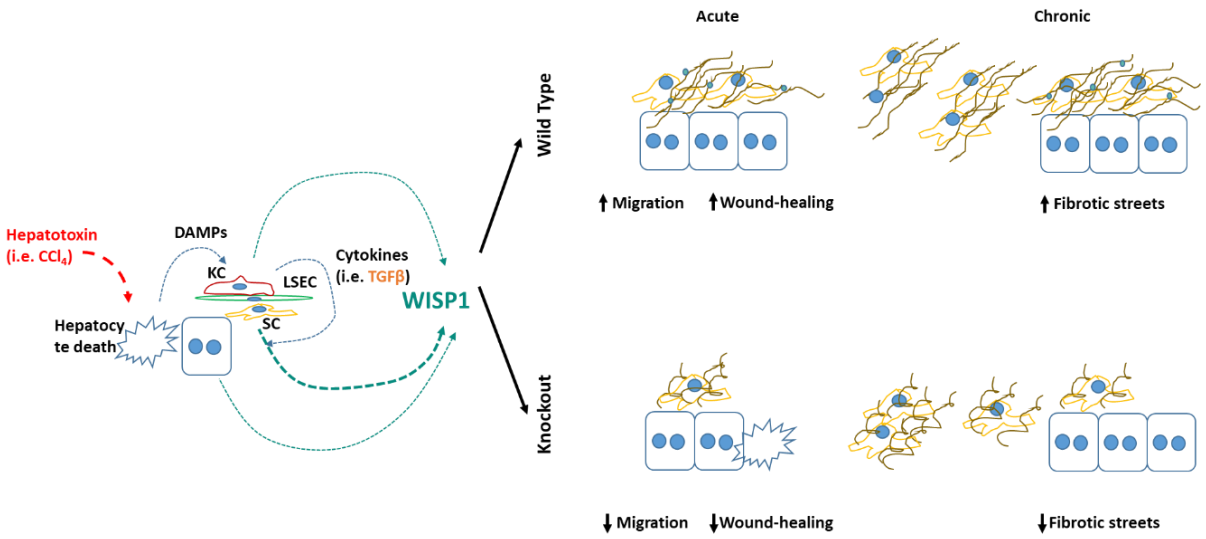

Figure 28. WISP1 role in acute and chronic liver damage hypothesis. After an insult, hepatocyte death occurs and DAMPs are released inducing the expression of cytokines. Cytokines like TGF-β induced the expression and secretion of WISP1 in all liver cells, especially in hepatic stellate cells. WISP1 can bind to collagen secreted by hepatic stellate cells, linearizing it and thus enhanced the cell migration to the damaged area. In the WISP1 knockout condition, collagen architecture remains unaltered and hepatic stellate cells migration is reduced. This condition can aggravate the acute scenario, however, can ameliorate the degree of fibrosis by reducing the fibrotic streets.

4.4 Conclusions and future perspectives

The work presented in this thesis gave strong evidence regarding the expression and secretion of WISP1 in healthy liver and under a damage condition. Moreover, the elucidation of the influence of WISP1 in hepatic stellate cell migration through collagen supports the known role of CCN proteins in the process of cell migration and implicates for the first time the role of WISP1 in the architecture of the extracellular matrix in the context of liver damage. Nevertheless, the *in vivo* data still needs further investigation to support the strong *in vitro* results and confirm the hypothesis of WISP1 as a novel downstream effector to remodel the extracellular matrix in the pathogenesis of liver fibrosis.

5 LIST OF FIGURES

6 LIST OF TABLES

REFERENCES

[1] R. Taub, “Liver regeneration: From myth to mechanism,” *Nat. Rev. Mol. Cell Biol.*, vol. 5, no. 10, pp. 836–847, 2004, doi: 10.1038/nrm1489.

[2] J.-F. Dufour and P.-A. Clavien, *Signaling Pathways in Liver Diseases*. Springer Berlin Heidelberg, 2005.

[3] H. Ishibashi, M. Nakamura, A. Komori, K. Migita, and S. Shimoda, “Liver architecture, cell function, and disease,” *Semin. Immunopathol.*, vol. 31, no. 3, pp. 399–409, 2009, doi: 10.1007/s00281-009-0155-6.

[4] K. Jungermann and T. Kietzmann, “Zonation of parenchymal and nonparenchymal metabolism in liver,” *Annu. Rev. Nutr.*, vol. 16, pp. 179–203, 1996, doi: 10.1146/annurev.nu.16.070196.001143.

[5] S. Colnot and C. Perret, *Molecular Pathology of Liver Diseases*, 1st ed. Springer US, 2011.

[6] T. Kietzmann, “Metabolic zonation of the liver: The oxygen gradient revisited,” *Redox Biol.*, vol. 11, no. December 2016, pp. 622–630, 2017, doi: 10.1016/j.redox.2017.01.012.

[7] E. L. LeCluyse, R. P. Witek, M. E. Andersen, and M. J. Powers, “Organotypic liver culture models: Meeting current challenges in toxicity testing,” *Crit. Rev. Toxicol.*, vol. 42, no. 6, pp. 501–548, 2012, doi: 10.3109/10408444.2012.682115.

[8] A. Braeuning *et al.*, “Differential gene expression in periportal and perivenous mouse hepatocytes,” *FEBS J.*, vol. 273, no. 22, pp. 5051–5061, 2006, doi: 10.1111/j.1742-4658.2006.05503.x.

[9] S. Sekine, B. Y. A. Lan, M. Bedolli, S. Feng, and M. Hebrok, “Liver-specific loss of β-catenin blocks glutamine synthesis pathway activity and cytochrome P450 expression in mice,” *Hepatology*, vol. 43, no. 4, pp. 817–825, 2006, doi: 10.1002/hep.21131.

[10] E. L. LeCluyse, L. M. Norona, and S. C. Presnell, *Liver—Structure and Microanatomy*, no. July. Elsevier Inc., 2018.

[11] R. Bataller and D. a Brenner, “Science in medicine Liver fibrosis,” *J. Clin. Invest.*, vol.

115, no. 2, pp. 209–218, 2005, doi: 10.1172/JCI200524282.The.

[12] P. A. Knolle and D. Wohlleber, “Immunological functions of liver sinusoidal endothelial cells,” *Cell. Mol. Immunol.*, vol. 13, no. 3, pp. 347–353, 2016, doi: 10.1038/cmi.2016.5.

[13] R. A. Roberts, P. E. Ganey, C. Ju, L. M. Kamendulis, I. Rusyn, and J. E. Klaunig, “Role of the Kupffer cell in mediating hepatic toxicity and carcinogenesis,” *Toxicol. Sci.*, vol. 96, no. 1, pp. 2–15, 2007, doi: 10.1093/toxsci/kfl173.

[14] T. Tsuchida and S. L. Friedman, “Mechanisms of hepatic stellate cell activation,” *Nat. Rev. Gastroenterol. Hepatol.*, vol. 14, no. 7, pp. 397–411, 2017, doi: 10.1038/nrgastro.2017.38.

[15] S. L. Friedman, “Liver fibrosis – from bench to bedside,” *J. Hepatol.*, vol. 38, pp. 38–53, Jan. 2003, doi: 10.1016/S0168-8278(02)00429-4.

[16] E. Arriazu *et al.*, “Extracellular Matrix and liver disease,” *Antioxid Redox Signal*, vol. 21, no. 6, pp. 1078–1097, 2014.

[17] M. Klaas *et al.*, “The alterations in the extracellular matrix composition guide the repair of damaged liver tissue,” *Sci. Rep.*, vol. 6, no. June, pp. 1–12, 2016, doi: 10.1038/srep27398.

[18] A. M. Andez and P. S. Amenta, “The extracellular matrix in hepatic regeneration,” *FASEB J.*, vol. 9, no. 14, pp. 1401–1410, 1995, doi: 10.1096/fasebj.9.14.7589981.

[19] M. K. Gordon and R. A. Hahn, “Collagens,” *Cell Tissue Res.*, vol. 339, no. 1, pp. 247–257, 2010, doi: 10.1007/s00441-009-0844-4.

[20] M. D. Shoulders and R. T. Raines, “Collagen structure and stability,” *Annu. Rev. Biochem.*, vol. 78, pp. 929–958, 2009, doi: 10.1146/annurev.biochem.77.032207.120833.

[21] L. F. Lau and D. Nathans, “Identification of a set of genes expressed during the G0/G1 transition of cultured mouse cells.,” *EMBO J.*, vol. 4, no. 12, pp. 3145–3151, 1985, doi: 10.1002/j.1460-2075.1985.tb04057.x.

[22] L. F. Lau and D. Nathans, “Expression of a set of growth-related immediate early genes in BALB/c 3T3 cells: Coordinate regulation with c-fos or c-myc,” *Proc. Natl. Acad. Sci. U. S. A.*, vol. 84, no. 5, pp. 1182–1186, 1987, doi: 10.1073/pnas.84.5.1182.

[23] J. Il Jun and L. F. Lau, “Taking aim at the extracellular matrix: CCN proteins as emerging therapeutic targets,” *Nat. Rev. Drug Discov.*, vol. 10, no. 12, pp. 945–963, 2011, doi: 10.1038/nrd3599.

[24] D. Pennica *et al.*, “WISP genes are members of the connective tissue growth factor family that are up-regulated in Wnt-1-transformed cells and aberrantly expressed in human colon tumors,” *Proc. Natl. Acad. Sci.*, vol. 95, no. 25, 1998.

[25] C. C. Chen and L. F. Lau, “Functions and mechanisms of action of CCN matricellular proteins,” *Int. J. Biochem. Cell Biol.*, vol. 41, no. 4, pp. 771–783, 2009, doi: 10.1016/j.biocel.2008.07.025.

[26] K. P. Holbourn, K. R. Acharya, and B. Perbal, “The CCN family of proteins: structure-function relationships,” *Trends Biochem. Sci.*, vol. 33, no. 10, pp. 461–473, 2008, doi: 10.1016/j.tibs.2008.07.006.

[27] L. F. Lau, “Cell surface receptors for CCN proteins,” *J. Cell Commun. Signal.*, vol. 10, no. 2, pp. 121–127, 2016, doi: 10.1007/s12079-016-0324-z.

[28] C. C. Chen, J. L. Young, R. I. Monzon, N. Chen, V. Todorović, and L. F. Lau, “Cytotoxicity of TNFα is regulated by integrin-mediated matrix signaling,” *EMBO J.*, vol. 26, no. 5, pp. 1257–1267, 2007, doi: 10.1038/sj.emboj.7601596.

[29] J. Il Jun and L. F. Lau, “The matricellular protein CCN1 induces fibroblast senescence and restricts fibrosis in cutaneous wound healing,” *Nat. Cell Biol.*, vol. 12, no. 7, pp. 676–685, 2010, doi: 10.1038/ncb2070.

[30] L. Xu, R. B. Corcoran, J. W. Welsh, D. Pennica, and A. J. Levine, “WISP-1 is a Wnt-1- and [illegible]-catenin- responsive oncogene,” pp. 585–595, 2000.

[31] M. Feng and S. Jia, “Dual effect of WISP-1 in diverse pathological processes,” *Chinese J. Cancer Res.*, vol. 28, no. 6, pp. 553–560, 2016, doi: 10.21147/j.issn.1000-9604.2016.06.01.

[32] K. Maiese, “WISP1: Clinical Insights for a Proliferative and Restorative Member of the CCN Family,” *Curr. Neurovasc. Res.*, vol. 11, no. 4, pp. 378–389, 2014, doi: 10.2174/1567202611666140912115107.

[33] H. Jaeschke, C. D. Williams, M. R. McGill, Y. Xie, and A. Ramachandran, “Models of drug-

induced liver injury for evaluation of phytotherapeutics and other natural products," *Food Chem. Toxicol.*, vol. 55, pp. 279–289, 2013, doi: 10.1016/j.fct.2012.12.063.

[34] H. Zaher *et al.*, "Protection against acetaminophen toxicity in CYP1A2 and CYP2E1 double- null mice," *Toxicol. Appl. Pharmacol.*, vol. 152, no. 1, pp. 193–199, 1998, doi: 10.1006/taap.1998.8501.

[35] J. Kale, E. J. Osterlund, and D. W. Andrews, "BCL-2 family proteins: Changing partners in the dance towards death," *Cell Death Differ.*, vol. 25, no. 1, pp. 65–80, 2018, doi: 10.1038/cdd.2017.186.

[36] K. Du, Y. Xie, M. R. Mcgill, and H. Jaeschke, "Pathophysiological significance of c-jun N -terminal kinase in acetaminophen hepatotoxicity," *Expert Opin. Drug Metab. Toxicol.*, pp. 1–11, 2015.

[37] N. Hanawa, M. Shinohara, B. Saberi, W. A. Gaarde, D. Han, and N. Kaplowitz, "Role of JNK Translocation to Mitochondria Leading to Inhibition of Mitochondria Bioenergetics in Acetaminophen-induced Liver Injury * □," vol. 283, no. 20, pp. 13565–13577, 2008, doi: 10.1074/jbc.M708916200.

[38] G. K. Michalopoulos, "Liver regeneration," *J. Cell. Physiol.*, vol. 213, no. 2, pp. 286–300, Nov. 2007, doi: 10.1002/jcp.21172.

[39] S. J. Forbes and N. Rosenthal, "Preparing the ground for tissue regeneration: From mechanism to therapy," *Nat. Med.*, vol. 20, no. 8, pp. 857–869, 2014, doi: 10.1038/nm.3653.

[40] N. Yamanaka *et al.*, "Dynamics of normal and injured human liver regeneration after hepatectomy as assessed on the basis of computed tomography and liver function," *Hepatology*, vol. 18, no. 1, pp. 79–85, 1993, doi: 10.1002/hep.1840180114.

[41] S. Hoehme *et al.*, "Prediction and validation of cell alignment along microvessels as order principle to restore tissue architecture in liver regeneration," *Proc. Natl. Acad. Sci. U. S. A.*, vol. 107, no. 23, pp. 10371–10376, 2010, doi: 10.1073/pnas.0909374107.

[42] J. P. Iredale *et al.*, "Mechanisms of Spontaneous Resolution of Rat Liver Fibrosis Hepatic Stellate Cell Apoptosis and Reduced Hepatic Expression of Metalloproteinase Inhibitors," *J. Clin. Invest.*, vol. 102, 1998, doi: 10.1172/JCI1018.

[43] B. Dewidar, J. Soukupova, I. Fabregat, and S. Dooley, “TGF-β in Hepatic Stellate Cell Activation and Liver Fibrogenesis: Updated,” *Curr. Pathobiol. Rep.*, vol. 3, no. 4, pp. 291–305, 2015, doi: 10.1007/s40139-015-0089-8.

[44] S. L. Nishimura, “Integrin-mediated transforming growth factor-βactivation, a potential therapeutic target in fibrogenic disorders,” *Am. J. Pathol.*, vol. 175, no. 4, pp. 1362–1370, 2009, doi: 10.2353/ajpath.2009.090393.

[45] Y. Inagaki and I. Okazaki, “Emerging insights into transforming growth factor β Smad signal in hepatic fibrogenesis,” *Gut*, vol. 56, no. 2, pp. 284–292, 2007, doi: 10.1136/gut.2005.088690.

[46] K. Breitkopf, P. Godoy, L. Ciuclan, M. V. Singer, and S. Dooley, “TGF-β/Smad signaling in the injured liver,” *Z. Gastroenterol.*, vol. 44, no. 1, pp. 57–66, 2006, doi: 10.1055/s-2005-858989.

[47] S. L. Friedman, “Hepatic fibrosis-Overview,” *Toxicology*, vol. 254, no. 3, pp. 120–129, 2008, doi: 10.1016/j.tox.2008.06.013.

[48] A. Pellicoro, P. Ramachandran, J. P. Iredale, and J. A. Fallowfield, “Liver fibrosis and repair: Immune regulation of wound healing in a solid organ,” *Nat. Rev. Immunol.*, vol. 14, no. 3, pp. 181–194, 2014, doi: 10.1038/nri3623.

[49] E. L. Ellis and D. A. Mann, “Clinical evidence for the regression of liver fibrosis,” *J. Hepatol.*, vol. 56, no. 5, pp. 1171–1180, 2012, doi: 10.1016/j.jhep.2011.09.024.

[50] J. P. Iredale, “Models of liver fibrosis: Exploring the dynamic nature of inflammation and repair in a solid organ,” *J. Clin. Invest.*, vol. 117, no. 3, pp. 539–548, 2007, doi: 10.1172/JCI30542.

[51] L. W. D. Weber, M. Boll, and A. Stampfl, “Hepatotoxicity and mechanism of action of haloalkanes: Carbon tetrachloride as a toxicological model,” *Crit. Rev. Toxicol.*, vol. 33, no. 2, pp. 105–136, 2003, doi: 10.1080/713611034.

[52] D. L. Tribble, T. Y. Aw, and D. P. Jones, “The pathophysiological significance of lipid peroxidation in oxidative cell injury,” *Hepatology*, vol. 7, no. 2, pp. 377–386, 1987, doi: 10.1002/hep.1840070227.

[53] G. Ramadori, F. Moriconi, I. Malik, and J. Dudas, “Physiology and pathophysiology of

liver inflammation, damage and repair," *J. Physiol. Pharmacol.*, vol. 59, no. SUPPL.1, pp. 107–117, 2008.

[54] K. Kiso *et al.*, "The role of kupffer cells in carbon tetrachloride intoxication in mice," *Biol. Pharm. Bull.*, vol. 35, no. 6, pp. 980–983, 2012, doi: 10.1248/bpb.35.980.

[55] S. Crespo Yanguas *et al.*, "Experimental models of liver fibrosis," *Arch. Toxicol.*, vol. 90, no. 5, pp. 1025–1048, May 2016, doi: 10.1007/s00204-015-1543-4.

[56] Y. Jiang, J. Liu, M. Waalkes, and Y. J. Kang, "Changes in the gene expression associated with carbon tetrachloride-induced liver fibrosis persist after cessation of dosing in mice," *Toxicol. Sci.*, vol. 79, no. 2, pp. 404–410, 2004, doi: 10.1093/toxsci/kfh120.

[57] A. Ghallab *et al.*, "Model-guided identification of a therapeutic strategy to reduce hyperammonemia in liver diseases," *J. Hepatol.*, vol. 64, no. 4, pp. 860–871, 2016, doi: 10.1016/j.jhep.2015.11.018.

[58] F. SWEAT, H. PUCHTLER, and S. I. ROSENTHAL, "SIRIUS RED F3BA AS A STAIN FOR CONNECTIVE TISSUE.," *Arch. Pathol.*, vol. 78, pp. 69–72, Jul. 1964.

[59] Y. Huang *et al.*, "Image analysis of liver collagen using sirius red is more accurate and correlates better with serum fibrosis markers than trichrome," *Liver Int.*, vol. 33, no. 8, pp. 1249–1256, 2013, doi: 10.1111/liv.12184.

[60] K. J. Livak and T. D. Schmittgen, "Analysis of relative gene expression data using real-time quantitative PCR and the 2-ΔΔCT method," *Methods*, vol. 25, no. 4, pp. 402–408, 2001, doi: 10.1006/meth.2001.1262.

[61] I. Mederacke, D. H. Dapito, S. Affò, H. Uchinami, and R. F. Schwabe, "High-yield and high-purity isolation of hepatic stellate cells from normal and fibrotic mouse livers," *Nat. Protoc.*, vol. 10, no. 2, pp. 305–315, Feb. 2015, doi: 10.1038/nprot.2015.017.

[62] P. Godoy *et al.*, *Recent advances in 2D and 3D in vitro systems using primary hepatocytes, alternative hepatocyte sources and non-parenchymal liver cells and their use in investigating mechanisms of hepatotoxicity, cell signaling and ADME*, vol. 87, no. 8. 2013.

[63] P. Maschmeyer, M. Flach, and F. Winau, "Seven steps to stellate cells," *J. Vis. Exp.*, no. 51, pp. 3–7, 2011, doi: 10.3791/2710.

[64] B. S. Boyden and D. Ph, “THE CHEMOTACTIC E F F E C T OF MIXTURES OF ANTIBODY AND ANTIGEN ON POLYMORPHONUCLEAR LEUCOCYTES (From the Department of Experimental Pathology , John Curtin School of Medical Research , Australian National University , Canberra) Materials and Methods,” *Assessment*, pp. 453–466, 1962.

[65] D. J. Webb, H. Zhang, and A. F. Horwitz, *Cell migration: an overview.*, vol. 294. 2005.

[66] H. Jia *et al.*, “ The tumor cell-secreted matricellular protein WISP 1 drives pro-metastatic collagen linearization ,” *EMBO J.*, vol. 38, no. 16, pp. 1–15, 2019, doi: 10.15252/embj.2018101302.

[67] A. Ghallab *et al.*, “Influence of Liver Fibrosis on Lobular Zonation,” *Cells*, vol. 8, no. 12, pp. 1–21, 2019, doi: 10.3390/cells8121556.

[68] G. Campos, “Genome-wide response patterns in stressed hepatocytes,” Technical University of Dortmund, Dortmund, 2014.

[69] G. Campos *et al.*, “Inflammation-associated suppression of metabolic gene networks in acute and chronic liver disease,” *Arch. Toxicol.*, vol. 94, no. 1, pp. 205–217, 2020, doi: 10.1007/s00204-019-02630-3.

[70] L. Pütter, “WNT1-inducible Signaling Pathway Protein-1 (WISP1), a Novel Critical Protein in Hepatotoxic Liver Injury,” *Phd-Thesis*, vol. 1, 2017.

[71] I. Gene, T. P. O. Brien, G. P. Yang, L. Sanders, and L. F. Lau, “Expression of cyr6l , a Growth Factor-Inducible,” *Mol. Cell. Biol.*, vol. 10, no. 7, pp. 3569–3577, 1990.

[72] Y. Tong *et al.*, “WISP1 mediates hepatic warm ischemia reperfusion injury via TLR4 signaling in mice,” *Sci. Rep.*, vol. 6, no. December 2015, pp. 1–11, 2016, doi: 10.1038/srep20141.

[73] X. Li *et al.*, “Blockade of CCN4 attenuates CCl4-induced liver fibrosis,” *Arch. Med. Sci.*, vol. 11, no. 3, pp. 647–653, 2015, doi: 10.5114/aoms.2015.52371.

[74] T. W. Jung *et al.*, “WISP1 promotes non-alcoholic fatty liver disease and skeletal muscle insulin resistance via TLR4/JNK signaling,” *J. Cell. Physiol.*, vol. 233, no. 8, pp. 6077–6087, 2018, doi: 10.1002/jcp.26449.

[75] C. T. Chen *et al.*, “Impacts of wnt1-inducible signaling pathway protein 1 polymorphism on hepatocellular carcinoma development,” *PLoS One*, vol. 13, no. 6, pp. 1–15, 2018,

doi: 10.1371/journal.pone.0198967.

[76] Q.-Y. Wang, Y.-J. Feng, and R. Ji, "High expression of WISP1 promotes metastasis and predicts poor prognosis in hepatocellular carcinoma.," *Eur. Rev. Med. Pharmacol. Sci.*, vol. 24, no. 20, pp. 10445–10451, Oct. 2020, doi: 10.26355/eurrev_202010_23396.

[77] S. Klee, M. Lehmann, D. E. Wagner, H. A. Baarsma, and M. Konigshoff, "WISP1 mediates IL-6-dependent proliferation in primary human lung fibroblasts," *Sci. Rep.*, vol. 6, no. November 2015, pp. 1–11, 2016, doi: 10.1038/srep20547.

[78] R. Hassan, "Mechanisms of activated hepatic stellate cell removal in acute and chronic liver injury," 2017.

[79] M. Y. Moon *et al.*, "Rap1 regulates hepatic stellate cell migration through the modulation of RhoA activity in response to TGF-β1," *Int. J. Mol. Med.*, vol. 44, no. 2, pp. 491–502, 2019, doi: 10.3892/ijmm.2019.4215.

[80] C. Yang *et al.*, "Liver fibrosis: Insights into migration of hepatic stellate cells in response to extracellular matrix and growth factors," *Gastroenterology*, vol. 124, no. 1, pp. 147–159, 2003, doi: 10.1053/gast.2003.50012.

[81] I. Mannaerts *et al.*, "Gene expression profiling of early hepatic stellate cell activation reveals a role for igfbp3 in cell migration," *PLoS One*, vol. 8, no. 12, pp. 1–13, 2013, doi: 10.1371/journal.pone.0084071.

[82] Y. Huang, X. Deng, and J. Liang, "Modulation of hepatic stellate cells and reversibility of hepatic fibrosis," *Exp. Cell Res.*, vol. 352, no. 2, pp. 420–426, 2017, doi: 10.1016/j.yexcr.2017.02.038.

[83] N. C. Henderson *et al.*, "Targeting of αv integrin identifies a core molecular pathway that regulates fibrosis in several organs," *Nat. Med.*, vol. 19, no. 12, pp. 1617–1624, 2013, doi: 10.1038/nm.3282.

[84] E. Olaso *et al.*, "DDR2 receptor promotes MMP-2-mediated proliferation and invasion by hepatic stellate cells," *J. Clin. Invest.*, vol. 108, no. 9, pp. 1369–1378, 2001, doi: 10.1172/JCI200112373.

[85] M. Ono *et al.*, "CCN4/WISP1 controls cutaneous wound healing by modulating proliferation, migration and ECM expression in dermal fibroblasts via α5β1 and TNFα,"

Matrix Biol., vol. 68–69, pp. 533–546, 2018, doi: 10.1016/j.matbio.2018.01.004.

[86] C. H. Hou, C. H. Tang, C. J. Hsu, S. M. Hou, and J. F. Liu, "CCN4 induces IL-6 production through αvβ5 receptor, PI3K, Akt, and NF-κB singling pathway in human synovial fibroblasts," *Arthritis Res. Ther.*, vol. 15, no. 1, p. R19, 2013, doi: 10.1186/ar4151.

[87] J. Ge *et al.*, "Effect of siRNA on Wisp-1 gene expression, proliferation, migration and adhesion of mouse hepatocellular carcinoma cells," *Asian Pac. J. Trop. Med.*, vol. 8, no. 10, pp. 821–828, 2015, doi: 10.1016/j.apjtm.2015.09.008.

[88] J. James, K. S. Bosch, D. C. Aronson, and J. M. Houtkooper, "Sirius Red histophotometry and spectrophotometry of sections in the assessment of the collagen content of liver tissue and its application in growing rat liver," *Liver*, vol. 10, no. 1, pp. 1–5, 1990, doi: 10.1111/j.1600-0676.1990.tb00428.x.

[89] H. Uchinami, E. Seki, D. A. Brenner, and J. D'Armiento, "Loss of MMP 13 attenuates murine hepatic injury and fibrosis during cholestasis," *Hepatology*, vol. 44, no. 2, pp. 420–429, 2006, doi: 10.1002/hep.21268.

[90] H. E. Tzeng *et al.*, "CCN6-mediated MMP-9 activation enhances metastatic potential of human chondrosarcoma," *Cell Death Dis.*, vol. 9, no. 10, 2018, doi: 10.1038/s41419-018-1008-9.

[91] C. H. Hou, Y. C. Chiang, Y. C. Fong, and C. H. Tang, "WISP-1 increases MMP-2 expression and cell motility in human chondrosarcoma cells," *Biochem. Pharmacol.*, vol. 81, no. 11, pp. 1286–1295, 2011, doi: 10.1016/j.bcp.2011.03.016.

[92] O. Krenkel, J. Hundertmark, T. Ritz, R. Weiskirchen, and F. Tacke, "Single Cell RNA Sequencing Identifies Subsets of Hepatic Stellate Cells and Myofibroblasts in Liver Fibrosis," *Cells*, vol. 8, no. 5, p. 503, 2019, doi: 10.3390/cells8050503.

ACKNOWLEDGMENTS

The completion of my PhD degree was challenging and would have never been possible without the support and guidance of numerous people. I am deeply grateful to everyone who contributed to this work and supported me throughout the whole time, only some of whom it is possible to give particular mention here.

First of all, I would like to express my sincere gratitude to my supervisor **Prof. Dr. med. Jan G. Hengstler** for giving me the chance to work in his laboratory at the Leibniz Research Center for Working Environment and Human Factors (IfADo) in Dortmund, Germany. His guidance, support and great ideas have contributed to my growth and development as a scientist, especially the last 2 challenging years of my PhD.

Moreover, I am deeply grateful to my co-supervisor and mentor **Dr. Patricio Godoy** for supporting me throughout the first years of my PhD. Without his trust, encouragement, guidance, patience and tremendous knowledge, this dissertation would not have been possible.

Many especial thanks to **Dr. Gisela Campos** who not only helped me at the beginning of my PhD in science related topics, but also to start my life in Germany. I will always be deeply grateful for all your support and kindness. In the same way, I am very grateful to **Dr. Agata Widera** for her help and ideas for my project but most importantly for her fun and cool advices for life.

I had the privilege to get to know and to work with many people who made the scientific life fun and more enjoyable, especially: **Katharina Belgasmi**, **Maiju Myllys**, **Sarah Metzler**, **Adelina Jashari**, **David Feuerborn** and **Patrick Nell**. Many thanks to the best technician I could ever ask for, **Katharina Belgasmi**. Her technical excellence was key when a new protocol needed to be established or a problem needed to be solved. Her help in the lab and "in general" was fundamental to complete this thesis. During the millions of perfusions and cell isolations we became very good friends. That friendship became stronger when **Maiju Myllys** joined our group, even with hugs from the very first day. Maiju's friendly and at the same time sarcastic personality made it easy to become friends with and to share the PhD student life. I am very grateful for all the talks and discussions, especially when trying to find some sense to our results. It is of course worth mentioning and thanking to her cute grumpy **Hansi**

boy, who created a sometimes “intense” office atmosphere but mostly a very happy one. Thanks to **Sarah Metzler** for being the best master student and for all the funny things that happened right from the beginning in our working time together and later in our friendship. For this and much more, I feel incredible lucky and grateful, to have found you **girls** and that you have become my family in Germany. I am very grateful to **Adelina Jashari**, one of the few “normal” people, for all the laughs and complaints during the best and not so good moments during our PhDs. Last but not least, thanks to “**the guys**” for the fruitful discussions, especially in our Livtox meetings, but most importantly thanks for the humor.

My sincere thanks go to **Elmar Kriek** and **Georgia Günther** for all your help, especially regarding the mice work and organization.

I have truly enjoyed the opportunity to work with and learn from my colleagues at IfADo: Dr. Rosemarie Marchan, Dr. Cristina Cadenas, Dr. Ahmed Ghallab, Dr. Karolina Edlund, Dr. Ayham Zaza, Brigitte Begher-Tibbe, Zaynab Hobloss, Larissa Pütter, Wiebke Albrech, Annika Glotzbach, Gregor Leonhardt, Philipp Gabrys, Anastasia Oprisko and many more. To all of you, thank you very much!

My gratitude also extends to **Monika Turajski** for helping me in any kind of paper work and organizational related problem.

Importantly I want to thank **my Eric** for completing my life here. Thanks for being my travel partner, my personal chef, my IT nerd, my support and love during the last 3 years. I am really looking forward for the next challenges and adventures in our lives together.

Nothing would have been possible without the support and love of my family and friends in Chile. Special thanks to my parents, **Raúl González** and **Eliana Leiva,** and to my sister **Paulina,** for being my cheerleaders my whole life. Thanks for always believing in me and telling me that I can achieve and concrete all my dreams.

Nada de esto podría haber sido posible sin el apoyo y amor de mi familia y amigos en Chile. Agradezco especialmente a mis padres, **Raúl González** y **Eliana Leiva**, y a mi hermana **Paulina**, por ser mis cheerleaders personales toda mi vida. Muchas gracias por siempre creer en mí, diciéndome que puedo alcanzar y cumplir todos mis sueños. Gracias por hacerme sentir que siempre estamos cerca a pesar de los más de 12.000 km de distancia; por los videos y fotos

de mis perritos que me animaron cada vez que sentí el estar lejos de casa. Por todo eso y mucho más, ¡gracias! Los amo.

Thank you all! Danke an alle! ¡Muchas gracias a todos!